STRUCTURE/PROPERTY RELATIONS OF ELASTOMERIC HYBRID ORGANIC-INORGANIC COMPOSITES

By

THOMAS M. MILLER

A DISSERTATION PRESENTED TO THE GRADUATE SCHOOL
OF THE UNIVERSITY OF FLORIDA IN PARTIAL FULFILLMENT
OF THE REQUIREMENTS FOR THE DEGREE OF
DOCTOR OF PHILOSOPHY

UNIVERSITY OF FLORIDA

1997

To Yvonne

ACKNOWLEDGMENTS

Sincere thanks go to my advisor Dr. Anthony Brennan for providing me the opportunity to educate myself in the field of polymer engineering. The challenges associated with working in his group and the enthusiasm he possesses for both his students and his profession have made my studies at UF enjoyable and rewarding. I would also like to thank Dr. Christopher Batich, Dr. Elliot Douglas, Dr. Eugene Goldberg and Dr. Kenneth Wagener for serving on my doctorate committee. Partial financial support for this research was made possible through a DuPont Young Faculty Investigator Award presented to Dr. Anthony Brennan. Additionally, support was provided by the National Institutes of Health under Grant DEO 9307-07, as well as a research grant awarded by PhotoSense LLC. As I have benefited from all of these contributions I gratefully acknowledge the support of DuPont, NIH and Dr. Alan Baron of PhotoSense. To this last individual I am especially grateful for both his enthusiasm as a project sponsor and the technical insights he has provided regarding the work detailed in Chapter 5. Also appreciated is the financial support of the Department of Materials Science and Engineering provided me during my first year of study. This assistance and the air of professionalism present within the MSE department were instrumental in my decision to attend the University of Florida.

Professional thanks go out to the members of Dr. Brennan's research group. I am indebted to Rick Feller and Yiqun Wang for their patience in explaining the operation of

laboratory equipment when I arrived, and for encouraging my own personal development with the occasional lack of help. Professional thanks are extended to Jesse Arnold and Mike Zamora for their unselfish donation of AFM skill and chemistry expertise, respectively. Additionally, their participation in numerous discussions has contributed immeasurably to the success of my research efforts. Also appreciated is the assistance of Licheng Zhao in the synthesis of the lumiphore containing samples evaluated in Chapter 5. The collection of the small angle X-ray scattering data presented in Chapter 4 was obtained by Dr. Jianye Wen at Virginia Polytechnic Institute and State University. His assistance is appreciated. Professional thanks are also extended to Dr. Bruce Carroll, Dr. Paul Hubner and Andy Winslow of the Department of Aerospace Engineering, Mechanics and Engineering Science at the University of Florida for their assistance in collecting the data necessary to measure the diffusivity of the hybrids. This work is detailed in Chapter 5. Personal thanks go out to all unmentioned members of the Brennan group and the remaining MAE students, for helping make graduate school fun. I thank my parents, Wayne and Peggy Miller, for their lifelong commitment to my education. Lastly, I thank my wife, Yvonne, for her patience as I completed these last few years of study.

TABLE OF CONTENTS

page

LIST OF TABLES

LIST OF FIGURES

Abstract of Dissertation Presented to the Graduate School
of the University of Florida in Partial Fulfillment of the
Requirements for the Degree of Doctor of Philosophy

STRUCTURE/PROPERTY RELATIONS OF
ELASTOMERIC HYBRID ORGANIC-INORGANIC COMPOSITES

By

Thomas M. Miller

December 1997

Chairman: Anthony B. Brennan
Major Department: Materials Science and Engineering

Hybrid organic-inorganic composites have been synthesized by the sol-gel processing of triethoxysilane end functionalized poly(tetramethylene oxide) and tetraethxoysilane. The resulting transparent materials are elastomeric gels crosslinked by an amorphous polysilicate phase. Elementary rubber-elasticity theory in conjunction with dynamic mechanical spectroscopy was applied to these seemingly nonideal networks to quantify the change in phase interaction induced by aging the benchmark acid catalyzed gels in a basic solution of 70% ethylamine in water. The change in the average molar mass between crosslinks explained the previously published mechanical and dynamic mechanical results. Furthermore, the application of this theory to these seemingly nonideal networks resulted in network parameters that were in excellent agreement with traditional equilibrium swelling estimates.

The work was then extended by utilizing this ethylamine solution to catalyze the sol-gel reaction in-situ. The effect of this change in catalyst upon the oxygen diffusivity of the hybrids as a function of polysilicate loading was investigated using a luminescence based approach. While the diffusivity of the acid catalyzed gels decreased with increasing loading, the base catalyzed gels did not indicating that the polysilicate domains resulting from the base catalysis possess considerable porosity. However, the pores appear to be much too small for Knudsen diffusion, a commonly observed gas separation mechanism in porous ceramic membranes.

To investigate the influence of polysilicate network polarity and spatial distribution, the sol-gel processing of the hybrids was adjusted to produce two classes of gels. One exhibited a more discrete polysilicate phase possessing greater network connectivity and reduced silanol content than the other. This was accomplished by using dimethylformamide in place of tetrahydrofuran as the organic solvent constituent of the sol. Poly(methacrylic acid)-PTMO-polysilicate semi-interpenetrating polymer networks (SIPNs) were then produced by γ polymerizing monomer swollen hybrids using a ^{60}Co source. Fourier transform infrared spectroscopy was used to confirm the reduced silanol content. Tensile testing revealed that the better developed, less polar inorganic network containing SIPNs exhibit decreased elongation at failure and post-yield elongation to strain hardening. Thus, the origin of the exceptionally high elongation of these SIPNs is a diffuse polysilicate network capable of extensive hydrogen bonding and deformation under load.

CHAPTER 1
INTRODUCTION

This dissertation is dedicated to the study of several aspects of hybrid organic-inorganic composites. The pervading theme throughout the work is an attempt to discern the role that the polysilicate reinforcing phase of a micro-phase separated, polymer matrix composite plays in dictating the mechanical, thermo-mechanical and gas transport properties of the overall materials system. The sol-gel process is utilized for composite consolidation. However, as there are many variables active in this process, the work specifically concentrates on the effects of spatial distribution and degree of network connectivity of the polysilicate phase as controlled by pre- and post-gelation exposure to network modifying solutions. More details regarding the specific studies will be given in the following paragraphs as each facet of this research is developed.

Composites play an ever increasing role in our daily lives. Driving forces such as reduction in weight, increases in stiffness or hardness and the ability to tailor a material response in a specific direction, if desirable, have spurred composite development. A general definition of a composite is that of a multiphase system in which one phase resides within the other and is responsible for the augmentation of an engineering property for the overall system. Such a material system is in contrast to a material blend in which one phase simply reduces the amount of the costlier phase while providing little to no increase in any engineering property.

Many types of composites exist within the ceramic, metal and polymer industries. Narrowing the discussion to the realm of polymer matrix composites, a plethora of composite systems still exist. For example, theromosets such as epoxy, polyester and polyurethane have all been used as matrix materials, as have thermoplastics such as poly(ether ether ketone), polyimides and polyamides. Similarly, a variety of reinforcing fibers exist. These may be ceramic, metal or polymer. The only design criterion that exists is that the modulus of the fiber must be much greater than the modulus of the matrix. Thus ensuring reinforcement of the matrix.

Traditionally, composite systems are classified according to the length of the fiber, i.e., continuous, discontinuous or particulate. However, with the advent of new processing techniques developed by materials chemists over the past several decades, composites can now be produced where the size of the reinforcing phase is on the nanometer scale. The development of these nanocomposites has been driven by groups interested in such aspects of materials science as the quantum confinement of electrons, self-assembling devices, high surface area catalyst supports and, an area of particular interest to this author, the extent that these nanophases are responsible for overall composite properties such as elasticity and gas transport.

Returning to the arena of nanocomposite processing, a variety of techniques have been developed enabling the synthesis of nanometer-in-size reinforcing phases. Examples such as sol-gel-processing, micellular formation, and in-situ growth of nanoclusters dominate the literature. However, regardless of the specific route utilized, all of these techniques rely on the same underlying approach, that of materials chemistry.

One class of nanocomposites that has been receiving a particularly large amount of attention in the past decade has been that of hybrid organic-inorganic composites. Hybrid composites, or simply hybrids, almost exclusively employ combinations of organic polymers or proteins and ceramic oxides or minerals. Numerous techniques have been developed for producing hybrids. However, with the exception of clay based composites, the review of hybrid technology provided in Chapter 2 will concentrate upon only sol-gel-derived composites. This is done to provide the reader with a detailed review of the processing routes, properties and applications of hybrid systems most closely related to the investigations detailed in Chapters 3, 4 and 5, which utilize the sol-gel-processing of ethoxysilane functionalized poly(tetramethylene oxide) (PTMO) and the silica precursor tetraethoxysilane (TEOS).

Intrinsic to hybrid composites, such as the PTMO-polysilicate system, is the influence of size, shape and continuity of the exceptionally small reinforcing polysilicate phase. For example, considering the significant increase in surface area relative to volume occurring as the particle size decreases, it should be clear that the interphase becomes increasingly important. In the case of sol-gel-derived composites, the spatial distribution of the reinforcing phase becomes particularly important given that the fractal nature of the inorganic structures produced via the sol-gel-process lead to extensive interaction between the matrix and the reinforcing phase. Probing the extent of PTMO and polysilicate interaction as a function of post-gelation processing is the focal point of Chapter 3, wherein elementary rubber-elasticity theory is employed in conjunction with dynamic mechanical spectroscopy as a tool for quantifying the extent of phase interaction.

Another critical issue when considering the increasing surface area contribution is that of surface chemistry. For example, the polysilicate networks that result from acid catalysis of silicon alkoxides are essentially defect laden structures containing alkoxy and hydroxyl groups that have not yet undergone complete hydrolysis and condensation. Hence the term polysilicate is used and not silica in reference to the lack of a well developed, oxygen-bridging network characteristic of fused silica. These unreacted polar species give rise to hydrogen bonding and other molecular forces that influence composite properties. Chapter 4 details investigations into the role that these defects play in dictating the mechanical response of poly(methacrylic acid)-based, semi-interpenetrating polymer networks (SIPNs) formed via the γ polymerization of methacrylic acid swollen PTMO-polysilicate hybrids. These SIPNs exhibit the exceptionally high stress and elongation at break characteristic of engineering thermoplastics despite the fact that poly(methacrylic acid) is an organic glass.

A final issue concerning the role of the polysilicate phase in determining the properties of sol-gel-derived hybrid composites is that of porosity. The sol processing conditions, such as the use of acidic versus basic catalysis, significantly influence the extent and continuity of the porosity present within the inorganic domains of these hybrid composites. Considering that the diameter of these pores may be as large as 10 nm, it is possible that the transport of gases is occurring via Knudsen diffusion at pressures less than ca. 15 atm. This transport mechanism is in contrast to the traditional solution and diffusion mechanism occurring within the elastomeric PTMO phase. Therefore, the investigations detailed in Chapter 5 addressing the transport of oxygen within these

PTMO-polysilicate hybrids as a function of inorganic loading and spatial distribution have allowed an assessment of the types of porosity present within these composites.

Detailed conclusions regarding each of these areas of investigation are provided at the ends of Chapters 3, 4 and 5. However, Chapter 6 will highlight some of these critical findings, summarize the overall impact of this research upon the field of hybrid technology and polymer science in general, and detail possible future directions for the research.

CHAPTER 2
THE DEVELOPMENT AND APPLICATION OF HYBRID COMPOSITES

Development and Detailing of Specific Composite Systems

As the following pages will demonstrate, many polymers and oligomers have been utilized in the synthesis of hybrid organic-inorganic composites. These include classes such as poly(alkenes, acrylates, ethers, esters, amides, imides and dienes). Similarly, a variety of inorganic alkoxides have been used. These include methoxides, ethoxides, isopropoxides and butoxides of silicon, titanium, zirconium and aluminum. Additionally, phenyl, vinyl and amino substituted derivatives of these silicon alkoxides have been incorporated into glassy networks. Despite the wide variety of components that have been mixed to date, the driving force for the development of hybrid composites remains to be the improvement in some material property arising from the synergistic combination of the organic and inorganic phases. Whether it is the improved reinforcement of a rubber over a conventional particulate filler, increased abrasion resistance of polymer glasses, improved temporal stability of embedded lumiphores or increased selectivity to gas mixtures permeating through the bulk, the key words are improved and increased. This section will provide some historical perspective for the development of these hybrid composites. However, the main focus is upon the information gained from the individual systems studied.

Poly(Dimethyl Siloxane)

Development of organic-inorganic networks began in the early to mid-1980s using poly(dimethyl siloxane) (PDMS) oligomers. This polymer was chosen because of the close similarity between the polysiloxane chains and the expected sol-gel-derived polysilicate chains. Hence, it is also an ideal organic-inorganic glass. Similar synthetic approaches were employed independently by two groups: J.E. Mark (The University of Cincinnati) and G.L. Wilkes (Virginia Polytechnic Institute and State University). However, the research goals of each group were different. Mark's approach focused on improving the mechanical properties of PDMS by using the sol-gel processing of metal alkoxides to generate inorganic fillers (silica, titania, alumina and zirconia) within the PDMS network.[1-8] In all cases, the hybrids generated by either the simultaneous curing and filling or the precipitation of the inorganic component within an existing swollen network (in-situ precipitation) showed significantly better reinforcement than the network containing fumed silica, an alternate reinforcing agent. Electron microscopy of the hybrids synthesized using the in-situ precipitated silica show that the inorganic phase did not agglomerate into large particles within the original PDMS network.[3,4] Rather, most "particles" fall in the range of 20 to 30 nanometers and were very finely dispersed. Small angle X-ray scattering experiments on these reinforced networks demonstrated that under strongly basic conditions and large excesses of water, uniformly dense particles (nonfractal) resulted.[5] Conversely, under acidic or neutral conditions more extended, less-dense inorganic structures resulted. Sohoni and Mark also studied the thermal stability of in-situ filled PDMS networks using thermogravimetric analysis (TGA) and

demonstrated that this type of reinforcement improved the thermo-oxidative stability of these materials more so than fumed-silica reinforced or ordinary PDMS.[8]

Simultaneous with Mark's research was that of Wilkes' group which also used PDMS as the polymer. Similarly, silica was used as the reinforcing phase. These materials were termed ceramers to denote the contributions of both the ceramic, inorganic glass and the polymeric, organic glass.[9-11] As the order of the name implies, i.e., not polymics, the emphasis was placed on developing sol-gel glasses containing more inorganic than organic material. The idea being to engineer glasses with controllable flexibility/brittleness rather than the reinforcement of rubbery systems as Mark was examining. An overview of the laboratory's contributions, as well as a general review of sol-gel-derived hybrid composites, has been recently published.[12]

Wilkes et al. research efforts examined the effect of silanol terminated PDMS as a function of loading upon the mechanical properties of these sol-gel-derived glasses. The principlal means of characterization were mechanical tensile testing, dynamic mechanical spectroscopy (DMS), and small angle X-ray scattering (SAXS). Since Mark had not utilized DMS, Wilkes et al. provided new insights into the structure-property behavior of these mixed-phase glasses. These insights included analysis of the tan δ response to discern information regarding polysilicate-polysiloxane interactions. A series of publications address the effects of varying the acid concentration, amount of water and tetraethoxysilane (TEOS) added as well as the molecular weight of the PDMS utilized.[9-11] These results indicated that the extent of hydrolysis and condensation that the network undergoes is a function of the amount of water added. Similarly, the simultaneous

hydrolysis and condensation of all alkoxysilanes may result in preferential reactions between inorganic TEOS monomer and itself along with silanol-terminated PDMS and itself. This would result in a phase separated morphology.

Chung et al.[13] and Hu and Mackenzie[14] have prepared rubbery ORMOSILS using PDMS and TEOS. An ORMOSIL is an organically modified silicate. Traditionally, such materials are comprised of organosilanes which, as the name implies, possess one or more organic pendant groups bonded to the tetrafunctional silicon atom. When reacted via the sol-gel process, these organic groups remain in the structure and impart flexibility to the resulting hybrid. Schmidt et al. have researched these materials thoroughly and a good review is available.[15] The ORMOSILS produced by Chung et al. differ somewhat from these original hybrids in that TEOS is not an organofunctional moiety. Nevertheless, these PDMS/TEOS materials do exhibit a high degree of rubber elasticity, which is a function of the sol-gel processing variables. The authors have suggested and evaluated different models, which in conjunction with mechanical tensile testing and electron microscopy, have helped determine the morphology of these materials.

Kohjiya et al.[16] and more recently Surivet et al.[17] have also published information on PDMS/silica based hybrids. In particular, Surivet et al. relate their work on ceramers to that of Wilkes's et al. discussed above.[9-11] Using differential scanning calorimetry (DSC), DMS and SAXS, these researchers investigated the structure-property relations of polyurethane-co-PDMS (PU-PDMS)/silica hybrids, as well as polybutadiene-based hybrids discussed shortly. Their results revealed that the PU-PDMS/silica system was a three phase, micro-phase separated system. This phase separation was due to

thermodynamic incompatibility between the siloxane backbone and the hard segments (urethane-urea linkages) used to cap the PDMS chains with multifunctional alkoxysilanes. Conversely, the polybutadiene based hybrids could be considered two-phase systems because of good miscibility between the polybutadiene backbone and urethane-urea linkages.[17] These early results indicated that significant gains in mechanical reinforcement could be achieved using hybrid technology. However, the systems produced exhibited micro-phase separation, a characteristic feature of virtually all hybrids produced using organic oligomers.

Poly(Tetramethylene Oxide)

It was speculated by Huang and Wilkes that the tendency of the PDMS and silica to phase separate was due to the immiscibility of the PDMS with the water added for hydrolysis and generated during condensation.[18] Therefore, new polymer systems were sought which had better mixing characteristics with water. Oligomers of PTMO were chosen for precisely this reason. However, the absence of the siloxane chain structure to compatiblize the organic polymer and inorganic glass was a concern. Previously, only silanol-terminated PDMS was all that was necessary to react with the in-situ generated silica. To improve the compatibility of the PTMO with silica, isocyanatopropyl-triethoxysilane was reacted with the oligomers. This reaction resulted in each oligomer possessing end groups capable of undergoing sol-gel processing. Similarly, it was assumed that the reactivity of the ethoxy groups on both the TEOS and the PTMO end groups would be the same. This would eliminate any preferential condensations as discussed above in the PDMS systems. With these concerns addressed, work was begun on the new hybrids and focused on the variables of oligomer molecular weight,

functionality, TEOS content, inorganic precursor, gel age, acid concentration and type, and processing temperatures and methods.[10,11,19-31] By using SAXS, DMS, mechanical tensile testing, infrared spectroscopy and NMR the structure-property relations of this class of hybrids were investigated. In particular, SAXS still revealed the presence of micro-phase separation within the transparent hybrids. However, the mechanical properties of the PTMO based system were much better than those of the PDMS/silica hybrids.

The observed benefits of near-molecular reinforcement over conventional reinforcement, as well as the potential of increased hardness, abrasion resistance and improved thermo-oxidative stability, sparked interest in the hybridization of other polymer systems. Although the reinforcement of rubbers continued to receive much interest, attention soon turned to the incorporation of inorganics into higher molar mass thermoplastics. The following sections detail some of the processing utilized and the resulting properties that could be developed in these materials.

Other Rubber Based Systems

Mauritz and Jones have synthesized homogeneous, translucent organic-inorganic "alloys" combining poly(n-butyl methacrylate) (Mn = 75,000 g/mol) with tetraethyl titanate (TET) and tertbutyl titanate (TBT).[32] The thermal stability of these networks was studied using thermogravimetric analysis (TGA), and it was determined that the thermal onset of significant network degradation could be increased by the addition of the titania phase. DSC revealed that crystallization of the amorphous TiO_2 to anatase, in the TET case, occurred at temperatures above the degradation temperature of the polymer.

Surivet et al. studied the thermo-mechanical properties of alkoxysilane-terminated hydrogenated polybutadiene-co-polyurethane (PU H-PBD) macromonomers of varying molar mass crosslinked via the sol-gel-derived silica phase.[17] Recall that these authors also investigated PU-PDMS of varying molar mass. Using a point source X-ray apparatus, SAXS investigations were made to determine the morphology of these heterogeneous materials. Those data, in conjunction with DMS and DSC measurements allowed these investigators to develop a qualitative morphological model for this new ceramer system. Unlike the earlier reported model for the PU-PDMS copolymers, which specified a three phase system composed of the pure PDMS regions, pure polysilicate regions and a distinct interfacial region arising from immiscibility of the urethane-urea end linkages, the PU H-PBD gels were distinctly two phase. This "improvement" in the level of miscibility is attributable to the increased solubility of H-BPD and the urethane-urea linkages.[33] These results highlight the importance of solubility in hybrid technology, for it is the level of mixing which gives rise to the improvements observed in hybrid systems.

Polyoxazolines

David and Scherer have synthesized a transparent, inorganic-organic glassy material composed of 50/50 volume percent TEOS-derived SiO_2 and 500 kg/mole poly(ethyloxazoline) (PEOX). Interestingly, there was no evidence of phase separation, as SAXS, DSC and TEM all indicated a homogeneous material.[34] The processing route and precursors utilized ensured that the two components were not covalently bonded. The absence of two-phase behavior is unusual for hybrids generated using a polymer of such

high molar mass. However, the strong hydrogen bonding ability of this polymer appeared to have provided the solubility enhancement necessary to prevent phase separation.

Additional evidence of such an occurrence is provided by Saegusa who has demonstrated the ability of polymers containing strong electron donor groups, such as poly(2-methyl-2-oxazoline) to be incorporated and well dispersed into the evolving inorganic glass.[35] Again, by improving the affinity of the two phases, which was demonstrated using FTIR, a more intimate level of mixing is achievable. One consequence of this increased level of mixing, that these researchers discuss and that is addressed later in the applications section, is the ability to create hybrids of controlled porosity via pyrolysis of the organic phase.

Vinylic Based Polymers

Fitzgerald et al. have investigated the dielectric and mechanical spectra of hybrids produced by mixing a poly(vinyl acetate) (PVAc)/THF solution with TEOS, followed by the addition of hydrochloric acid.[36] Mixtures were made believed to be 0, 5, 10, 15 and 20 wt.% SiO_2. These composites were transparent and, not surprisingly, FTIR revealed hydrogen bonding between the silicate network and carbonyl units of the PVAc. Interestingly, no shift in the Tg of the composites from that of the pure PVAc was observed. Similarly, the activation energies were calculated and shown to be independent of SiO_2 loading. However, the breadth of the tan δ associated Tg relaxations did increase with increased filler content.

Landry et al. have also produced transparent, homogeneous hybrids using a 50/50 wt.% PVAc and TEOS mixture and acid catalysis.[37] Just as in the preceding paragraph,

DSC and DMS indicated only a slight increase in the Tg of the hybrid with incorporation of silica. Also, dynamic mechanical tan δ responses indicate a strong interaction between the organic and inorganic phases, which lead to well-dispersed phases and high modulus rubbery plateaus. The absence of a discernible increase in the Tg of these PVAc composites is in agreement with the finding of Fitzgerald et al. described above.[36] These findings lead to the conclusion that hydrogen bonding is not energetic enough and that covalent bonds need to be present for an increase in the Tg to occur.

Saegusa and coworkers have utilized the hydrogen bonding affinity of the organic and inorganic phase to produce transparent PVP-silica hybrids.[35,38] Using atomic force microscopy (AFM) and BET analysis these researchers demonstrated that the composite possessed a very dense microstructure exhibiting little porosity, i.e., the silica domains in this material have much less pore volume than sol-gel-derived silica. This observation is important in that the section on membranology later in this chapter discusses the influence of porosity within the hybrids.

Similar to the work of Saegusa, Novak et al. have also found that polymers possessing functional groups such as amines and pyridines are soluble in the pre-gelled sol solutions, especially, poly(2-vinyl-pyridine) and poly(n-vinyl pyrrolidone).[39] However, unlike the work of Saegusa et al., Novak's work focuses on the synthesis of non-shrinking, sol-gel-derived networks utilizing acid based, acrylate monomers to functionalize the alkoxysilanes prior to sol-gel processing. Upon hydrolysis these macroalkoxysilanes release the acrylate monomers as the hydrolysis by-product. These groups then undergo traditional free radical polymerization simultaneous with the

polycondensation reaction of the silane. As the hydrolysis by-product is polymerizable, no mass loss and corresponding shrinkage is observed.[39]

Extensive work has been done at the Eastman Kodak Corporate Research Labs by Landry et al. towards determining the chemical nature of the organic-inorganic interaction and the thermo-mechanical properties that result from the non-covalently bonded phases interacting within acrylic glasses.[37,40,41] Like many of their coworkers, this group found that the ability to produce well-dispersed networks is attributable to hydrogen bonding between the silanol groups and, in this case, the carbonyl units in the poly(methyl methacrylate) (PMMA).[37] Hence, the highly hydrated, open polysiloxane chains resulting from the acid-catalyzed sol-gel process were shown to form more homogeneous, transparent hybrids. Somewhat surprisingly, these hybrids exhibited enhanced mechanical properties beyond the Tg. However, the mechanical properties were also affected by curing time and temperature.[41] It was also noted that transparency was a function of the temperature of the substrate the films were cast on, e.g., ≥30°C resulted in films exhibiting no macrophase-separation. Base catalyzed systems, films cast on cooler substrates and non-hydrogen bonding capable polymers produced cloudy, poorly dispersed glasses. Another interesting feature of these reports is microscopy images provided that show asymmetric particulate formation in some of these hybrids.

Pope et al. have studied the properties of porous, sol-gel-derived glass impregnated with benzoyl peroxide (BPO) initiated PMMA. The effect of silane coupling agents was evaluated also.[42] It was found that the density, elastic modulus, modulus of rupture (MOR) and compressive strength of the material decreased as the volume fraction

of PMMA increases. Conversely, the refractive index increases as the volume fraction of PMMA increases. Methacryloxypropyltrimethoxysilane was then used as a coupling agent to improve the adhesion between the silica glass and the PMMA. As expected, the result was an increase in the MOR as the amount of coupling agent employed increased.

Klein and Abramoff also examined PMMA impregnated sol-gel-derived silica gels.[43] Long-wave UV illumination was employed in addition to benzoyl peroxide for PMMA polymerization. This method prohibited the degradation of the silica xerogel due to moisture adsorption and desorption. Overall, the material behaved more like bulk PMMA than bulk silica, with the exception of hardness.

Wei et al. have reported the synthesis of poly(allyl methacrylate-co-methyl methacrylate) containing hybrids using group-transfer polymerization.[44] The allyl methacrylate homopolymers (PAMA) were then functionalized by hydrosilylation of the allylic segments using Speier's catalyst. When mixed with tetrafunctional metal alkoxides in the presence of HCl or methanesulfonic acid and water, transparent, sol-gel-derived glasses were produced over a wide range of TEOS:triethoxysilyl group ratios. However, when copolymers of the functionalized PAMA and PMMA were used, only the methanesulfonic acid produced transparent hybrid glasses. Similarly, lower fractions of the functionalized PAMA, i.e. <10%, tended to produce grainy and opaque materials. The lack of a well-defined Tg in the DSC traces of the polyacrylate suggested good dispersion of the organic and inorganic phases. Titanium alkoxides were also employed, but met with less success.

High Performance Thermoplastics

The lure of improved mechanical response, thermo-mechanical response and increased degradation temperatures attainable with hybrid technology has spurred development of high performance thermoplastic hybrids. For example, polymers such as poly(ether ketone) and polyimide have been used in the synthesis of hybrid composites. As was the case for the previously discussed thermoplastics, solubility continues to drive hybrid morphology and response. However, steps can be taken to promote mixing.

Considering poly(ether ketone) (PEK) first, Noell et al. have successfully produced transparent hybrids of varying inorganic contents using triethoxysilane end functionalized PEK oligomers and TEOS.[45] It was demonstrated that the Tg dependence on the curing temperature was governable by the time-temperature transformation behavior described by Gillham for network development, i.e., by increasing the cure temperature the diffusion limited curing associated with vitrification could be avoided.[46] As a result, better phase mixing was obtainable. However, SAXS experiments confirmed the characteristic presence of micro-phase separation. The importance of this work is that it demonstrated the ability to produce transparent, highly loaded hybrids exhibiting Tgs as high as 200°C from 4,000 g/mole oligomers. Additionally, this oligomer based route circumvented the poor solubility experienced by Landry et al. in the synthesis of PMMA and other acrylic hybrids.[37,40,41]

A similar oligomeric approach was used by Brennan, who has employed transimidization to functionalize polyimide oligomers. These reactive oligomers were

subsequently used to produce polyimide/titania hybrids.[47] This technique resulted in the successful synthesis of transparent materials composed of 18%, 37%, and 54% titania.

In an alternative synthesis route, Morikawa et al. synthesized hybrid glassy materials using polyamic acid and TEOS.[48] The resulting films consisted of non-covalently bonded polyimide/silica species, and the results were quite different from those of Brennan. Specifically, transparent, organic-inorganic networks resulted only when the wt.% silica was less than or equal to 8% (assuming 100% conversion to an oxygen bridging network). Beyond the 8% limit, only opaque films resulted. All of the 0 wt.% to 70 wt.% SiO_2 containing films exhibited considerable flexibility. These materials are in sharp contrast to the PEK hybrids that contained up to ca. 30-40 vol.% silica and the PI hybrids of 54 wt.% titania.[45,47] This comparison demonstrates the importance of a mechanism for improving compatibility, e.g., covalent or hydrogen bonding.

Nafion® Membranes

Nafion® membranes represent a unique and interesting area in hybrid technology. These membranes are perfluorosulfonate ionomers possessing a morphology composed of 3-5 nm clusters of SO_3X (where X is a proton or cation) terminated side chains residing within a semi-crystalline, tetrafluoroethylene matrix.[49] Their use in the preparation of hybrids stems from two sources. First, their physicochemical stability and excellent ion transport properties have resulted in their application in electrochemical cells and as templates/acid catalysts for chemical reactions.[50] Secondly, the presence of these well dispersed, nanometer-scale, polar micro-domains is anticipated to provide an ordering influence for an in-situ precipitated, inorganic network.[51]

The research conducted on hybrids produced from these membranes is becoming extensive, with Mauritz's group at the University of Southern Mississippi contributing a significant portion.[49-55] The preponderance of the literature confirms that these polar groups do affect the in-situ precipitation of alkoxide swollen membranes. Perhaps the best study illustrating the influence of this template approach to hybrid synthesis was that utilizing SAXS.[53] In the report, it was demonstrated that as the silicate loading increased from 0% to 74% (mass/mass) the correlation distance or interdomain spacing remained unchanged. This is in contrast to the studies of Wilkes' group using the sol-gel processing of triethoxysilane end functionalizd PTMO oligomers and various metal alkoxides. For these systems, increasing interdomain spacings with increasing silica and titania content were clearly observed.[30]

Recent research on hybrid Nafion® based composites has focused on their use as asymmetric membranes for gas separation.[54,55] These application oriented studies are detailed under the membrane application section later in this chapter.

Clay Based Hybrids

Clay has received considerable attention in the synthesis of hybrid organic-inorganic composites. Recently, an excellent review of this field has been published by Giannelis providing a good overview of the properties attainable in these composites.[56] For example, researchers in this area have demonstrated the ability to achieve excellent mechanical reinforcement with less inorganic than alternative glass based nanocomposites.[57] Therefore, less of the inorganic phase is needed and weight can be saved. Another inherent advantage is the self-extinguishing characteristics of this class of

materials.[56] The key to this approach is the ability of organic monomers to intercalate into the layers of these silicate based minerals prior to polymerization initiation.

For example, Yano et al. have produced molecularly mixed composites of montmorillonite clay and polyimide. These hybrids were synthesized using montmorillonite intercalated with the ammonium salt of dodecylamine. Polymerization occurred in the presence of dimethylacetamide and polyamic acid, and the resulting dispersion was cast onto glass plates and cured. The cured films were as transparent as polyimide but exhibited reduced gas permeability and a lower coefficient of thermal expansion (CTE) than ordinary polyimides.[58] The reduced permeability is not surprising, as fillers often reduce the ability of gases to permeate through polymers. Nevertheless, applications such as low cost, more effective barrier coatings can be realized.

Okada et al. have produced nylon-6/montmorillonite clay hybrids via intercalation of 12-aminolauric acid. When mixed with ε-caprolactam and polymerized at 100°C for 30 min, a nylon/clay hybrid (NCH) was produced. TEM and X-ray diffraction of the NCHs confirm both the intercalation and molecular level of mixing between the two phases. The benefits of such materials over ordinary nylon-6 or non-molecularly mixed, clay-reinforced nylon-6 included increased heat distortion temperature, elastic modulus, tensile strength and dynamic elastic modulus throughout the -150°C to 250°C temperature range.[59, 60] Additional studies by this group have also demonstrated increases in elastic modulus and strength, without a simultaneous drop in impact strength for a 4 wt.% Nylon-6 nanocomposite relative to that of Nylon-6. Perhaps most impressively, the heat distortion temperature increased from 65°C to 145°C as a result of hybridization.[57]

In addition to the improved final properties of these clay hybrids, advantages also exist in the processing stages. For example, this group has synthesized vulcanized rubber sheets of nitrile rubber and montmorillonite intercalated with Hycar ATBN (a butadiene acrylonitrile copolymer).[61] Although these rubber hybrids showed enhanced reinforcement relative to both carbon black containing and pure nitrile rubber materials, they were easier to process than carbon black-filled rubbers. This leads to less wear on the processing equipment and lower energy consumption for production.

Applications Utilizing Hybrid Technology

The following sections highlight the major fields of science and industry in which hybrid composites are being developed and applied. Although some of the sections are short and provide only a quick summary, others such as the areas of luminescent technologies and membranology provide more detail. This is owing to their relevance to the studies presented in Chapter 5.

When reviewing the literature on hybrid technology, the line between hybrids that actually combine an organic and inorganic phase to produce a synergistic change in a property and researcher-proclaimed hybrids merely incorporating a dispersed organic within the matrix begin to blur. For the applications previewed in the following sections, both types of materials will be discussed. However, it will be made clear if the work under discussion is relying solely on a dispersion and not on a property enhancement resulting from the combination of a multiphase system. For example, an excellent review of organically doped, porous sol-gel glasses has been published recently and addresses the incorporation of organics such as enzymes, proteins and liquid crystals (LC) within the gel

structure.[62] Both the advantages and disadvantages of sol-gel processing are discussed with particular emphasis placed upon immobilization procedures.

Microelectronics Usage

Schmidt and Wolter have developed an organically modified ceramic (ORMOCER) system based on the sol-gel processing of phenyl and vinyl substituted organosilanes and silica.[63] The system can be cured either thermally or using photopolymerization of the vinyl groups. The properties of this coating include excellent electrical properties, such as low dielectric constant and high surface and bulk resistance, even after weathering. Additionally, the material was stable up to 260°C.

Popall et al. have developed several coating compositions based on organically substituted silicon and aluminum alkoxides, e.g., vinyltrimethoxysilane and aluminum tri-sec-butylate. After mixing these solutions with photoinitiators, the resulting sols were spin coated onto various substrates and photocured to produce patterned microelectronic devices.[64] Polymerization can be induced using either a high wattage UV light or a frequency doubled argon laser.

Abrasion Resistant Coatings

Melamine, tris(m-aminophenyl)phosphine oxide (TAPO), diethylenetriamine (DETA), polyethyleneimine (PEI), 4,4 diamino diphenyl sulfone (DDS), bis(3-aminophenoxy-4,-phenyl) phosphine oxide (BAPPO), and epoxy have all been functionalized by the Wilkes group using a triethoxysilane coupling agent to produce molecules capable of sol-gel processing.[65-67] These functionalized species may or may not be reacted with additional metal alkoxides. Once the sol-gel process is initiated, but

before significant gelation occurs, these sols can be spin coated onto substrates where they are allowed to finish gelling. Additionally, curing at elevated temperatures may also be employed. The resulting coatings are glasses composed of organic moieties or oligomers covalently bonded via siloxane linkages. These coatings have been shown to significantly enhance the abrasion resistance of a Lexan® substrate, and do so with increasing effectiveness as the curing temperature increases.[65,66] Similarly, when additional metal alkoxides such as titanium or zirconium are employed in conjunction with the functionalized moieties, significant increases in the refractive index of the coatings result.[65]

Schmidt and Wolter have also studied the ability of ORMOCERs based on alumina, zirconia, titania or silica and mixtures of each to function as abrasion resistant coatings.[63] For example, polycarbonate, when coated with an epoxy/alumino-silicate system, experienced a significant reduction in the degree of hazing induced by an abrader, as compared to uncoated polycarbonate.

Solid Polymer Electrolytes

Fujita and Honda have reported the successful synthesis of a transparent solid polymer electrolyte (SPE) based on PEO and alkoxysilanes.[68] The material possessed good mechanical properties and high ionic conductivity, ca. 1.8×10^{-5} S cm^{-1} @ 25°C, dependent upon the organic-inorganic ratio and PEO chain length.

Crosslinking Agents

Munteanu has published a review article addressing the use of polyfunctional organosilanes as crosslinking agents for a variety of polyolefins.[69] Most techniques

employ a grafting initiator, usually an organic peroxide, which is mixed with the polyolefin prior to extrusion. Upon heating, the initiator thermally decomposes to free radicals. These radicals then abstract hydrogen from the polyolefin backbone and thereby promote grafting of the organosilane onto the chain. Subsequent hydrolysis and condensation of the alkoxysilanes, with or without a catalyst, after polymer processing and shaping induce crosslinking in the preformed product. These methods have the advantage of not requiring treatment at elevated temperatures, e.g., above the crystalline melting point, to induce the crosslinking in the final part, as is the case for peroxide induced crosslinking. Hence, dimensional stability is maintained throughout crosslinking.

Traditionally, peroxide and radiation were used to induce crosslinking. However, numerous patents exist regarding this novel organosilane crosslinking method and Munteanu provides an excellent review.[69] Similarly, Munteanu also reviews the complete spectrum of actual and potential applications of this technology.

Nonlinear Optical Materials

This class of materials is established owing to the nonlinear change in optical response that polarizable molecules exhibit in the presence of an intense electric field.[70] The refractive index of a material is an example of a first-order, linear response whereupon the electron cloud of a molecule becomes delocalized, producing a dipole. However, under intense electric field, e.g., a laser, linear polarization fails and higher-order responses are observed such as frequency doubling, termed secondary harmonic generation (SHG), and occasionally frequency tripling, termed third harmonic generation (THG). Although these higher order responses are observable in the individual molecules, special processing is necessary to orient materials or glasses doped with these optically active species as they

destructively interfere with one another and negate any SHG. For polymers, a common approach is to heat the material above the Tg, expose it to a magnetic field and then quench/cool back below the Tg under the influence of the field. For thermosets, such as sol-gel-derived hybrids doped with these compounds, the equivalent processing would be to delay polycondensation until the magnetic field is established and allow the sample to gel under the fields influence.

Numerous researchers have synthesized transparent sol-gel-derived glasses containing optically active compounds that give rise to nonlinear optical activity.[71-75] An inherent advantage of the silica gel matrix over organic glasses is its greater ability to stabilize the organic dopants, i.e., prevent these poled molecules from randomizing over time. This can be attributed to the network structure, which can be thought of as possessing a very high crosslink density. To enhance the temporal stability of the active compounds, which is a function of the mobility, researchers either covalently react the molecules to the gel matrix or produce optically active polymers/oligomers with decreased mobility. For example, equal amounts of the prepolymer of hexakis-(methoxymethyl)melamine and an optically active molecule created by reacting (3-glycidoxypropyl)trimethoxysilane and 4-[(4'-nitrophenyl)azo]phenylamine can be processed using sol-gel techniques to produce a hybrid composed of a highly crosslinked organic melamine phase covalently bonded to a polysilicate phase. Furthermore, the pendent group of the alkoxysilane monomer is the optically active group.[71-75] The combination of high crosslink density afforded by the silica and melamine network and covalent bonding with the molecularly dispersed, two-phase matrix dramatically increased the temporal stability of the SHG for the poled composite.

Wung et al. have synthesized an organic-inorganic hybrid utilizing a very ingenious approach.[75] By mixing a sulphonium polyelectrolyte precursor for PPV and TMOS together and subsequently polymerizing the organic precursor via thermolysis, a hybrid network was formed. The catalyst required for the polymerization of the TMOS was supplied as a by-product of the thermolysis. Similar to the findings of others, the polymer doped glass exhibited improved optical quality over that of pure PPV. Although these researchers view the primary application of this material as a wavequide, the sol-gel processing of the TMOS appeared to have resulted in the shortening of the conjugation length in the PPV as observed in the above studies.

Luminescent Based Instrumentation and Devices

The porosity present in sol-gel-derived glasses and leached glasses, such as Vycor, have spurred development of instrumentation that utilizes this pore network to provide the pathways necessary for either gases or liquids to reach chemical probes dispersed within the gel. By incorporating an organic phase, increased ductility for the glasses and/or environmental stability for the embedded molecules can be achieved. The key to these technologies is the response of the organic lumiphore to sensitizing agents such as metal ions, oxygen, ammonia, etc. Nearly always, the detection mechanism is the change in spectral emission wavelength or intensity. Therefore, these devices rely heavily upon computers to monitor and quantify the spectral emissions.

One of the more unique sensors developed has incorporated chemically active proteins within the pore structure of sol-gel-derived glass. These proteins exhibit changes in the visible absorption spectra reflective of the chemical reactions they have undergone upon exposure to cyanide gas and metal containing solutions.[76] The key, of course, is the

change induced in the luminescence of the molecules upon contact with the sensitizing agent.

The sensing of both atmospheric and dissolved oxygen has received considerable attention and current efforts rely primarily upon the dispersion of an oxygen sensitive lumiphore within porous glass fibers and films.[77-79] Additionally, silica particles have been coated with these lumiphores, which are then generously dispersed in a polymeric binder and applied to the substrate.[80,81] This approach to doping/coating highly porous glass results in sensors capable of responding to changes in oxygen concentration within 0.5-3 seconds. However, a concern regarding the validity of the relationship between luminescent intensity and molecular oxygen concentration arises for glass filled, polymer matrix composites and organic glasses.[82] The origins of these problems and the impact on the hybrid composites reported in Chapter 5 will be addressed in this later chapter.

Although this review reveals that functioning devices can be produced from doped silica gels, several researchers have noted that improvements can be made in the quality and long-term performance of these devices by the incorporation of organosilanes.[83-85] For example, when 3-aminopropyltriethoxysilane (3-APTS) is used in conjunction with TEOS, the quality and clarity of the doped silica films produced are enhanced. Additionally, the tendency of fluoroescein isothiocyanate (FITC), the optically active agent, to leach from the films is reduced.[83,84] The reduction in leaching arises from the immobilization of the FITC to the gel matrix via the formation of a thiourea linkage with the 3-APTS. Similar increases in film quality and emission intensity were observed upon the addition of 3-(trimethoxysilyl)propylmethacrylate to TEOS.[85] An excellent example,

in terms of demonstrating the improvements possible, is in the production of hybrid-based light emitting diodes (LEDs).

The low cost of plastics, multitude of manufacturing techniques relative to ceramics and the design flexibility of polymeric structures ensure that polymeric LEDs will be able to compete for markets such as flat panel displays. However, a key to their success is improving their longevity by reducing the influence of thermal vibration and chain mobility. To this end, recently published research has focused on the formation of a poly(phenylene vinylene)-organopolysilicate interpenetrating polymer network.[86] Thin films were first fabricated by spin coating sols containing a PPV thermally-activated precursor and alkoxides of TEOS, methyltriethoxysilane and dimethyldiethoxysilane sols of varying molar ratios on indium tin oxide wafers. Heat treatment of these sols at 200°C initiated polymerization of the PPV precursor and drove the polycondensation reaction. These films exhibited blue shifts with increasing connectivity of the silicate phase, as controlled by the ratio of the organo-substituted alkoxides. As a result, a fourfold increase in photoluminescent intensity at the highest polysilicate loading was measured. Additionally, LED devices were fabricated by coating the exposed surface of these films with aluminum. The results showed that the electroluminescent intensity per unit current increases with increasing connectivity of the glass network as well. This behavior is attributed to the ability of the gelling glass to shorten the conjugation length of the polymerizing PPV precursor by hindering the molar mass build-up. In terms of lifetime, the hybrid glass/PPV LEDs exhibited double the usage lifetime. However, the decay in intensity with increasing time remained unchanged by IPN formation.

An alternative approach to altering the emission spectra of PPV is that of alkoxysilane functionalization of PPV oligomers prior to the sol-gel reaction. Such an approach has been taken recently, with the focus of the work being the influence of the central moiety of arylenevinylene oligomers on photoluminescence.[87] Although no devices were produced, these investigations did probe the influence of the silica network upon the conformation of these fixed molar mass oligomers. Unlike the just discussed research, which exhibited blue shifts with increasing silica gel connectivity, this research revealed that overall photoluminescence intensity decreases as a result of incorporation into a gel as opposed to in solution. Additionally, red-shifts were observed and attributed to the increase in planarity induced by the surrounding gel structure.

A study investigating the thermal stability of optically active chromophores was published by Schutte et al. This study details the thermo-oxidative stability of coatings produced by either covalently or non-covalently incorporating 2,4-dinitroaniline into an inorganic silicate network coated onto a sapphire substrate.[88] Although some increase in the thermal stability of the chromophore was observed using UV-Vis spectroscopy, the authors conclude that this sol-gel method of chromophore encapsulation did not provide any real thermal and/or oxidative protection in either the covalently or non-covalently bonded state.

Air/Gas and Liquid Separation Membranes

This area of science is an extremely diverse and economically driven area of research at both the academic and corporate levels.[89,90] This research is driven by the gas separation industry which is interested in the rapid separation of gases such as nitrogen

from air for inert blanketing, high hydrocarbons from natural gas and hydrogen streams, and organic vapors from air and nitrogen streams.[89,91] Essentially, only two main approaches can be taken when designing a membrane for gas separation: the use of a highly selective organic polymer or the use of a microporous ceramic. The next two sections detail the strengths of each class of material and develop the transport concepts necessary to understand the processes likely to occur in hybrid organic-inorganic composites. A review of the published research on hybrid membranes is then provided in the third section.

Diffusion in porous materials

The unquestionable benefits of inorganic porous membranes include exceptional high temperature stability, corrosion resistance to solvents, excellent mechanical integrity and high permeation rates. However, numerous disadvantages also exist for this class of membranes. For example, although a separation mechanism exists, via Knudsen diffusion, the selectivity of this process is less than that exhibited by polymers. This is particularly true of organic glasses which exhibit significantly greater selectivity and will be discussed in the next section.

Considering porous materials, such as sol-gel-derived gas separation membranes or ultrafiltration membranes, several regimes of gas transport exist. The specific mechanism is dependent upon the Knudsen number, K_n, which is defined as

$$K_n = \frac{\lambda_{gas}}{d_{pore}} \tag{2.1}$$

where d_{pore} is the diameter of the pore and λ_{gas} is the mean free path of the gas.[92] Schematically, these regimes are illustrated in Figure 2.1. If K_n is much less than 1, which

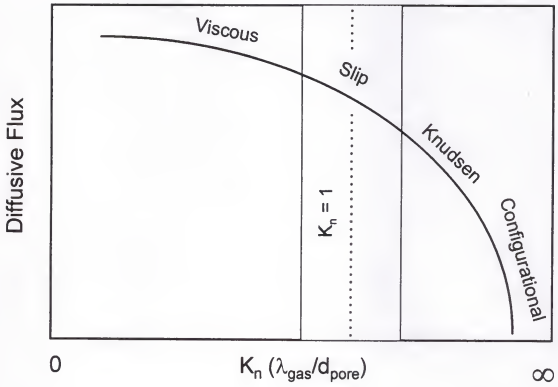

Figure 2.1 Schematic illustration of the relative change in diffusive flux accompanying a change in pore diameter for a gas of constant mean free path.

is the case for large pores relative to the mean free path of the gas, then molecule-molecule collisions predominate. However, the few molecule-wall collisions that do occur result in a loss of momentum for the molecules. Upon reflection from the wall, these molecules immediately collide with other gas molecules and regain their momentum. The continual loss and regaining of momentum via collisions leads to formation of a stable boundary layer moving at a speed dictated by the rate of the collisions. Momentum transfer ensures that all of the gas molecules in the stream move at the same pace. An important consequence of this process is that no mechanism of gas separation exists.

As the diameter of the pore decreases, and λ_{gas} begins to approach the dimensions of the pores, K_n approaches unity. In this regime, some gas molecules collide with one another while others collide with the pore walls. As in the previous case, those molecules colliding with the wall loose momentum. However, the decreased pore diameter ensures that some of the rebounding molecules strike another wall before colliding with other gas molecules. As a result, these molecules do not regain their momentum, and the previously stable boundary layer breaks down. As a consequence, the speed of the gas stream begins to become independent of the rate of collisions. This lapse, or slip, in the momentum transfer gives rise to this transition regime. Continuing, as the diameter of the pore decreases further, virtually all of the collisions occurring are between the individual gas molecules and the pore walls. As a result, a complete loss of momentum transfer occurs and each molecule begins to travel at a velocity independent of other molecules. The speed of travel is dictated solely by the molar mass and collision diameter of the species. Consequently, gas molecules of differing molar masses, e.g., oxygen and nitrogen, would move at differing velocities, thereby giving rise to a separation mechanism. This regime is

termed the Knudsen diffusion regime. The limiting case of diffusion is when the Knudsen number approaches infinity. At this point, the diameter of the pore approaches the diameter of the molecule and spatial configurations of both the pore and gas molecules become significant, hence, the term configurational diffusion.

As oxygen diffusion in hybrids will be studied in Chapter 5, it is useful to determine its mean free path at temperatures and pressures relevant to the previously described potential applications. Employing the kinetic theory of gases, the mean free path of a gas can be calculated from the expression

$$\lambda_{gas} = \frac{\eta}{p}\left(\frac{\pi RT}{2M}\right)^{\frac{1}{2}} \tag{2.2}$$

where p is the pressure, R is the gas constant, T is absolute temperature and M is the molar mass of the gas. The term η, the viscosity of the gas, can be calculated using the expression

$$\eta = \frac{M}{2}\left(\frac{8RT}{\pi M}\right)^{\frac{1}{2}}\left(\frac{1}{\sqrt{2}\pi\sigma^2 L}\right) \tag{2.3}$$

where the terms σ and L refer to the molecular diameter of the gas and Avogadros number, respectively. Review of the above relations reveals that pressure and temperature are the two parameters that dictate the mean free path independent of gas type. For example, Figure 2.2 illustrates the effect of pressure upon the mean free path of oxygen at 0°C and 100°C, which are the extreme temperatures most likely encountered by applications such as oxygen sensing instrumentation for use in wastewater treatment, biomedical applications and aerodynamic testing.[78,81,93] The upper limit of 20 atm represents the commonly observed pressure limit utilized for research on organic polymer

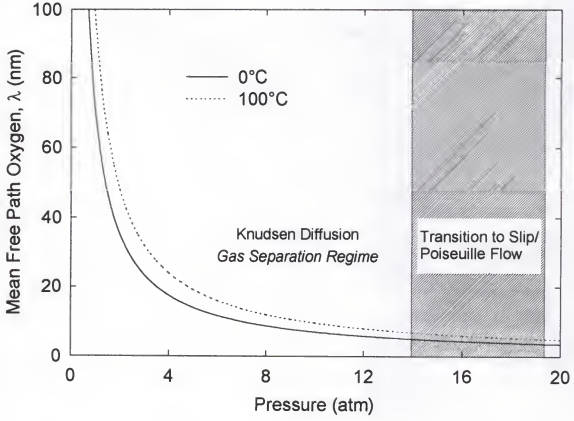

Figure 2.2 The pressure dependence of the mean free path of oxygen at 0°C and 100°C, which are the temperature extremes most likely to be encountered in oxygen sensing applications.

membranes.[94,95] These calculated values are in agreement with those tabulated in the literature stating that the mean free paths of common non-condensible gases at ambient conditions fall between 80 nm and 130 nm.[96]

Although strongly dependent upon processing history, the average diameter of the pores present in sol-gel-derived silica ranges from 2 nm to 20 nm. For example, Fosmoe and Hench report that Type VI gel silica is composed of interconnected pores of diameter equal to 10 nm.[97,98] Therefore, Knudsen diffusion should dominate the flow, and indeed these researchers results confirm this.[98] Similar pore diameters and Knudsen diffusion dependence were reported by Klein and Giszpenc for nitric acid catalyzed TEOS membranes.[99] Lastly, the Saegusa group has reported BET analysis results of poly(vinyl pyrrolidone)/silica hybrid composites showing hydraulic radius values of 2 nm. However, no gas permeability measurements were reported or were indicated to be underway.[38] Therefore, in keeping with these results, the porosity likely present within the inorganic domains of the hybrid composites to be produced in this study should lie in the 1 to 10 nm diameter range. Using 10 nm as the upper limit for pore diameter, Figure 2.2 reveals that at 0°C the K_n begins to approach unity at a pressure of 14 atmospheres. Given that the mean free path increases with decreasing pressures, the diffusion of gas through these pores at anticipated use temperatures and pressures will likely occur via a Knudsen diffusion mechanism.

One issue remains, however, and that is the size of these pores relative to the collision diameter of the gases. In the case of oxygen the effective molecular diameter is 0.346 nm.[89] If the pores within the inorganic domains of the hybrids are ca. 1 nm then it

is quite possible that the diffusion may be occurring in the configurational regime. Evidence supporting this speculation exists in the literature. For example, the diffusivity of methane in a single zeolite possessing a minimum pore diameter of ca. 0.56 nm is $8x10^{-6}$ cm^2/sec. Furthermore, the authors allude to the influence of pore shape when discussing the results.[100] The diffusivity of methane within a porous solid containing pores of 0.56 nm diameter can be calculated from the relation given by Cunningham and Williams:

$$D_K = \frac{2}{3} r \bar{v} \frac{1}{\xi} \tag{2.4}$$

where r is the pore radius.[92] Additionally, $\bar{v}$ is the average speed of the penetrant gas and ξ is a shape factor defined by Knudsen as the diffuse reflection. Assuming that the diffuse reflection is equal to 1 and knowing that the average speed of a gas is given as

$$\bar{v} = \left(\frac{8RT}{\pi M}\right)^{\frac{1}{2}} \tag{2.5}$$

where R is the gas constant, T is the absolute temperature and M is the molecular weight of the gas species, then the diffusion coefficient for the Knudsen regime can be written as

$$D_K = \frac{4r}{3}\left(\frac{2RT}{\pi M}\right)^{\frac{1}{2}}. \tag{2.6}$$

The molecular weight of methane is 16 g/mole. Given a pore radius of 0.25 nm, the theoretical diffusivity at 25°C is $1x10^{-3}$ cm^2/sec. This value is two orders of magnitude larger than the measured value, which was shown to be in good agreement with other reported values of zeolite diffusivities.[100] These data suggest, along with other published results on pyrolyzed organic-inorganic hybrid membranes to be presented shortly, that Knudsen diffusion is not operative in materials with pores this small. Consequently, it may

not be operative in unpyrolyzed hybrids unless special precautions are taken to ensure that the pore structures are on the order of 5-10 nm.

Diffusion in polymeric materials

An excellent historical perspective of the transport of gases in polymer membranes was published by Stannett in 1978.[101] More recent accounts are also available detailing the history of the field with additional information regarding industrial interest.[89] Both reveal that the earliest study addressing gas transport through a membrane was conducted by Graham in 1829. Additionally, research in the field of membranology was well established by 1900 and many of the most important concepts developed by 1950. Research within the past two decades has focused on the use on glassy polymers owing to their increased selectivity.

Gas transport through nonporous materials such as rubbers and organic glasses essentially relies upon the solution of the gas in the up-stream surface, diffusion through the bulk, and evaporation from the down-stream side of the material.[102] Credit for this concept is given to Graham, and the theory underlies all diffusion in polymeric materials.[102,103] However, theories differ in their treatment of diffusion through rubbers and organic glasses. A rubber, more specifically a polymer with a Tg less than room temperature, is the simplest case. Diffusion of a non-condensible gas through an elastomer is described by a combination of Fick's first law,

$$J = -D\left(\frac{dC}{dx}\right) \tag{2.7}$$

where J is the flux, D is the diffusivity, C is the concentration and x is the one-dimensional position of the penetrant within the bulk. Henry's law states that

$$C = Sp, \tag{2.8}$$

where, again, C is the concentration, S is the solubility and p is the pressure of the penetrant "above" the bulk. Under conditions of steady-state diffusion Fick's first law can be integrated from the up-stream face to the down-stream face to produce the relation

$$J = D\left(\frac{C_u - C_d}{t}\right) \tag{2.9}$$

where the subscripts d and u denote downstream and upstream concentrations, respectively, and t is the thickness of the rubber. Henry's law can also be written with similar face-dependent concentrations:

$$C_u = Sp_u \text{ and } C_d = Sp_d. \tag{2.10 and 2.11}$$

Substitution of these Henry's law concentrations into Equation 2.9 yields

$$J_H = D_H S\left(\frac{p_u - p_d}{t}\right). \tag{2.12}$$

The product DS is termed the permeability, P, and the subscript H denotes the Henry's law dependence of the flux and diffusivity. The most common method of measuring the permeability, diffusivity and solubility (also termed sorption) is the time-lag method. The enabling concept is the solution to Fick's second law for a plane sheet where the upstream surface at x=0 is kept at constant concentration, C_1, and the downstream surface at x=1 is kept at constant concentration, C_2=0, i.e., vacuum.[104]

$$Q = \frac{DC_1}{l}\left(t - \frac{l^2}{6D}\right). \tag{2.13}$$

In this equation Q is the total volume of material that has passed through the sheet, t is the elapsed time, and l is the thickness of the polymer sheet. During the first few moments of the process adsorption is occurring and the volume of material traversing the sheet

continues to grow until conditions of steady-state flux are achieved. This established, the volume of penetrant having traversed the sheet becomes linear with time, and the slope is the permeability. Extrapolation of the linear portion of the total volume traversed, Q, as a function of time curve to the abscissa, i.e., solving for t when Q equals zero, produces the relation

$$\Theta = \frac{l^2}{6D} \tag{2.14}$$

where Θ is the extrapolated time value. From this equation, D can be determined. Knowing P and D then the average solubility, S, can be calculated. It is generally recognized that a time of 3Θ should be allowed for steady-state permeation to develop before the linear portion should be extrapolated and D calculated.[89] For unfilled, i.e., non-reinforced, rubbers this technique works very well. However, some complications are observed when the time-lag approach to gas transport is used on filled rubbers and organic glasses.

The origin of the problem is easiest to understand in rubbers containing absorptive fillers such as zeolites.[105-107] The presence of these porous gas sinks leads to an increase in the time required for steady-state permeation to occur. Therefore, Θ is unusually large and the corresponding gas diffusivities calculated from it, in turn, are unusually low. Van Amerongen accounted for the presence of these fillers by introducing a tortuosity factor, τ, to account for the reduced diffusivity, D^*, where

$$D^* = \frac{D}{\tau}. \tag{2.15}$$

In this equation, D is the diffusivity of the unfilled rubber.[108] The term τ was interpreted as a geometric obstruction factor introduced by the particulate. There is validity to this geometric origin, as 23 years later studies on block copolymers of polystyrene and polybutadiene of varying morphologies demonstrated geometric dependent changes in the diffusivity of CO_2.[109] However, the series of publications by Paul et al. investigating the absorptive nature of embedded zeolites suggested that the ability of the filler to immobilize the sorbed gas directly effects the value of Θ.[105-107] The equation relating Θ and D (Equation 2.14) for polymers containing adsorptive fillers had been derived earlier, and was found to be applicable to these zeolite embedded polymers:[110]

$$\Theta = \frac{l^2}{6D}\left[1 + Kf(y)\right]. \tag{2.16}$$

In this equation the new quantity Kf(y) incorporated a Langmuir isotherm of the form

$$C_A = \frac{C'_A bp}{1 + bp}, \tag{2.17}$$

where C_A is the concentration of the permeant in the filler, b is the hole affinity constant and C'_A is the hole saturation constant.[89] The results of new studies incorporating this dual-sorption theory showed that although the time to reach equilibrium permeation was increased significantly the actual change in diffusivity was not nearly as severe as van Amerongen predicted.[106]

Paul's and other researchers' interest in polymers soon turned to organic glasses, which exhibited overall lower permeability than rubbers but significantly improved selectivity, that is, the ability of the polymer to transport one component of a gas mixture at a faster rate.[95,111-115] The adsorptive nature observed in the filled rubbers was also

observable in the organic glasses studied, and a postulate was soon put forth suggesting that since a glass is not an equilibrium structure then regions within the glass do possess localized order. A complete discussion of the impacts of this order upon the transport characteristics of glasses is provided by Kesting and Fritzsche.[89] However, at this point it is sufficient to say that the dual-sorption theory provides the underpinnings of the study of glassy polymer membranes and still finds near universal application in some form or another today. Furthermore, even with the complexities present in the study of organic glasses, the promise of increased selectivity, higher temperature separation processes and better mechanical strength continues to drive the development of the next generation of gas separation membranes.[90]

This review of the transport phenomena present in both porous and polymeric materials provides sufficient understanding of the multiple diffusion mechanisms possibly occurring in hybrid organic-inorganic composite membranes. Therefore, the following section reviews the research published to date on this newly emerging field of membranology.

Hybrid organic-inorganic composite membranes

The bulk of the work on hybrid gas separation membranes focuses on the use of the organic phase as a template for creating the desired pore size within the membrane. The most common approach is to blend organoalkoxysilanes with tetraalkoxysilanes to produce organically doped glass networks.[116-119] The permeation properties of the membranes produced are strongly dependent upon the post gelation processing, and the work of Shelekhin et al. provides an excellent review relating the changes in transport

mechanisms and rates with morphological changes and pore development.[116] The majority of researchers have found average pore sizes on the order of 0.5 nm to 2 nm. Additionally, an absence of Knudsen diffusion was observed in all of these studies. Much more common were results on the permeation of a variety of inert gases, e.g., He, H_2, O_2, CH_4, CO_2 and SF_6 that demonstrated little dependence of He permeability with processing/firing temperatures. Conversely, considerable changes in the permeability of "larger" gases were observed with firing. This indicated that the size of the molecule was dictating the overall permeability.[116,117] As all of these gases lie in the 0.26 nm to 0.38 nm range, the conclusion of sub-nanometer pore diameters was substantiated.

Fortunately, several studies investigating the influence of the organic dopant levels upon the membranes without the use of pyrolysis do exist.[119,120] An investigation by Smaihi et al. utilizing DSC, NMR and SAXS techniques to compliment the permeability data obtained on phenyltrimethoxysilane versus diphenyldimethoxysilane doped tetramethoxysilane revealed that the mono-substituted organoalkoxysilane gels possessed greater connectivity and increased He/N_2 selectivity with increasing phenyl concentration.[119] Conversely, the network connectivity and selectivity remained unchanged with increasing (di)phenyl content. Furthermore, the selectivity for these diphenyl derived membranes was equal to theoretical Knudsen diffusion selectivity values of 2.6, while the selectivity of the phenyl derived membranes reached values as high as ca. 80 at an organoalkoxide to tetramethoxysilane molar ratio of 0.8. These results, although lacking in an estimation of pore size, strongly support the argument that highly

homogeneous, well developed polysilicate phases within hybrid composites/membranes do not exhibit Knudsen diffusion.

In a switch from the investigations of organoalkoxysilane doped glasses, Guizard and Lacan have researched membranes prepared from diethoxysilane and triethoxysilane end functionalized terephtaloyl-based molecules.[120] Analysis of the permeability selectivity values for O_2/N_2 obtained on membranes resulting from acid catalysis of 100% of the diethoxy based reactive molecules indicated that Knudsen diffusion is not occurring. However, selectivity values for the triethoxy based reactive molecules processed using an equivalent acid/alkoxy ratio suggested that Knudsen diffusion was occurring. Thus the membrane possessed considerable porosity in the range of 5 nm and larger. The selectivity results of these triethoxysilane end functionalized molecules represent the lone deviation from configurational diffusion within these sol-gel derived hybrid membranes.[120]

CHAPTER 3
RUBBER ELASTICITY EVALUATED USING DYNAMIC MECHANICAL SPECTROSCOPY AND EQUILIBRIUM SWELLING

Relevant Background

One issue consistently at the forefront of composite research is the effect of the interphase upon the mechanical and physical properties of the composite. Similar issues surround hybrids and to this end previous investigations have addressed modifications to both the organic and inorganic phases with the goal of understanding the structure/property relations of these near homogeneous composites.[121,122]

With regard to modifications of the inorganic polysilicate phase, previous results revealed that gels derived from an acid catalyzed mixture of 60% (mass/mass) PTMO and 40% TEOS, which were subsequently swollen in a basic 70% ethylamine in water solution for up to 24 hr, exhibit enhanced phase separation of the PTMO and polysilicate phases.[121,123] This enhancement was not accompanied by a loss of optical transparency. Additionally, changes in dynamic mechanical response were observed in that the thermally induced syneresis typically exhibited by these polysilicate crosslinked composites could be eliminated by aging the gels in the basic solution. These results, as well as infrared evidence to be presented shortly, suggest that during the first hour of exposure the ethylamine treatment is the chemical analog of a thermal cure in that exposure to the basic solution for one hour drives the condensation reaction to virtual completion. Beyond the first hour, however, increased phase separation is observed in the DMS data as evidenced

by the onset of PTMO crystallization. Such crystallization would occur only when the PTMO chains are set free of significant interactions with the vitreous polysilicate chains and thereby gain the mobility necessary to crystallize. It has been proposed that this phase separation, which does not occur on the macro-optical scale, occurs via a simultaneous dissolution and reprecipitation process. This process is analogous to the ripening observed in pure silicates exposed to basic conditions.[124] In an attempt to quantify the changes induced by this polysilicate ripening upon the network structure of the hybrid composite elementary rubber elasticity theory has been applied in conjunction with dynamic mechanical spectroscopy. It will be shown that this somewhat unorthodox approach not only provides valuable qualitative insights into the interactions present within these near molecularly mixed composites but also that there is excellent quantitative agreement with values calculated from equilibrium swelling.

Rubber elasticity theory should serve as a useful tool for quantifying the reduced elasticity of the PTMO chains in that interpenetration of polysilicate and PTMO chains should lead to entanglements or labile crosslinks that reduce the average molar mass between crosslinks, $\overline{M}_c$. Consequently, the more interactive or mixed that the phases are; the lower that the average chain length should be. The exceptional linearity of the DMS storage modulus versus temperature plots, to be shown shortly, suggest that the data could be used to calculate $\overline{M}_c$ based on the thermodynamic derivation of the elasticity relation[125]

$$G = \overline{N}_v kT = \frac{\rho RT}{\overline{M}_c} \qquad (3.1)$$

where G is the shear modulus, $\overline{N}_V$ is the average number of covalently bonded, elastically active network chains per unit volume, k is the Boltzmann constant, R is the gas constant, T is absolute temperature, ρ is the density, and $\overline{M}_C$ is the average molar mass between crosslink junctions. If the sample is assumed to have a Poisson ratio, υ, of 0.5 throughout the temperature range of interest, then the elastic modulus, E, which is related to the shear modulus by the equation

$$E = 2G(1+\upsilon), \tag{3.2}$$

is equal to 3G. Additionally, if the characteristic relaxation time of the gel is less than the time-scale of the dynamic modulus measurement, then the storage modulus, E', is effectively an equilibrium measurement equivalent to the equilibrium elastic modulus, E. Equation 3.1 can then be updated to the form

$$E' = 3\overline{N}_V kT = \frac{3\rho RT}{\overline{M}_C}. \tag{3.3}$$

Examination of this equation reveals that a linear regression through a plot of E' vs. 3kT yields a slope of $\overline{N}_V$ and a crosslink density of $\overline{N}_V/2$, assuming tetrafunctional crosslink junctions. Equating the second and third expressions of the equalities in Equation 3.3 produces the relation

$$\overline{M}_C = \frac{\rho L}{\overline{N}_V} \tag{3.4}$$

where L is the Avogadro constant, and again, ρ is the density of the gel.

A check on the values obtained using Equation 3.4 above can be made using the more traditional equilibrium swelling technique in conjunction with the Flory-Rehner Equation for a perfect network

$$-\ln\left[(1-\nu_{2m})+\nu_{2m}+\chi_{1,2}\nu_{2m}^2\right]=\frac{V_1\rho}{\overline{M}_c}\left(\nu_{2m}^{1/3}-\frac{\nu_{2m}}{2}\right), \tag{3.5}$$

where ν_{2m} is the volume fraction of polymer in the equilibrium swollen mass, V_1 is the molar volume of the solvent, and $\chi_{1,2}$ is the Flory-Huggins interaction parameter.[126,127] The volume fraction of polymer in the swollen mass can be calculated using the equation

$$\nu_{2m}=\frac{V_2}{V_1+V_2}=\frac{\dfrac{M_2}{\rho_2}}{\dfrac{M_2}{\rho_2}+\dfrac{M_1}{\rho_1}} \tag{3.6}$$

where V, M and ρ are the volume, mass and density, respectively, and the subscripts 1 and 2 correspond to the solvent and polymer, respectively. Note that the values estimated using this swelling technique have not been corrected for the volume fraction of polysilicate present, i.e., ν_{2m} is based on volume fraction of solids in the swollen mass determined during extraction of the gels in tetrahydrofuran, a good solvent.

The χ-parameter needed for determination of $\overline{M}_c$ using swelling can be estimated from the difference in solubility parameters of the gel and solvent using

$$\chi_{1,2}=\frac{V_1}{RT}(\delta_1-\delta_2)^2 \tag{3.7}$$

where, again, the subscripts 1 and 2 denote the solvent and hybrid gel, respectively.[128] The value of δ_2 for the benchmark 40% (mass/mass) TEOS-based gel containing 19 vol.% polysilicate has been previously measured by swelling pieces of the gel in solvents of different Hildebrand parameters with the solvent inducing the maximum swelling taken as the estimated value.[122,123] For this report, this same value was used for all the

ethylamine exposure times thereby assuming that swelling in the ethylamine solution produces no change in the Hildebrand parameter of the 19 vol.% polysilicate hybrid gel.

These relations, having been developed under the stated assumptions, permit both a mechanical, elasticity-based and equilibrium swelling-based estimation of $\overline{M}_c$ for the PTMO chains present within the polysilicate crosslinked gels. Therefore, it will be possible to compare the values obtained using the two approaches with insights gained into the effectiveness of DMS as a basis for such measurements. Secondly, it will be possible to use the measured values to quantify the extent of interaction, as evidenced by the change in average PTMO chain molar mass, between the organic and inorganic phases present in these hybrids.

Experimental

Details regarding the synthesis of the gels used in this investigation have been published previously along with complete mechanical and dynamic mechanical characterization results.[121,123] Consequently, the experimental techniques and testing parameters therein described pertain to this report also. Briefly, a dissolved mixture of 60%:40% (mass/mass) PTMO:TEOS, henceforth referred to as TEOS(40), were cast into polystyrene petri dishes from an acidified isopropyl alcohol-tetrahydrofuran (4:1) co-solvent system. The PTMO oligomers used in this study had been functionalized by reacting isocyanatopropyltriethoxysilane with 2,000 g/mole poly(tetramethylene ether) glycol in bulk at 70°C for 4 days to produce reactive oligomers capable of undergoing sol-gel processing in the presence of additional metal alkoxides, such as TEOS. This reaction and the resulting end functionalized oligomer are shown in Figure 3.1. After casting, the

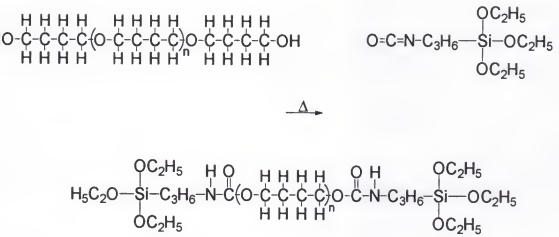

Figure 3.1 Reaction schematic illustrating the synthesis of end functionalized poly(tetramethylene oxide) via the reaction of a 2% molar excess of isocyanatopropyl-triethoxysilane and 2,000 g/mole poly(tetramethylene ether) glycol.

gels were covered and allowed to gel for 4 days. Subsequently, the gels were uncovered for 2 days to allow evaporation of any residual alcohol, water or tetrahydrofuran (THF). Next, the gels were immersed in THF and were allowed to swell at ambient for 24 hr. This swelling was followed in series by vacuum drying at 40°C and 10 Torr for 24 hr, swelling again in water at ambient for 24 hr and a final vacuum drying at 40°C and 10 Torr for 24 hr. After this processing the gels were considered benchmarks and were ready for modification using the 70% ethylamine in water solution.

The standardized PTMO-polysilicate gels were placed into Pyrex petri dishes pre-filled with the aqueous ethylamine solution (pH of 12.5) for 1, 4, 7, 13 and 25 hr. After swelling, the gels were removed and de-swollen in water with multiple rinses until the pH of the de-swelling water had returned to its proper value of 6.5 (ca. 8 hr). Vacuum drying under the conditions described in the previous paragraph completed the ethylamine processing.

For the sake of comparison, gels were made by crosslinking the PTMO chains without adding TEOS. These gels are referred to as TEOS(0) gels. The sol-gel processing of these reactive oligomers in the absence of TEOS produced an elastomeric gel containing ca. 4.5 vol.% polysilicate. This gel underwent the same swelling/extraction and vacuum drying process as the TEOS(40) gels.

Multiple characterization techniques were utilized for this study. Dynamic mechanical spectroscopy (DMS) was performed using a Seiko DMS 200(FT) interfaced with a Seiko Rheostation Model SDM/5600H. Testing for all composites was carried out from -150°C to 200°C at a heating rate of 0.75°C/min in a dry nitrogen atmosphere

maintained at an approximate flow rate of 200 ml/min. The test frequencies ranged from 0.1 to 10 Hz with a strain amplitude of 0.1%.

Thermogravimetric analysis was performed using a Seiko TG/DTA 320 interfaced with the same Seiko Rheostation Model SDM/5600H as the DMS 200(FT). A heating rate of 10°C/min in a dry air atmosphere maintained at a flow rate of approximately 100 ml/min was used. The temperature range investigated was 25°C to 1,000°C.

Swelling measurements were obtained by immersing three 9.5 mm diameter disks, which had been punched from the cast films using a No. 6 cork-borer, into small petri dishes filled with THF. The averages and standard deviations given throughout this work are based upon the swelling values for these three samples.

Density measurements were obtained using a Mettler density determination kit employing distilled water at ambient conditions. Five samples were used for each ethylamine exposure time with the averages and standard deviations displayed in all figures.

Fourier transform infrared spectroscopy (FTIR) was performed using a Nicolet 20SXB FT-IR spectrometer. A Perkin-Elmer attenuated total reflection (ATR) stage was set to 45° using a KRS-5 trapezoidal crystal obtained from Spectra-Tech, Inc. In all cases, 32 scans were sufficient to collect reproducible spectra with an instrumental resolution of 4 cm^{-1}. All spectral subtractions were performed automatically using the OMNIC FT-IR software package supplied by Nicolet.

Results and Discussion

Physical Characteristics

The density and percent residue on ignition of the benchmark TEOS(0) and TEOS (40) gels as well as the TEOS(40) gels exposed to the ethylamine and water solution for up to 25 hr are given in Table 3.1. Examination of this data reveals that, as expected, the density of the gels and the percent residue on ignition increase as the mass loading of TEOS increases from 0% to 40% of the initial sol. Similarly, there is another slight increase in the residue mass for the 40% samples exposed to the ethylamine for 1 hr. The density, however, decreases somewhat after the first hour of exposure. Changes such as these are possible if the number of organic defects, such as the hydroxyl groups known to be present in the polysilicate domains, are converted to oxygen bridges during the initial swelling stages thereby producing a more highly connected polysilicate phase containing fewer volatiles.[129] A strong base such as the ethylamine solution employed in this study would be an effective catalyst for such rapid refinements in the polysilicate phase and FTIR results presented next confirm these changes. However, for the gel density to decrease upon exposure to the ethylamine solution a volume expansion within the PTMO

Table 3.1 Room temperature densities of the TEOS(40) gels investigated.

Gel Type	Density @ 25°C (g/cm^3)	% Residue on Ignition to 1,000 °C (10°C/min, air flow at 100 ml/min)
TEOS(0) Benchmark	1.028 ± 0.00312	2.5
TEOS(40) Benchmark	1.154 ± 0.00230	20.5, 20.7
TEOS(40) 1 Hr Exp.	1.146 ± 0.00173	21.2, 21.1
TEOS(40) 4 Hr. Exp.	1.145 ± 0.00300	21.0, 21.0
TEOS(40) 13 Hr. Exp.	1.147 ± 0.00207	20.9, 20.8
TEOS(40) 25 Hr Exp.	1.143 ± 0.00245	20.8, 21.0

phase must occur that offsets the increased polysilicate phase density. Results presented in the following sections will help explain this trend. Of critical importance, however, is that beyond the first hour of exposure of the gels to the basic solution there appears to be no significant change in either gel density or mass residue on ignition. Similarly, this exposure does not result in any detectable loss of polysilicate in the bulk gels.

ATR-FTIR Spectroscopy

In addition to verifying the hypothesis of silica refinement via enhanced condensation of unreacted hydroxyl groups during the first hour of exposure, an analysis of the polysilicate structures present is necessary to confirm that beyond this first hour of exposure no chemical changes leading to increased crosslink density are occurring. Such changes would artificially increase the slope of the modulus versus temperature plots within the rubbery regimes of these gels. FTIR provides the insight needed to examine these chemical changes. However, the thickness of the hybrids, ca. 0.3 mm negates the use of transmission FTIR. Therefore, the ATR technique was utilized on all gels.

The contributions of the polysilicate phase in all of these hybrids can be observed in two regions. Figure 3.2 displays the lower wavenumber region, or fingerprint region, dominated by the stretching of the ether linkages in the PTMO at 1100 cm^{-1}, the asymmetric stretching of the Si-O-Si groups at 1050 cm^{-1} and the Si-OH stretch at 955 cm^{-1}.[130-132] Additionally, subtle silicate-based absorbances are observable in the symmetric stretching/bending of Si-O-Si at ca. 800 cm^{-1} and what has been attributed to skeletal motion of 4-fold siloxane ring structures at ca. 570 cm^{-1}.[130,131,133] The second, or high wavenumber region where silicate absorbance occurs is shown in Figure 3.3 where absorbed water and free Si-OH stretching is observable at ca. 3300 cm^{-1}.

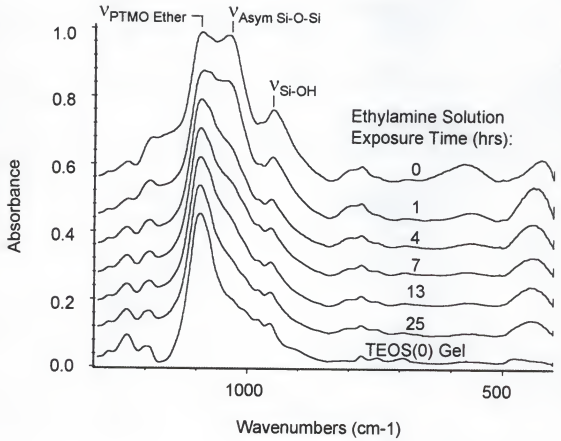

Figure 3.2 Low wavenumber region of the ATR-FTIR spectra of a benchmark TEOS(0) gel, benchmark TEOS(40) gel and TEOS(40) gels exposed to the ethylamine water solution for the indicated times.

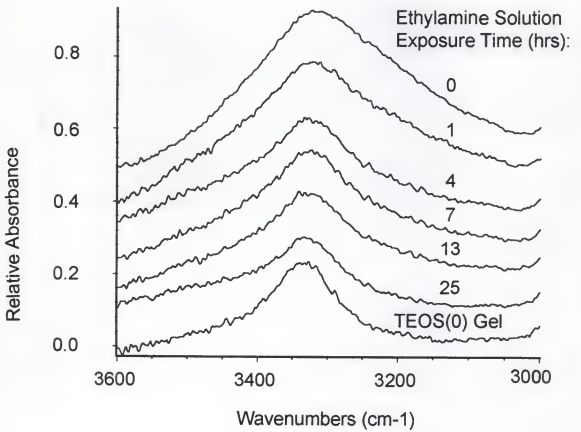

Figure 3.3 High wavenumber region of the ATR-FTIR spectra of a benchmark TEOS(0) gel, benchmark TEOS(40) gel and TEOS(40) gels exposed to the ethylamine water solution for the indicated times.

Considering the spectra shown in Figure 3.2, the most pronounced change induced by continued exposure to the ethylamine solution is that of the decreasing intensity of the asymmetric Si-O-Si stretching and Si-OH stretching. By taking the ratio of the $\nu_{Asymm\ (Si\text{-}O\text{-}Si)}$ to the $\nu_{C\text{-}O\text{-}C}$ peak, shown as the lower plot in Figure 3.4, it is clear that there is a continued decrease in the strength of the Si-O-Si band with increasing exposure. The depth of penetration of an IR beam is a function of wavelength, angle of incidence and the index of refraction of the material and crystal.[134] Based on these variables, the outermost 2 μm of the sample surface, or ca. 0.7% of total thickness, is being probed at 1050 cm^{-1}. This indicates that there is a reduction in the amount of polysilicate being detected near the surface of the gels after a day of exposure. The TGA data presented in Table 3.1, however, confirms that this reduction is negligible and that the overall amount of silica is virtually unchanged.

The issue that remains is what changes are the ethylamine solution inducing in the polysilicate phase that remains behind? This question can be answered by subtracting out the contribution of the crosslinked PTMO, i.e., the benchmark TEOS(0) gel, and examining the spectral response of the polysilicate phase alone. Figure 3.5 displays the resulting spectra, which are dominated by the previously discussed asymmetric stretching of silica and silanol groups. However, there is another peak present at ca. 1165 cm^{-1} in all 5 of the spectra that is not immediately discernible in Figure 3.2 but is commonly observed in the spectra of gel derived silica. There is, however, some ambiguity surrounding its origin in that this peak/shoulder has been attributed to both the 3-fold degenerate stretching frequencies of SiO_4 tetrahedron and the longitudinal optic mode of the asymmetric Si-O-Si stretch.[131,132] Regardless, it is a common characteristic of silica.

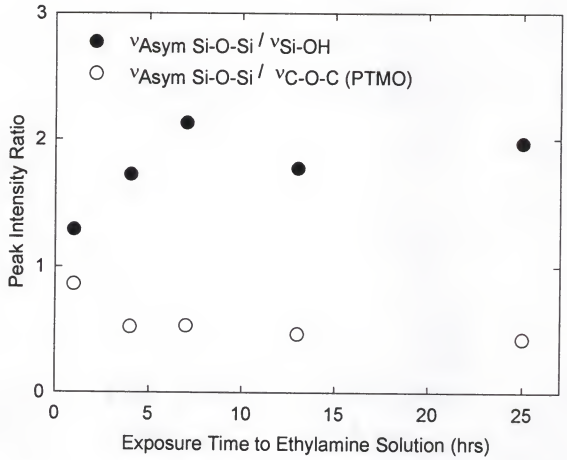

Figure 3.4 The ratio of peak intensities for the asymmetric Si-O-Si and Si-OH stretches (1050/955 cm^{-1}) as well as the ether linkage of the PTMO and Si-OH stretch (1100/955 cm^{-1}).

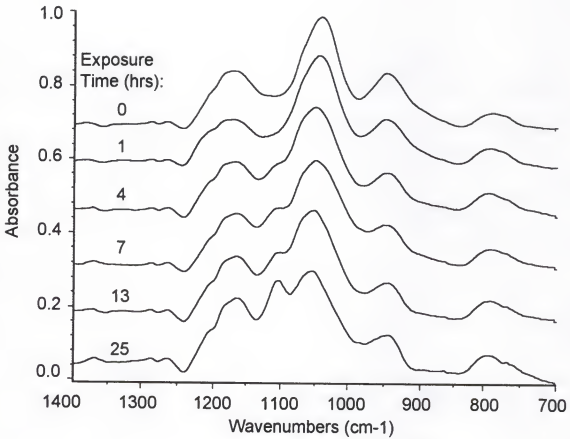

Figure 3.5 Low wavenumber region of the ATR-FTIR spectra of the TEOS(40) gels exposed to the ethylamine water solution for the indicated times after subtracting out the benchmark TEOS(0) spectra. The spectra, therefore, are those of the polysilicate phases in the TEOS(40) hybrids.

The fact that all three significant peaks associated with silica are observable at the proper locations lends credence to the subtraction and ATR technique employed in this study. Unfortunately, one artifact of the subtraction does become visible as the exposure time increases. This artifact is the ether linkage of the PTMO at 1100 cm^{-1}, which becomes more visible as the polysilicate at the surface of the samples begins to dissolve.

Returning to an analysis of the nature of the polysilicate phase, a technique has been developed by Mauritz et al. on similar hybrid systems utilizing the ratio of $\nu_{Asymm\ Si\text{-}O\text{-}Si}$ / $\nu_{Si\text{-}OH}$ (1050 cm^{-1} / 955 cm^{-1}) as a semi-quantitative/qualitative assessment of the degree of silica development present in hybrids.[50,54] This technique can be employed on the gels in this study to examine the changes induced by the ethylamine processing. The ratio of these peaks as a function of the ethylamine exposure time are displayed as the upper plot in Figure 3.4 and reveal that at least 4 hr is needed before there is an indiscernible change in the number of silanol species relative to oxygen-bridged Si atoms. Alternately stated, the first hour of exposure does not provide sufficient time for an equilibrium silicate structure to develop within the hybrid. Beyond this first hour, during which much of the absorption leading to equilibrium solvent uptake occurs, it appears that the silicate phase experiences no further change in its degree of condensation. A similar trend is observed in Figure 3.3 in that after the first hour of exposure, the number of the silanol species present, as evidenced by the area under the absorbance at ca. 3,300 cm^{-1}, seems to remain unchanged and approximates the number present in the benchmark TEOS(0) gel.

To summarize the results of the ATR-FTIR analysis, it appears that increased connectivity of the polysilicate phase is occurring at the surface of the gels. Based on the previously discussed changes in density, percent residue on ignition and DMS results

presented in the next section, these changes are most certainly occurring throughout the bulk of the gel as well. Additionally, some dissolution is taking place at the surface of the sample. However, this amount of loss is negligible and undoubtedly has little influence on the bulk properties of the gels.

DMS and Estimation of Average Molar Mass Between Crosslinks

The dynamic mechanical storage modulus, E', of the benchmark TEOS(0) and TEOS(40) gels, as well as the TEOS(40) gels which have been exposed to the ethylamine in water solution for up to 25 hr, appear in Figure 3.6. The features of interest include the glass to rubber transition, Tg, at ca. -80°C for all of the gels and the presence of crystallization and onset of crystallization in the TEOS(0) and TEOS(40) gel exposed to ethylamine for 25 hr, respectively. This onset of crystallization is evidence of increased phase separation induced by the ripening process. At temperatures greater than the Tg and crystalline melting point, the rubbery regimes of the TEOS(0) gel and ethylamine exposed TEOS(40) gels exhibit significant linearity with increasing temperature and prompt the analysis developed in the Introduction. Additionally, there is a region between ca. 30°C and 130°C where the benchmark TEOS(40) gel exhibits appreciable linearity. The first equality in Equation 3.3 necessitates a plot of E' vs. 3kT in the rubbery regime to determine the average number of elastically active network chains per unit volume. This data is displayed in Figure 3.7, where differences in slopes are observable. Although only the 0.1 Hz data is shown, Table 3.2 displays the slopes, $\overline{N}_v$, for all frequencies investigated. The exceptional linearity is confirmed by the regression coefficient, r^2, for each gel, which ranges from 0.995 to 0.998. If tetrafunctional crosslink junctions are

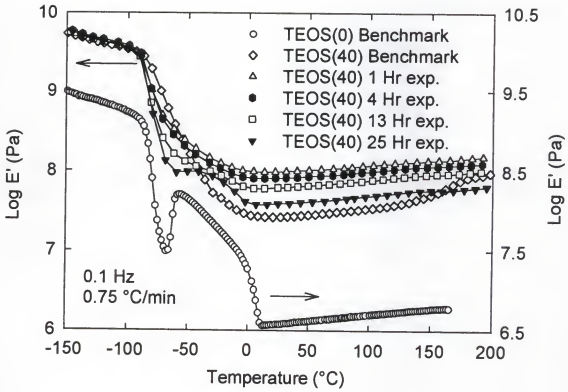

Figure 3.6 Dynamic mechanical storage modulus, E', as a function of temperature for the indicated gels. Note the different storage modulus range for the TEOS(0) gel, which was done to clearly show the crystallization observed.

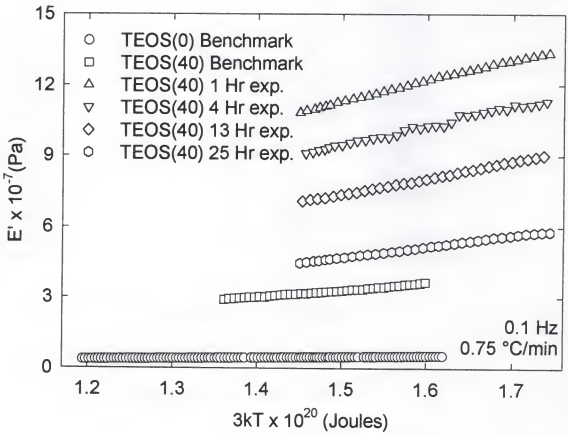

Figure 3.7 The rubbery regime of the gels investigated expressed in terms of thermal energy. The slope of each line is the number of elastically active network chains per unit volume, $\overline{N_v}$.

Table 3.2 Number of elastically active network chains per unit volume at each frequency measured using the dynamic mechanical spectrometer. $\overline{N}_V \times 10^{-27}$ (chains/m^3).

	Test Frequency (Hz)					
Gel Type	0.1	0.5	1	2	5	10
TEOS(0) Benchmark	0.401	--	0.394	--	--	0.388
TEOS(40) Benchmark	2.99	2.90	2.86	2.85	2.74	2.65
TEOS(40) 1 Hr Exp.	8.84	8.79	8.77	8.75	8.67	8.53
TEOS(40) 4 Hr. Exp.	8.05	8.03	8.00	7.91	7.86	7.80
TEOS(40) 13 Hr. Exp.	6.98	7.02	6.99	7.01	6.99	6.86
TEOS(40) 25 Hr Exp.	4.75	4.77	4.74	4.73	4.68	4.60

assumed, then the crosslink density is equal to $\overline{N}_V/2$. A review of the frequency dependence of $\overline{N}_V$ in Table 3.2 reveals that as the test frequency increases there are fewer chains contributing to the elastic force. This trend will be discussed in more detail shortly.

The average molar mass between crosslinks can be calculated using the second equality in Equation 3.2 and the density values given in Table 3.1. Figure 3.8 displays the estimated $\overline{M}_C$ values as a function of frequency. Recalling that the molar mass of the PTMO prior to triethoxysilane functionalization is ca. 2000 g/mole, values in the range of 1550-1600 g/mole for the TEOS(0) gels are promising. This is especially true given that estimations of polysilicate volume based on molar mass changes upon condensation and additive volumes indicate that ca. 4.5 vol.% polysilicate exists within the TEOS(0) gel. These calculations assume a 75% conversion of ethoxysilane species to oxygen-bridging SiO_4 tetrahedron. As expected, as the volume of polysilicate increases to 19% for the TEOS(40) gels the average molar mass between crosslinks decreases to a range of 230-260 g/mole. Both the TEOS(0) and TEOS(40) benchmark gels, each with the potential for thermally induced ripening, exhibit an increase in $\overline{M}_C$ with increasing frequency.

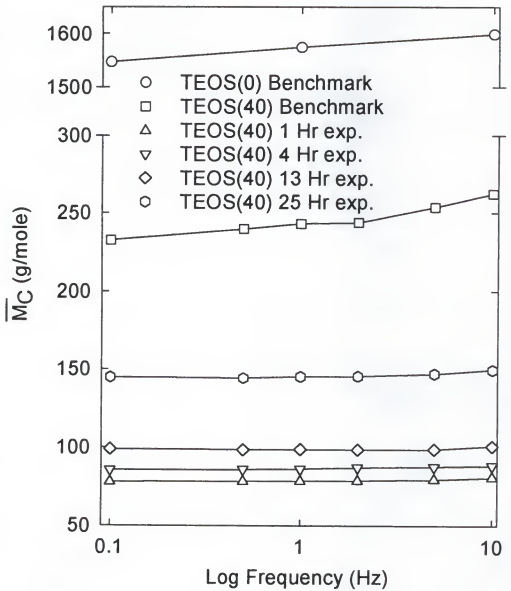

Figure 3.8 Frequency dependence of the average molar mass between crosslinks, $\overline{M}_c$, for the indicated gels.

However, less significant increases are observable for the TEOS(40) ethylamine exposed gels, which were just shown to possess chemically stable polysilicate phases. Additionally, the values for $\overline{M}_c$ are significantly reduced for the ethylamine exposed gels, and a minimum value of approximately 75 g/mole is exhibited by the gel exposed for 1 hr. As the exposure time increases to a maximum of 25 hr the value of $\overline{M}_c$ increases and reaches a maximum of ca. 145 g/mole.

A reduction in the average molar mass between crosslinks is to be anticipated based upon the incorporation of the anelastic (from the standpoint of entropy driven polymer elasticity) polysilicate phase. For the sake of comparison, if only the volume fraction of PTMO is assumed elastic, then a rule of mixtures predicts that $\overline{M}_c$ values of 1920 g/mole and 1620 g/mole should be observed for the TEOS(0) and TEOS(40) gels, respectively, regardless of ethylamine exposure since the total mass percent of polysilicate remains unchanged for all exposure times investigated (Table 3.1). As these values are much greater than those predicted from Equation 3.3 and displayed in Figure 3.8, the employment of rubber elasticity theory reveals that the near molecular level of mixing occurring in these acid catalyzed gels gives rise to strong restriction of the PTMO chains by the polysilicate chains. Furthermore, the ripening induced by the ethylamine treatment does indeed result in phase sharpening, as evidenced by the increasing average chain length between crosslinks with increasing exposure time. This interaction-based analysis completely explains the mechanical, dynamic mechanical, density and swelling response previously observed for these gels.[121] Another question remains, however, regarding the accuracy of the measured values, especially considering the use of dynamic moduli data

and the possible chemical curing contributions known to be operative in the as cast (0 hr) and 1 hr exposed samples. To test the validity of the values calculated from Equation 3.3, equilibrium swelling measurements were made with the goal of using Equation 3.5 to predict $\overline{M}_c$ values for the same gels.

Equilibrium Swelling and Estimation of Average Molar Mass Between Crosslinks

Equation 3.5 necessitates knowledge of the volume fraction of polymer in the swollen state, v_{2m}, and the Flory-Huggins interaction parameter, $\chi_{1,2}$, for the given polymer-solvent-temperature combination used. With regard to the former values, equilibrium mass uptake of THF for the TEOS(40) and ethylamine exposed TEOS(40) gels was measured at room temperature and the volume fraction of polymer calculated using Equation 3.6. The results are displayed in Figure 3.9 as a function of ethylamine solution exposure. Consistent with results predicted from the above analysis, as the benchmark TEOS(40) gel possess the greatest average molar mass between crosslinks, it swells the most and consequently has the lowest v_{2m} value. The gel exposed for 1 hr had the lowest value of $\overline{M}_c$ and, therefore, swells the least and has the largest v_{2m} value. Continued exposure to the ethylamine induces phase separation and frees the previously restrained PTMO chains thereby increasing $\overline{M}_c$, allowing more swelling and decreasing v_{2m} values.

Determination of the Flory-Huggins interaction parameter for such a complex composite system necessitates an experimental estimate. Previous measurements of the solubility parameter for the TEOS(40) based systems have been made by swelling the gel in solvents of differing Hildebrand parameters and using the maximum in the gel swelling

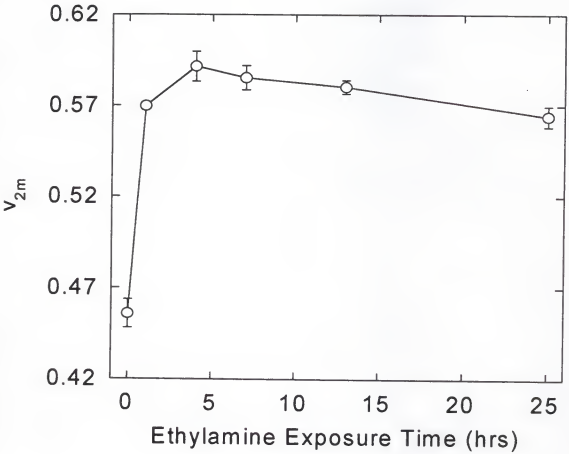

Figure 3.9 Values of the equilibrium volume fraction of polymer present in the swollen network, v_{2m}, for TEOS(40) gels as a function of ethylamine solution exposure time.

coefficient, 19.1 $MPa^{1/2}$, as an estimate of the Hildebrand parameter of the gels.[122] Employing Equation 3.7 and knowing that THF has a Hildebrand parameter of 18.6 $MPa^{1/2}$ and molar volume of 8.11×10^{-5} m^3/mole, $\chi_{1,2}$ is calculated to be 0.0082. The exceptionally low value is not unreasonable considering the affinity the polymer should have for THF since PTMO is made from the ring opening polymerization of this solvent.

A concern arises regarding the incorporation of the lattice constant of entropic origin that some authors have put forth requiring that an additional value of ca. 0.34 be added to the $\chi_{1,2}$ value calculated using Equation 3.7.[128] For the sake of comparison, calculations of $\overline{M}_C$ using swelling were performed using both a $\chi_{1,2}$ of 0.0082 and 0.3482. These results are displayed in Figure 3.10 along with the values of $\overline{M}_C$ calculated using the 0.1 Hz and 10 Hz DMS data from Figure 3.8. The overall good agreement between the two techniques is very encouraging considering the ease with which the dynamic technique can be accomplished relative to the various swelling experiments. The choice of Hildebrand parameter is of obvious importance and a value neglecting the entropic-derived 0.34 contribution appears to fit best over most of the range, the exception being the 25 hr exposure time to ethylamine solution.

Conclusions

Dynamic mechanical spectroscopy was performed on polysilicate crosslinked PTMO based gels containing an estimated 4.5 and 19 vol.% polysilicate. Additionally, DMS was performed on samples of the 19% polysilicate gel, which had been exposed to a basic ethylamine and water solution for times ranging from 0 to 25 hr. The data revealed exceptional linearity in the storage modulus versus temperature plots warranting

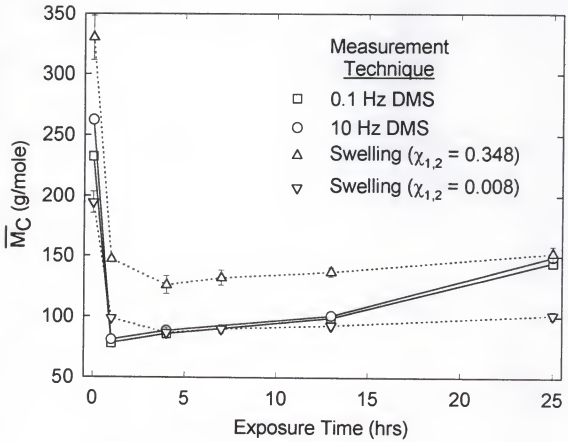

Figure 3.10 Comparison of the values for $\overline{M}_C$ calculated using Equations 3.5, 3.6 and 3.7 based on equilibrium swelling using two values of $\chi_{1,2}$, as well as values for $\overline{M}_C$ obtained using Equations 3.4 and 3.5 for the 0.1 Hz and 10 Hz data from the DMS.

the use of elementary rubber elasticity theory as a tool for measuring the average molar mass between crosslinks. FTIR analysis revealed that although some chemical change occurred during the first hour of exposure, discrediting the predicted values of $\overline{M}_c$, continued exposure resulted in equilibrium polysilicate structures. The significantly reduced values of $\overline{M}_c$ obtained using the DMS based technique relative to those predicted by a rule of mixture for both the benchmark and ethylamine exposed TEOS(40) gels confirm extensive interaction between the vitreous polysilicate phase and elastomeric PTMO phase. Furthermore, the increase in $\overline{M}_c$ with increasing exposure times to ethylamine is in good agreement with the onset of phase separation observable in the DMS data. Most interestingly, both the trend observed for the ethylamine exposed gels and the magnitude of the $\overline{M}_c$ values calculated were confirmed using equilibrium swelling calculations in conjunction with the Flory-Rehner Equation. This excellent agreement suggests that elementary rubber elasticity theory is a good tool for investigating the extent of phase interaction occurring in these hybrid composites and that dynamic mechanical spectroscopy provides a valid basis for collection of the data necessary for estimation of network parameters.

CHAPTER 4
STRUCTURE/PROPERTY BEHAVIOR OF ORGANIC-INORGANIC SEMI-IPNS: EFFECT OF POLYSILICATE LOADING AND CO-SOLVENT SYSTEM

Relevant Background

Previous investigations in our laboratories have focused on the development of semi-interpenetrating polymer networks (SIPNs) generated by the γ polymerization of methacrylic acid, n-vinylpyrrolidone and cyclohexylmethacrylate swollen hybrid composites.[122,123] The most striking results showed that γ polymerization of methacrylic acid (MAA) within a poly(tetramethylene oxide) (PTMO)/polysilicate hybrid gel, henceforth referred to as a PMAA-PTMO SIPN, produced an SIPN that exhibited exceptionally high stress and elongation at break. A significant 3,000% increase in the tensile elastic modulus was observed over that of the benchmark hybrid. Accompanying the increased modulus was the observance of yielding, a mechanism that had not been observed in the elastomeric benchmark hybrid prior to SIPN formation. These significant changes in the mechanical response of the organic-inorganic hybrids were attributed to the formation of a PMAA-PTMO copolymer upon exposure of the MAA swollen gel to high energy γ radiation and/or hydrogen bonding between the less than fully developed, acid catalyzed polysilicate network present in the hybrid and the polar acid groups of the PMAA. It is likely that both mechanisms are at work given the high energy polymerization route employed. However, by suitable choice of the solvent system it is possible to gain some insights into the mechanical response of the PMAA-PTMO SIPNs

as dictated by the hydrogen bonding ability and spatial distribution of the polysilicate phase present in the benchmark gels during γ polymerization of MAA. It has been shown that the use of dimethylformamide (DMF), a drying control chemical additive (DCCA), in place of tetrahydrofuran (THF) as the organic solvent constituent in the organic solvent/isopropyl alcohol (IPA) co-solvent solution used to process the hybrids results in enhanced phase separation between the PTMO and polysilicate phases of the resulting gel.[30] Several relevant investigations of the role of DCCAs in the sol-gel-processing of pure silicon alkoxide systems have been published and provide insight into the origin of this solvent enhanced micro-phase separation in hybrid PTMO/polysilicate composites.

Detailed studies by Orcel et al. utilizing formamide, perhaps the most potent DCCA, in acid catalyzed sol systems have shown that hydrogen bonding occurs between the formamide molecule and silanol species of hydrolyzed tetramethoxysilane.[135,136] This hydrogen bonding was shown to decrease the rate of hydrolysis and slightly increase the rate of polycondensation. This change in the rate constants led to larger sol particles and the subsequent formation of a gel exhibiting decreased interparticle connectivity, surface area and silanol concentration but increased mean pore size. A structural investigation was conducted in neutral conditions comparing the morphologies of several gels resulting from the gelation of sols based on a variety of DCCAs, including formamide and DMF.[137] It was concluded that the dimethyl substitution reduced the effectiveness of the formamide DCCA, i.e., DMF was less effective at producing large structural units possessing greater pore diameters. Fortunately, a complimentary mechanism-based investigation exists detailing the influence of formamide and DMF in neutral sol

systems.[138] It also compares these DCCA dependent gels to an aqueous ammonia catalyzed system. This study revealed several differences in the gel structures produced by these two DCCAs and also some similarity between the DMF and base catalyzed gels. The rate of hydrolysis was concluded to decrease in those systems containing either formamide or DMF, in agreement with Orcel et al. However, it was suggested that the rate of polycondensation also decreased for the DMF containing sols. This is in contrast to the increased rate of polycondensation previously observed for the formamide containing sols. Small angle X-ray scattering, gas chromatography and nitrogen adsorption experiments revealed that DMF containing sols did produce large gel clusters. Of additional importance, however, is that a significantly greater number of oxygen bridges were formed in DMF-based gels relative to either formamide or ammonia catalyzed gels. Inherent in the increased network connectivity is a reduced silanol concentration. With regard to particulate size, the radius of gyration values calculated from the Guineir region of the SAXS profiles indicated that the DMF gels were composed of colloidal-like particles similar in size to that characteristic of ammonia gels.[138] By comparison, the addition of formamide produced colloidal particles larger than the DMF or ammonia gels, while uncatalyzed sols resulted in the smallest radius of gyration of all four systems investigated.

As the findings of the above studies yield similar results for the effect of formamide in either acidic or neutral sol systems, it seems analogous that DMF would behave the same in either acidic or neutral solutions as well. Therefore, it is possible to summarize that the addition of DMF to an acidic or neutral sol system results in the formation of a polymeric silicate, or polysilicate, network exhibiting a high degree of network

connectivity that mimics that of a true base catalyzed system. These findings are interesting in that the similarities in gel structure hold even though the mechanism of formation is completely different: electrophilic attack by protons in acidic sols versus nucleophilic substitution in basic sols.[124,139]

It is anticipated that hybrid organic-inorganic composites produced using DMF would possess a polysilicate morphology/spatial distribution similar to that observed in pure polysilicate systems, i.e., a polymer-like, colloidal phase exhibiting little interaction with the surrounding polymer matrix. In contrast, a hybrid produced using a THF-based sol would possess a comparatively less interconnected and consequently more highly interactive polysilicate phase. In addition to the difference in morphology, it is anticipated that the increased degree of connectivity of the DMF-based hybrid relative to that of the THF-based hybrid would lead to a decreased silanol concentration. Therefore, by synthesizing PMAA-PTMO SIPNs from hybrids resulting from gelation of these two different sols a method exists to examine the combined influence of spatial distribution and silanol concentration on the exceptional mechanical response of the PMAA-PTMO SIPNs. Indeed, this approach has been undertaken in this study.

In addition to the combined effects of hydrogen bonding and spatial distribution, the polysilicate loading was also considered an experimental variable and adjusted to provide four loadings in the benchmark PTMO-polysilicate gels used for PMAA-based SIPN synthesis: 4.5, 11, 19 and 33% by volume. Clearly stated, the objective of this study was to determine the origin of the greatly improved mechanical response of these polysilicate containing PMAA-PTMO SIPNs. To accomplish this objective three main characterization techniques were employed: DMS, static tensile testing and Fourier

·transform infrared spectroscopy (FTIR). Additionally, atomic force microscopy (AFM) and SAXS were utilized to probe the morphology of some of these mixed-phase hybrids and hybrid SIPNs.

Experimental

Triethoxysilane functionalized PTMO was prepared by the reaction of 2,000 g/mole hydroxyl-terminated poly(tetramethylene ether) glycol (Polysciences, Inc.) and isocyanatopropyl-triethoxysilane (IPTS) (United Chemical Technologies, Inc.) Prior to the end functionalization reaction the PTMO was vacuum dried overnight at 40°C/10 Torr. Additionally, the IPTS was vacuum distilled and the middle 80% used for this reaction. The purity of the "middle 80" was verified at 99+% using gas chromatography. The end functionalization reaction involving a 1:2.09 molar ratio of PTMO:IPTS was carried out in a glycerin bath maintained at 70±5°C. Constant mechanical stirring of the PTMO/IPTS solution under nitrogen was continued until FTIR indicated no further changes in the ratio of intensities of the diminishing isocyanate peak at 2250 cm^{-1} and the developing carbonyl peak at 1715 cm^{-1}, ca. 4 days.

The hybrid composites were synthesized by dissolving masses of 10, 8, 6 and 4 g of the end functionalized PTMO each into a mixture of either 8 ml of IPA and 2 ml of THF, "THF-based system," or 5 ml of IPA and 5 ml of DMF, "DMF-based system." All solvents were used as received (Fisher Scientific-HPLC grade). Continuous stirring for 15 minutes in covered 25 ml polypropylene Erlenmeyer flasks resulted in clear solutions to which 0, 2, 4 and 6 g of tetraethoxysilane (TEOS) were added, respectively. After 5 minutes had elapsed, the stoichiometric amount of water required for the hydrolysis of

every ethoxy group was added along with 0.0165 equivalents of 10N HCl. Each of the 2 co-solvent classes comprises 4 sols containing 0, 20, 40 and 60 wt.% TEOS, henceforth abbreviated TEOS(0), TEOS(20), etc., relative to end functionalized PTMO. The contents of each beaker were then cast into four polystyrene petri dishes, which were then covered for 4 days allowing the sols to gel to transparent films. The covers were removed for 2 days to evaporate any residual alcohol, water and THF/DMF, and then covered again and stored under vacuum for later use. These thin films were used as the benchmarks against which the effects of radiation and SIPN formation are compared.

The synthesis of PMAA-PTMO SIPNs was accomplished by cutting portions of the benchmark gels into rectangular pieces approximately 1.1 cm wide and 5 to 7 cm long. Typical sample thickness for the inorganic loadings evaluated were between 0.1 mm for the TEOS(60) gels and 0.5 mm for the TEOS(0) gels with the difference in thickness attributable to increasing polymerization shrinkage with increasing TEOS loading. The strips were cut into characteristic shapes and the initial weights recorded so that mass increases of each could be monitored throughout the processing. The rectangular samples from each TEOS loading were placed in Pyrex petri dishes each containing 45 ml of distilled MAA. After 2 hours the monomer swollen strips were removed, blotted dry and the mass uptake of monomer recorded. Each was immediately placed into a pre-filled test tube containing 10% (mass/mass) MAA in deionized water. Water was chosen because of its poor ability to swell the benchmark gels.[121] However, MAA is soluble in water. Therefore, a 10% (mass/mass) monomer in water solution was used to reduce the concentration gradient and hence the driving-force for monomer desorption.

The sample containing test tubes were then purged by bubbling ultrahigh purity nitrogen through each tube for ca. 15 seconds. Additionally, test tubes containing samples of the benchmark gels suspended in deionized water only were also purged with nitrogen for 15 seconds. The tubes were then sealed with polyethylene caps and were positioned radially 4 inches from a ^{60}Co γ radiation source for 3 hours and 18 minutes. The dose rate was ca. 350 rads/min for a total dose of 0.069 Mrads. This total dose is in keeping with earlier experiments.[123] Upon removal from the source, the MAA solutions in the test tubes had gelled to a transparent water swollen network, which adhered to the surfaces of the samples when removed from the tubes. To facilitate removal of the clinging polymer all of the samples were swollen in water for 24 hr with multiple washings. Vacuum drying at 40°C for 24 hr/10 Torr followed by another 24 hr of swelling in THF and an additional vacuum drying completed the processing of the polysilicate containing PMAA-PTMO SIPNs. These SIPNs were stored in a desiccator under vacuum until tested.

The mechanical tensile properties of the benchmark gels, γ–irradiated gels and PMAA-PTMO SIPNs were all evaluated using an Instron Model 1122 equipped with a 200 lb load cell at ambient conditions (23±1°C, ~50% RH). The strain rate was 2.5 mm/min. Dumbbell-shaped samples were cut using the Type III ASTM die described in ASTM test D638M-84. The grip-to-grip distance was 25 mm, which combined with the 2.5 mm/min crosshead velocity produced a strain rate of 10%/min. Between 4 and 6 samples were tested for the benchmark gels, γ–irradiated benchmark gels and the majority of the PMAA-PTMO SIPNs at the 0, 20, 40 and 60% (mass/mass) TEOS loadings. However, only 2 samples were available for testing the TEOS(0) THF-based benchmark gel and TEOS(0) PMAA-PTMO THF-based SIPNs due to material limitations. Densities

were obtained using a Mettler density determination kit relying upon Archimedes' principle and water with between 8 and 10 samples per datum. The error bars shown on all figures represent one standard deviation from the mean.

Dynamic mechanical spectroscopy was performed using a Seiko DMS 200(FT) interfaced with a Seiko Rheostation Model SDM5600H. Testing for all of the SIPNs was carried out from -145°C to 300°C at a heating rate of 0.75°C/min in a dry nitrogen atmosphere maintained at a minimum flow rate of 200 ml/min. All spectra presented are those obtained at 1 Hz.

Fourier transform infrared spectroscopy was performed using a Nicolet 20SXB FT-IR spectrometer. For the poly(tetramethylene ether) glycol and end functionalized PTMO transmission spectroscopy was performed using NaCl crystals with 32 scans collected. However, for the thicker, cast gels it was necessary to utilize a Perkin-Elmer attenuated total reflection (ATR) stage set at 45° and a KRS-5 trapezoidal crystal obtained from Spectra-Tech, Inc. In the case of the ATR, 128 scans were sufficient to collect reproducible spectra. For both techniques, the instrumental resolution was 4 cm^{-1}. All spectral subtractions were performed automatically using the OMNIC FTIR software package supplied by Nicolet.

Atomic force microscopy was performed in tapping mode using a Nanoscope III instrument manufactured by Digital Instruments on the fracture surfaces of samples loaded while immersed in liquid nitrogen. Small angle X-ray scattering data was acquired using a Siemens Kratky camera employing a M. Braun position-sensitive detector from Innovative Technologies.

Results and Discussion

Physical Characteristics

To facilitate understanding of the effect of polysilicate loading upon SIPN formation the experimental results obtained will be presented as a function of the estimated volume of polysilicate present within the gels. Table 4.1 lists the densities of both classes of the benchmark hybrids and the γ-irradiated gels as a function of TEOS loading. The estimated polysilicate volume percentage is based upon the benchmark gel density measurements and calculations similar to those of Huang et al. accomplished by scaling the density with the molar mass change as the sol converts to a gel.[19] A maximum 75% conversion of the TEOS to an oxygen-bridging network of SiO_2 is assumed.[129] It is evident from the density measurements that neither the co-solvent system employed nor exposure to the γ radiation results in a significant change in the gel density at the loadings investigated.

Table 4.1 Densities of the benchmark and γ-irradiated gels, as well as the estimated volume of polysilicate based upon the benchmark PTMO-polysilicate gel densities and calculations similar to those of Huang et al.[19]

TEOS(X)	Co-solvent System	Benchmark Gel Density (g/cm^3)	γ-Irradiated Gel Density (g/cm^3)	Estimated Volume Polysilicate (%)
0	1:1 IPA:THF	1.028±3.12E-3	1.029±3.68E-3	4.5
0	4:1 IPA:DMF	1.030±3.87E-3	1.030±3.87E-3	4.5
20	1:1 IPA:THF	1.071±2.34E-3	1.074±2.34E-3	11
20	4:1 IPA:DMF	1.076±1.80E-3	1.077±3.97E-3	11
40	1:1 IPA:THF	1.147±2.97E-3	1.150±2.48E-3	19
40	4:1 IPA:DMF	1.149±5.45E-3	1.142±5.24E-3	19
60	1:1 IPA:THF	1.261±6.76E-3	1.273±1.16E-3	33
60	4:1 IPA:DMF	1.254±8.97E-3	1.254±6.83E-3	33

FTIR Spectroscopy

The structure and connectivity of the polysilicate phase present within the hybrid gels prior to swelling in MAA and γ polymerization is important in terms of understanding the interactions that may be driving monomer uptake, morphology and ultimately, the mechanical response of the SIPNs. To begin, the transmission spectra of the molten, dry poly(tetramethylene ether) glycol and the subsequent end functionalized PTMO after reaction with the IPTS are shown in Figure 4.1. The primary features of the polyether glycol include the C-O-C stretch at 1113 cm^{-1}, CH_2 bending (scissoring, twisting and wagging) in the 1200 cm^{-1} to 1550 cm^{-1} region, CH_2 rocking at 747 cm^{-1} and symmetric and asymmetric CH_2 stretching at 2857 cm^{-1} and 2940 cm^{-1}, respectively.[140] The glycol groups are observable via the OH stretch centered at 3477 cm^{-1}.[140] After reaction with the IPTS several changes are evident, with perhaps the most pronounced being the presence of a carbonyl at 1715 cm^{-1} resulting from the reaction between the isocyanate groups of the IPTS and alcohol groups of the ether glycol to form a urethane linkage. The N-H stretch of this secondary amine is observable in the characteristic bimodal absorbance centered at ca. 3325 cm^{-1}.[140] Less significant changes are also observable. For example, the appearance of asymmetric stretching of the SiO_3 groups on the chain ends at ca. 790 cm^{-1}, CH_3 rocking from the ethoxy groups at 960 cm^{-1}, C-N stretching at 1240 cm^{-1}, and NH bending from the secondary amine at 1560 cm^{-1}.[140,141]

The end functionalized oligomers having been characterized, the next step is an analysis of the gels resulting from mixing of these oligomers with TEOS in the THF- and DMF-based solvent systems. As the changes in the polysilicate phase resulting from

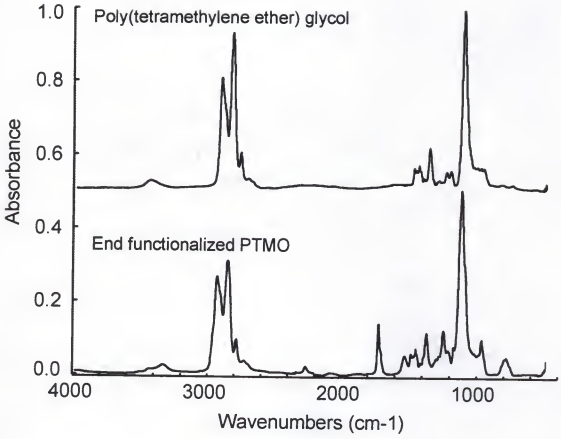

Figure 4.1 Transmission FTIR spectra for poly(tetramethylene ether) glycol and the subsequent triethoxysilane functionalized poly(tetramethylene oxide).

gelation of these two sol classes are of primary importance, the ATR-FTIR results of the silicate "finger print" region of the benchmark gels employing each co-solvent system at the four loadings investigated are displayed in Figure 4.2. Consider first the 4.5% polysilicate loaded gel, which possesses a spectrum dominated by the IR characteristics of PTMO described in the preceding paragraph. Significant changes are observable in the 500 cm^{-1} to 1250 cm^{-1} region, however, and a review of the infrared characteristics of silica is in order.

The major absorbances known to occur in this region for gel-derived silica are given in Table 4.2 along with other relevant information. As the lower limit of the detector in this investigation was ca. 460 cm^{-1}, it is not possible to examine the absorbance band occurring in this low wavenumber region. However, three major absorbances can be investigated: the silicate bending region at 800 cm^{-1}, the silanol stretching at ca. 960 cm^{-1} and the asymmetric Si-O-Si stretching in the 1050 cm^{-1} to 1220 cm^{-1} region. To verify that the absorbances occurring in these regions of the benchmark hybrids are attributable to the polysilicate phase, the ratio of the maximum of each of these absorbances to the PTMO associated ether stretch at 1100 cm^{-1} was plotted versus the estimated volume of polysilicate present in the gels. These results are shown in Figure 4.3 for both co-solvent systems, where it is evident that the intensities of each of the silicate associated absorbances increases nearly linearly in intensity with increasing polysilicate loading. In addition to the increase in intensity ratio with increasing glass loading, the 1040 cm^{-1} absorbance associated with asymmetric Si-O-Si stretching is more intense for the DMF-based gels. Conversely, the defect-associated absorbances at ca. 565 cm^{-1} and 950 cm^{-1} are less intense for the DMF-based gels. These trends, which will be substantiated in an

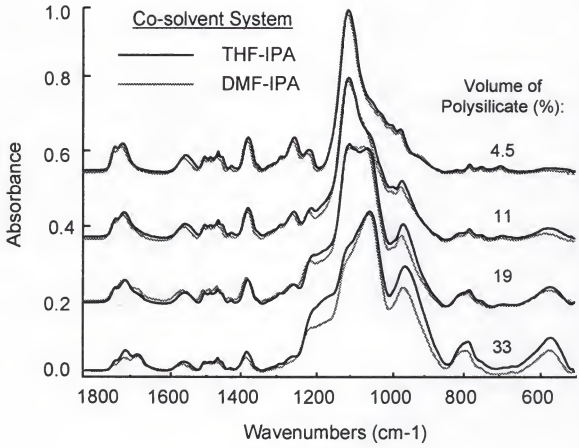

Figure 4.2 ATR-FTIR spectra of the silicate fingerprint region of the THF-IPA and DMF-IPA benchmark gels at the indicted polysilicate loadings.

Table 4.2 Primary absorbances occurring in the infrared for gel derived silica.

Wavenumber (cm^{-1})*	Optically Active Regions and Absorbance Assignments
	Silicate Bending/Rocking
450[141]	Rocking motion of oxygen ⊥ to Si-O-Si plane, some Si motion
468[142]	Si-O-Si bending
475[131]	Lower wavenumber indicates increasing network rigidity
550[132]	Decreases in intensity with heat treatment (can be eliminated)
578[130]	Si-OH rocking (absorbance is not observed in fused silica)
550–600[133]	Skeletal motion of 4-fold siloxane rings
800[130,132,133,140]	Symmetric stretching of oxygen along the bisector of the Si-O-Si bridge with some Si motion
805[142]	Si stretching with broadening possibly due to random packing of SiO_4 units and Si-O-Si bending
800-810[131]	
	Si-OH Stretching
940-970[130-132]	Si-OH or Si-O stretching. Reduced intensity with heating.[132]
957-975[143]	Si-OH that increases in wavenumber with increasing gel age
	Asymmetric Si-O-Si Stretching
1090(1185)[131,144]	SiO_4 tetrahedra stretching. More intense if base catalyzed.
1108(1190)[142]	Si-O stretching (spectrum similar to low temperature tridymite)
1080(1163[130,141], 1220[132])	Transverse optical component.[130, 141] The shoulder is the longitudinal optical component, which decreases in intensity upon heat treatment of gels.[132]
1000[51,54]	Tentatively assigned to branched structural component
1050 and 1080[51,54]	Linear and cyclic structural components, respectively
1080 and 1155[143]	Observed during first 7 hr of polycondensation
1155→1190-1210[143]	Evolution to higher wavenumber of 1155 cm^{-1} absorbance as age approaches 500 hr
	Molecularly Bonded Water
	-Low wavenumber region-
1630[131,132]	Molecular water vibration from hydrogen bonded water (disappears upon drying and/or heat treating to <700°C)
	-High wavenumber region-
3200 - 3450[144,145]	Absorbed water and/or hydrogen bonded Si-OH groups
3650-3680[130,131]	Free Si-OH stretching

* Parentheses denote approximate locations of significant shoulders.

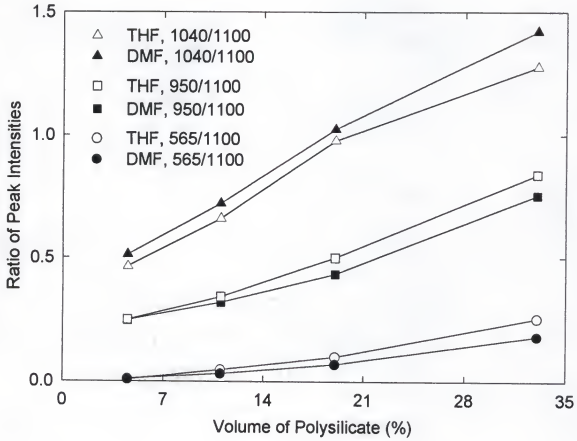

Figure 4.3 The ratio of the asymmetric Si-O-Si stretch (1040 cm^{-1}), Si-OH stretch (960 cm^{-1}) and Si-OH rocking/siloxane ring stretching (565 cm^{-1}) to the ether stretch attributed to the PTMO (1100 cm^{-1}) as a function of the polysilicate loading for both co-solvent classes.

analysis presented shortly, suggest that the polysilicate phase generated in the DMF-based sol possesses a better developed glass network, i.e., is less defect ridden and closer to a melt derived glass than the THF-based polysilicate phase.[132,144]

To more closely examine the structure of the polysilicate phases present in each gel the 4.5% polysilicate containing gel was subtracted from each of the 3 higher loadings to obtain the spectrum of the "TEOS derived" glassy phase. The peaks present between 1300 cm^{-1} and 1600 cm^{-1} are of unchanging position and common intensities for all 4 sets of spectra shown in Figure 4.2. Therefore, they are used as the reference peaks for conducting the spectral subtractions that appear in Figure 4.4. The complete absence of the reference peaks in the subtracted spectra lend credence to their use.[146] At the low wavenumber end of the spectra, the skeletal motion of the siloxane rings (possibly augmented by Si-OH rocking) is observable at ca. 565 cm^{-1}.[130,133] As the wavenumber increases, the symmetric Si-O-Si stretching, also assigned to Si-O-Si bending by some authors, can be seen at ca. 790 cm^{-1}.[130-132,142] Si-OH stretching is observable at 950 cm^{-1} as is the asymmetric Si-O-Si stretching at 1040 cm^{-1}.[51,54,130-133,143,144] A distinct absorbance at 1160 cm^{-1} exists, and is in contrast to the characteristic broad shoulder typically present in the spectra of gel derived and fused silica. Nevertheless, the location of this absorbance and its relative intensity to the asymmetric Si-O-Si stretch at 1040 cm^{-1} is in good agreement with the literature, which traditionally assigns this band to the longitudinal optical component of the stretch.[130-132,141,142] A final comment is due regarding the bands at ca. 1700 cm^{-1}, which are composed of two mechanisms. The first is the aforementioned carbonyl at 1715 cm^{-1}, while the second, centered at ca. 1680

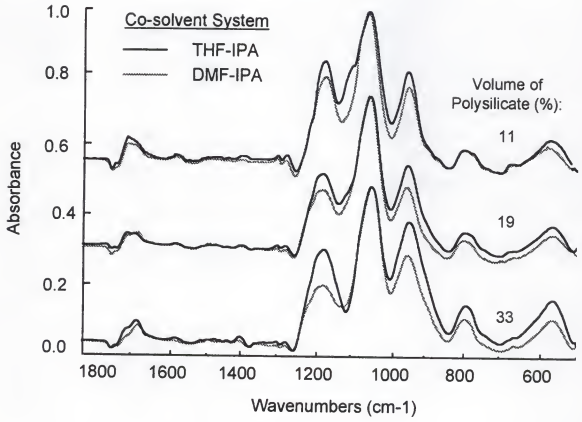

Figure 4.4 ATR-FTIR spectra of the polysilicate phases present in the gels synthesized from sols employing tetraethoxysilane. Spectra were obtained by subtracting the 4.5 vol.% gel spectra from each of the three higher loadings.

cm^{-1}, is most likely attributable to deformation of water that is hydrogen bonded to the silanol species present in the gels.[131,132] This explains why the apparent carbonyl peak does not vanish upon subtraction of the 4.5% gel from the higher loaded films.

An examination of Figure 4.4 reveals that the absorbance bands associated with the DMF-based gels (aside from the dominant 1040 cm^{-1} to which each spectra has been scaled) are all less intense than the corresponding THF-based gel bands. This is in agreement with the comments made earlier postulating fewer defects in the DMF gels. Figure 4.5 displays the ratio of the bands associated with gel silica to the primary Si-O-Si asymmetric stretch at 1040 cm^{-1}. It can be seen that for all three ratio sets, the DMF gels exhibit less intense gel associated absorbances. This is in agreement with several published investigations which have shown that the band located at ca. 550 cm^{-1} for gel derived silica, which is only a weak shoulder in fused silica, disappears upon heat treatment at elevated temperatures, as does the silanol stretch at 960 cm^{-1}.[132] Additionally, a decrease in the intensity of the 1196 cm^{-1} shoulder for the DMF gels compared to equivalently loaded THF gels provides additional evidence that the DMF gel possesses a network structure closer to that of fused silica.[130] The one exception to the claim of increased network ideality is that of the 790 cm^{-1} peak, which is less intense for the DMF-based gels. This contrasts the typical increase in intensity observed for gel silica when heat treated.[132] It is not clear at this time why the intensity is not greater for the DMF-based gels relative to the THF-based gels.

Overall, there appears to be a preponderance of evidence supporting the claim that the polysilicate phase generated in the presence of DMF possesses a vitreous structure

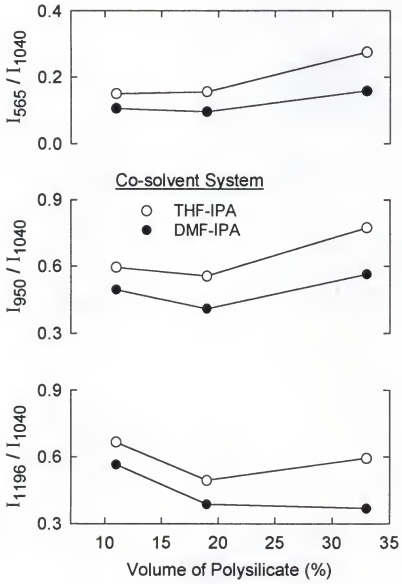

Figure 4.5 The ratio of Si-OH rocking/siloxane ring stretch (565 cm-1), Si-OH stretch (960 cm-1) and high wavenumber shoulder of the primary absorbance band in silica (1196 cm-1) to the characteristic asymmetric Si-O-Si stretch at 1040 cm-1 as a function of polysilicate loading for both classes of gels.

closer to that of fused silica, i.e., containing fewer defects such as silanol groups. This analysis paired with the investigation described in the Introduction utilizing SAXS to probe the structure/spatial distribution of the gel compliment each other well and establish the differences in the gels produced from these two co-solvent systems.[30] In the case of the THF-based gels, a highly interactive, spatially diffuse polysilicate phase containing a high number of silanol species exists. In contrast, the DMF-based gels are comprised of a less spatially diffuse polysilicate phase containing fewer silanol species. Having established the characteristics of the polysilicate phase present in these two classes of gels, the influence upon the mechanical response of PMAA-based SIPNs can be studied.

Effect of Radiation on Mechanical Tensile Response

Before presenting the results of the mechanical tensile testing it is necessary to point out a disparity that exists in the age of the THF compared to DMF benchmark gels, γ–irradiated gels, and PMAA-PTMO SIPNs when tested. In the case of the THF class of gels, 29 days had elapsed after casting before testing was conducted, while 52 days had elapsed for the DMF class of gels. Huang et al. have shown that as the age of a THF-based, 50% (mass/mass) TEOS gel increases the modulus increases and the elongation to break decreases.[19] Specifically, gels tested after 24 days and 53 days exhibited Young's moduli of 2.8 and 4.8 MPa, respectively, while the elongation at break decreased from 68% to 44% as a result of aging for an additional 29 days. SAXS studies on these gels revealed an increase in the scattering intensity with no change in the peak intensity position or tail region decay. Both the mechanical and X-ray scattering changes are attributable to an increased degree of network connectivity owing to continued

polycondensation of the less than fully developed polysilicate phase. These findings are in agreement with similar measurements made by Scherer on sol-gel-derived, TEOS-based gels synthesized using similar water and acid concentrations but no organic polymer.[147] Considering that the FTIR analysis above demonstrated a more highly developed polysilicate network in the DMF gels, it is anticipated that the magnitude of the changes exhibited by aging of the gels described in this work would be reduced significantly. Similarly, the influence of the polysilicate aging becomes less pronounced as the loading of polysilicate decreases. Therefore, although the ages of the gels are given as a reminder, the true effect of the age difference is considered relatively insignificant when compared to the magnitude of the changes exhibited after formation of the PMAA-PTMO SIPNs.

The effect of high energy γ radiation upon gels synthesized using 40% (mass/mass) TEOS was previously shown to increase the network crosslink density thereby increasing the elastic modulus and decreasing the swelling in THF, a good solvent.[122,123] To more completely evaluate the influence of the glassy phase upon the radiation induced crosslinking of the benchmark gels the elastic modulus, stress at failure and elongation at failure as a function of the polysilicate loadings were determined for both co-solvent systems. These results are displayed in Figure 4.6. Typical engineering stress-elongation responses are not shown as the gels exhibit linearly increasing stress with increasing elongation up to the point of failure given in Figure 4.6. Alternately stated, no yielding was observed for any of the inorganic loadings evaluated either before or after γ irradiation.

Consistent with our earlier reports, the irradiation of both classes of the benchmark gels resulted in an increase in the elastic modulus and decrease in elongation to failure.

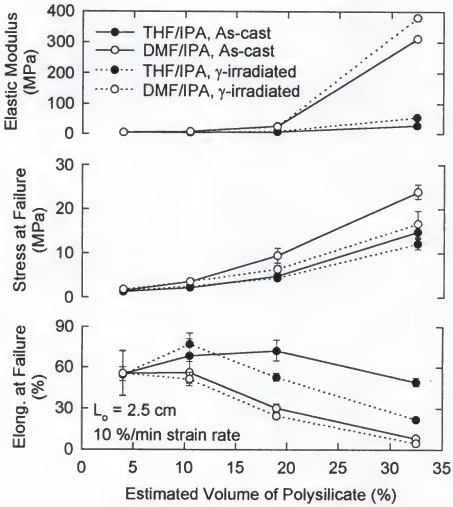

Figure 4.6 Effect of polysilicate loading upon the tensile mechanical response of the benchmark and g irradiated PTMO-silica hybrids exposed to 350 rads/min for a total dose of 0.069 Mrads. The age of the THF-IPA gels was 29 days, while the age of the DMF-IPA gels was 52 days.

However, the stress at failure decreased for both co-solvent systems upon irradiation, which is a reversal of previous observations and will be addressed shortly.[122,123] The magnitude of the change in modulus and elongation at failure increases as the inorganic loading increases, suggesting that the γ radiation interacts with the polysilicate phase possibly leading to its densification via localized heating. This increased degree of condensation should manifest itself in an increased gel density. However, as the data in Table 4.1 indicates, there is no apparent increase in overall density of the hybrid gels, seemingly discounting that minimal additional consolidation occurs as a result of irradiation at this dose rate. The overall magnitude of the changes for the TEOS(40) gel observed in this study are less than those observed in previous investigations.[122,123] Although the total dose is the same, the dose rate in prior investigations was 580 rads/min. This increased dose rate most likely lead to more heat being generated, a higher extent of silicate consolidation and the increased elastic modulus and stress at failure observed previously.

Monomer Swelling and Polymer Formation

The effect of the inorganic loading upon the mass uptake of MAA and subsequent polymerization to PMAA as a function of the co-solvent system and polysilicate loading is displayed in Figure 4.7. It is evident that within each solvent system as the volume of polysilicate increases, the swelling of the benchmark hybrid decreases. However, even though less monomer is absorbed as the volume of polysilicate increases, more is retained within the hybrid structure after γ polymerization. This behavior suggests that the PTMO phase absorbs the MAA but that both the monomer and subsequent polymer possess an

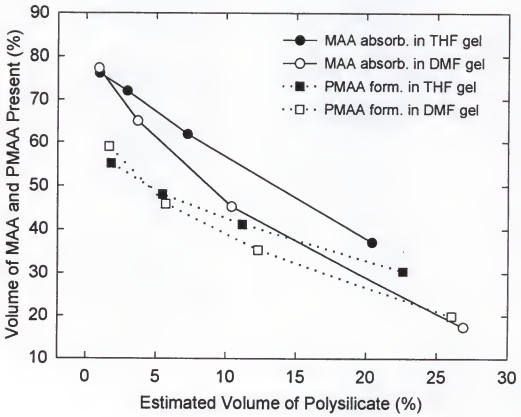

Figure 4.7 The effect of polysilicate loading upon the equilibrium MAA absorption and PMAA SIPN formation for the benchmark PTMO-silica hybrids.

affinity for the polysilicate phase. Furthermore, this affinity is greater in the THF-based gels as they absorb more monomer and retain more polymer after γ polymerization for all polysilicate loadings investigated. However, the lower modulus undoubtedly contributes to increased swelling also. The swelling response of these hybrids can be explained in terms of two competing mechanisms: the kinetics of monomer desorption versus polymer formation.

At low polysilicate loadings, and hence minimal restriction of the PTMO chains by the vitreous polysilicate chains, both the concentration gradient and hydrophobic nature of PTMO ensure that the rate of MAA desorption will be great. As the inorganic volume increases, the vitreous chains restrict the mobility of the PTMO chains and hinder their ability to collapse in the aqueous medium. Consequently, the magnitude of this contribution to monomer desorption is diminished. At the highest polysilicate loading investigated extensive interaction and restriction of the mobility of the PTMO chains occurs thereby resulting in the slowest rate of MAA desorption. The limiting case would be a 100% microporous silica gel in which the only mechanism for monomer desorption would be concentration induced Fickian diffusion. The reduced monomer desorption rate with increasing polysilicate loading allows the formation and retention of increasing amounts of PMAA. As a consequence of increased PMAA formation the hydrophobic nature of the PTMO is offset, thus lessening the rate of desorption as polymerization continues. In addition to the PTMO influence, polar interactions between the acid groups of the MAA and the hydroxyl containing, less than fully developed polysilicate networks diminish the driving force for desorption of MAA from the gels. The overall decrease in both monomer and polymer absorption for the DMF-based gels relative to the THF-based

gels, especially at the higher polysilicate loadings, is attributable to the greater elastic modulus of the DMF-based gels and a lower propensity for the hydrogen bonding. It seems reasonable that the preferred morphology resulting from the above-described swelling and formation kinetics would entail PMAA-PTMO SIPN formation adjacent to and possibly interpenetrating with the polysilicate rich domains.

Mechanical Response of PMAA-PTMO SIPNs

The typical engineering stress as a function of the percent elongation for each of the polysilicate loadings is shown in Figure 4.8 for the THF-based SIPNs and Figure 4.9 for the DMF-based SIPNs (note the difference in axis range). The elastic tensile moduli and stress and elongation at failure are given in Table 4.3 for both. The elongation values shown and reported are calculated using the crosshead extension as a measure of elongation up to the yield point. Beyond the yield, the gauge length of the Type III die, 7.5 mm, was used. This switch in gauge length accounts for the viscous flow that visibly occurs only in the parallel-sided test section of the dumbbell shaped sample. The result, however, is artificially high elongation. Preliminary results utilizing a video camera and tick marks 7.5 mm apart within the parallel sided test section indicate that the true elongation at failure are approximately half the value shown and tabulated. Nevertheless, the relative differences in elongation for the samples tested at the various volume percentages of polysilicate are valid and comparable to those reported previously for PMAA-PTMO SIPNs synthesized using higher dose rates of γ radiation.[123] With regard to the mechanical response of the 1.6% polysilicate DMF gel and 1.8% THF gel, several of the samples tested were ca. twice the thickness of the remaining 3 loadings owing to the large monomer absorption and subsequent polymer formation (Figure 4.7). Experiments

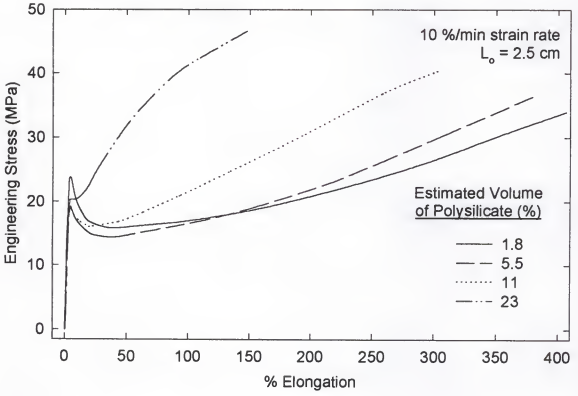

Figure 4.8 The effect of polysilicate loading upon the tensile mechanical response of 29 day old THF-based PMAA-PTMO SIPNs.

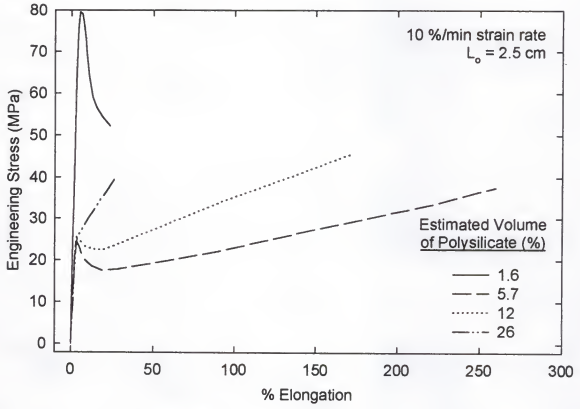

Figure 4.9 The effect of polysilicate loading upon the tensile mechanical response of 52 day old DMF-based PMAA-PTMO SIPNs.

Table 4.3 The effect of polysilicate loading upon the stress and elongation at failure of the PMAA-PTMO SIPNs for both co-solvent systems.

Estimated Volume of Polysilicate (%)	Elastic Modulus (MPa)	Stress at Failure (MPa)	Elongation at Failure (%)
	29 Day Old THF-Based SIPNs		
1.8	930, 1170	34, 35	410, 360
5.5	750±130	37±3.7	390±63
11	870±71	39±1.5	300±24
23	920±140	46±1.2	140±17
	52 Day Old DMF-Based SIPNs		
1.6	2150±140	51±1.1	26±5.5
5.7	1070±98	41±3.0	270±30
12	970±150	45±2.9	170±20
26	980±280	40±3.5	27±10

indicate that there is a definite thickness dependence in that exceptionally thick samples of both the DMF- and THF- based PMAA-PTMO SIPNs exhibit much higher yield strength and much lower elongation at failure than equivalent composition thin samples. For this reason only samples of reasonably similar thickness are displayed with the exception of the 1.6% polysilicate DMF-based PMAA-PTMO SIPN, which illustrates this dependence.

All of the inorganic loadings evaluated exhibit significant increases in the mechanical response as compared to the benchmark and γ–irradiated gels. Indeed, greatly increased stress and elongation to failure along with yielding indicate significant changes in the morphology of the hybrids as a result of PMAA-PTMO SIPN formation. Considering Table 4.3, there is no clear dependence of the elastic modulus upon the inorganic loading for either co-solvent system. However, for the THF-based gels there is the trend of increasing stress at failure and decreasing elongation at failure with increasing polysilicate

loading. Only the decreasing elongation at failure holds for the DMF-based gels when the thickness dependent response of the 1.6 vol.% polysilicate loaded SIPN is ignored.

The stress and elongation at yield values are given in Table 4.4 along with the post-yield (P.Y.) stress drop and elongation prior to strain hardening, i.e., the percent elongation occurring after yield but before the onset of strain hardening. These post-yield values are depicted graphically in Figure 4.10 as a function of polysilicate volume fraction. The data in Table 4.4 indicates that the stress at yield and elongation at which yielding occurs exhibit no correlation with inorganic loading. However, a clear trend of diminishing post-yield stress drop and post-yield elongation prior to strain hardening with increasing inorganic loading is observable in Figure 4.10. Excluding the DMF-based 1.6% polysilicate samples there is little difference between the post-yield stress drop of the two co-solvent systems. There is, however, a greater post-yield elongation prior to strain hardening for the THF-based gels.

Table 4.4 The effect of polysilicate loading upon the tensile yield stress and elongation and post-yield (P.Y.) response of the PMAA-PTMO SIPNs for both co-solvent systems.

Estimated Volume of Polysilicate (%)	Stress at Yield (MPa)	Elongation at Yield (%)	P.Y. Stress Drop (MPa)	P.Y. Elongation Prior to Strain Hardening (%)
29 Day Old THF-Based SIPNs				
1.8	24, 26	3.7, 3.6	7.9, 8.6	14, 10
5.5	19±1.4	4.3±0.90	4.7±0.48	12±2.2
11	18±1.1	3.6±0.10	2.7±0.21	6.7±0.25
23	22±2.5	4.0±0.22	None Observed	None Observed
52 Day Old DMF-Based SIPNs				
1.6	76±3.1	5.4±0.12	25±2.1	16±1.1
5.7	26±1.9	3.5±0.07	6.6±0.61	17±1.7
12	24±3.5	3.7±0.14	2.2±0.84	12±1.3
26	27±3.1	3.8±0.10	None Observed	None Observed

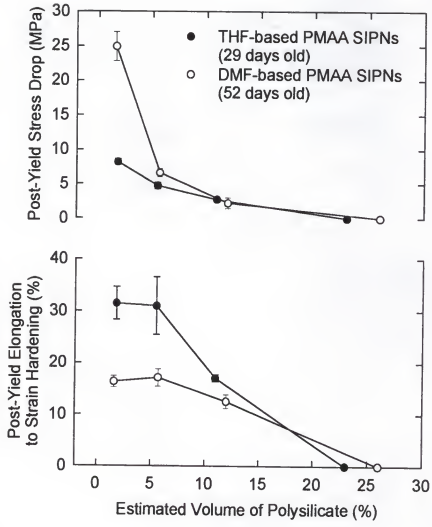

Figure 4.10 Post-yield stress drop and elongation prior to strain hardening as influenced by polysilicate loading and co-solvent system employed.

Traditionally, the phenomenon of yielding originates from the ability of a material to undergo viscous motion during applied stress and thereby dissipate energy.[148] This reorientation initiates by the formation of a neck in the sample. As the elongation increases, this neck grows at a rate dictated by the natural draw ratio of the material. This growth is generally accompanied by an increase in stress and modulus owing to the increased molecular orientation. Hence the term strain hardening is used to describe the process. In terms of the response of these SIPNs, the lower plot in Figure 4.10 indicates that the more spatially diffuse and polar THF-based polysilicate SIPNs are capable of undergoing greater elongation prior to the increase in stress attributable to complete reorientation. Considering the effect of the polysilicate loading, the observed decrease in both the post-yield stress drop and elongation prior to strain hardening for both co-solvent system indicates that as the continuity of the polysilicate phase increases, and presumably approaches a phase inversion, it increasingly hinders the ability of the SIPNs to undergo viscous motion.

Dynamic Mechanical Response of the SIPNs

Dynamic mechanical spectroscopy was performed on all the SIPNs of the same age with the storage modulus, E', and tan δ response as a function of temperature appearing in Figures 4.11 and 4.12, respectively. Considering the storage modulus first, all 8 of the PMAA-PTMO SIPNs exhibit similar thermo-mechanical response. As the temperature increases from -145°C there is a gradual decay in the glassy modulus at ca. 0°C for all samples. The Tg of PTMO gels containing no PMAA or polysilicate (other than the triethoxysilane crosslinks) is ca. -78°C. Therefore, the observance of this decay at much higher temperatures indicates good miscibility of the initial hybrid structure and

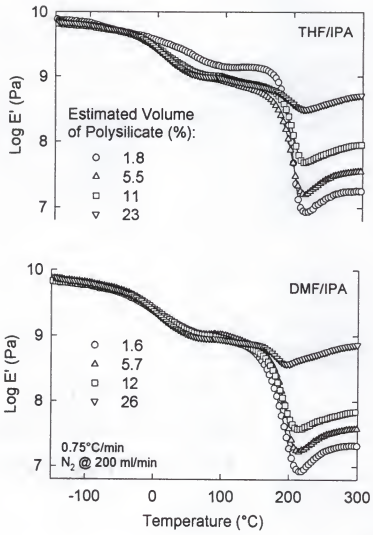

Figure 4.11 Dynamic mechanical storage modulus, E', for both the THF- and DMF-based PMAA-PTMO SIPNs of the same age as a function of temperature for the polysilicate loadings indicated.

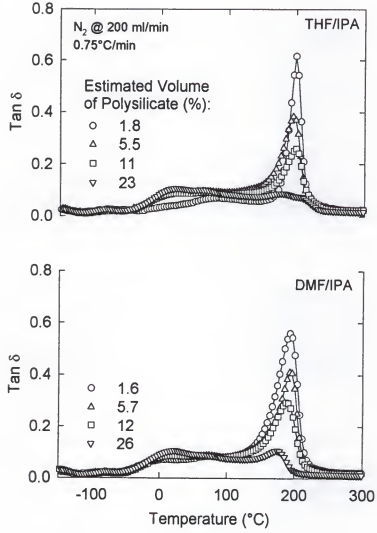

Figure 4.12 Dynamic mechanical tan δ response for both the THF- and DMF-based PMAA-PTMO SIPNs of the same age as a function of temperature for the polysilicate loadings indicated.

the γ polymerized PMAA. A plateau then follows till ca. 150°C at which point the most significant decay in the storage modulus begins. This decay is centered at ca. 200°C, which is close to the reported Tg of 230°C for PMAA.[149] Additionally, the magnitude of the decay is dependent upon the polysilicate loading and co-solvent system in that increasing levels of the inorganic phase reduce the decay associated with the Tg. Above the Tg of the PMAA phase the low volume percent polysilicate containing samples exhibit the thermally induced syneresis which has been observed in Chapter 3 and explained in a previous publication.[121] Interestingly, the effect of this syneresis is virtually undetectable in the samples containing more polysilicate. The exceptionally high value for the 0°C to 150°C storage modulus region of the 1.8 vol.% polysilicate THF-based sample is indicative of the thickness effects discussed earlier. Conversely, the thinner 1.6 vol.% polysilicate DMF-based gel shown in the lower plot exhibits values consistent with other samples of the same relative thickness.

Considering next the tan δ response as a function of temperature displayed in Figure 4.12, multi-modal relaxations are observed in the spectrum of all samples investigated indicating that a wide variety of molecular environments exist within these gels. The overall breadth of the relaxations suggests that much mixing of the PTMO, polysilicate and PMAA phases is occurring. The intense relaxations centered at ca. 190°C for all eight of the samples tested are attributed to the Tg of the PMAA phase. The increase in intensity of these relaxation with decreasing polysilicate loadings and hence increasing PMAA loadings suggest that the PMAA phase constitutes a significant portion of the molecular environment within these gels. This is further supported by the significant strength and modulus increases observed in the tensile samples.

Preliminary Investigations into SIPN Morphology

Further evidence of the affinity of the PMAA for the polysilicate phase is provided by the atomic force microscopy images shown in Figures 4.13 and 4.14 of the fracture surfaces of both the TEOS(40) benchmark gel and TEOS(40) derived, 11 vol.% polysilicate loaded THF-based PMAA-PTMO SIPN, respectively. The tapping mode images clearly indicate that the tortuous, micro-phase separated polysilicate domains clearly observable in the benchmark gel are smoothed over in the SIPN gels. The morphological similarities of this polysilicate containing PMAA-PTMO-SIPN to those images collected by Toki et al. on the surface of poly(n-vinylpyrrolidone) (PVP)-silica hybrids are striking.[38] Their attribution of the homogeneity of the PVP-silica gel to hydrogen-bond formation between the PVP carbonyl groups and residual silanols, as measured using NMR, lends further support to the proposed poly(methacrylic acid)-polysilicate interactions discussed in this work.

Small angle X-ray scattering was performed to evaluate the effect of SIPN formation upon the average electron density fluctuations present within the gels. Figure 4.15 illustrates the changing scattering response observed upon formation of the SIPN within a benchmark 19 vol.% polysilicate containing gel. The scattering profile before swelling and γ polymerization exhibits a maximum characteristic of these micro-phase separated gels.[30] An interdomain spacing of ca. 13 nm can be estimated from the reciprocal of the scattering vector at the maximum scattering intensity, I(s), for the starting gel. Upon polymerization of the adsorbed MAA the overall scattering intensity is reduced due to the lower volume fraction of the relatively electron rich inorganic phase.

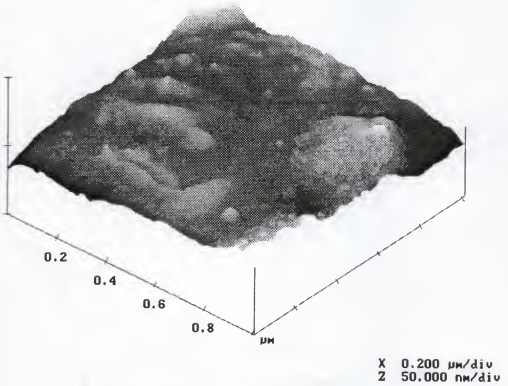

Figure 4.13 Atomic force microscopy image of the fracture surface of a 19 vol.% percent polysilicate, THF-based benchmark PTMO-silica gel collected using tapping mode.

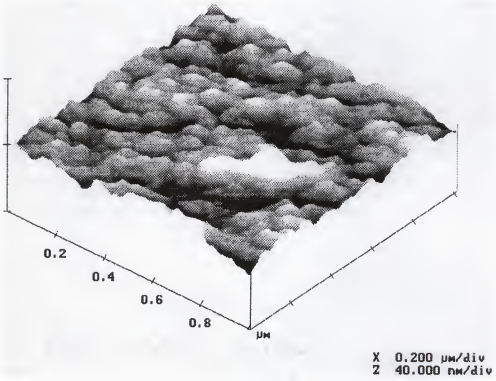

Figure 4.14 Atomic force microscopy image of the fracture surface of an 12 vol.% percent polysilicate, THF-based, PMAA-PTMO SIPN gel collected using tapping mode. This SIPN is formed from the same "parent" PTMO-silica gel as the piece imaged in Figure 4.13.

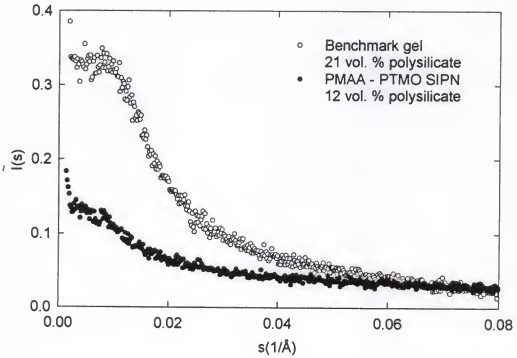

Figure 4.15 Small angle X-ray scattering profiles of the 19 vol.% polysilicate, THF-based benchmark gel and the subsequent 12 vol.% polysilicate, THF-based PMAA-PTMO SIPN resulting from γ polymerization of the MAA swollen "parent" gel.

Additionally, there is no clear maximum in the scattering profile indicating that the PMAA and polysilicate phases have mixed and thereby reduced the electron density gradient. This data in conjunction with the DMS results presented above strongly suggests that mixing occurs in these PMAA-PTMO-silica SIPNs and is driven by the affinity of the PMAA and polysilicate phases for one another.

Conclusions

Significant changes in the tensile mechanical response of the benchmark PMTO-polysilicate hybrid composites can be induced by formation of PMAA-PTMO SIPNs. Additionally, the presumed spatial distribution and demonstrated polarity differences induced in the polysilicate phase by the use of two different co-solvent systems significantly affects the mechanical response of these γ polymerized SIPNs. Overall, this transformation involves the conversion of elastomeric hybrids to high strength, high elongation organic glasses exhibiting yielding. The effect of increasing polysilicate loading upon the tensile mechanical properties of the SIPNs synthesized from both co-solvent systems has been found to increase the stress at failure, decrease the elongation to failure, decrease the magnitude of the post-yield stress drop and decrease the post-yield elongation prior to strain hardening. Within the individual co-solvent systems the THF-based SIPNs exhibit greater elongation than the near equivalently loaded DMF-based SIPNs. This indicates that less fully developed polysilicate networks are capable of undergoing greater viscous motion. It is unclear at this time whether the hydrogen bonding ability of the polysilicate phase directly influences the degree of viscous motion or is just an indicator of this less than fully developed glass network. Atomic force

microscopy and small angle X-ray scattering data suggest the formation of a PMAA rich SIPN phase adjacent to the polar polysilicate domains. Therefore, even if this hydrogen bonding does not directly contribute to the mechanical response, it does dictate the morphology of the SIPNs.

CHAPTER 5
THE EFFECT OF SOL CATALYST UPON OXYGEN DIFFUSION

Relevant Background

Motivation

The potential of high temperature, gas separation processes in corrosive environments is driving the development of porous ceramic membranes. For these membranes to provide a separation mechanism, the pore diameters must be small enough for Knudsen diffusion to predominate. Although this mechanism is functional and has found use in the separation of uranium isotopes for the manufacturing of nuclear weapons, it is a slow process exhibiting relatively low gas selectivity. This selectivity can be greatly improved by using polymeric membranes. In general, rubbers exhibit the highest gas permeability of all the polymer classes. However, permeability and selectivity are virtually always inversely proportional.[95] Therefore, although organic glasses such as polycarbonate, polyimide and polysulfone exhibit lower permeability than organic rubbers, the selectivity is improved.[113,114,150] Surprisingly, little research has been performed on materials capable of true mixed-mode diffusion. Rather, the current interest is in understanding and modeling the dual-sorption characteristics of glassy polymers. However, an understanding of the gas transport mechanisms present in rubber/porous ceramic composites would provide a good foundation for further study of more refractory and corrosion resistant polymer-porous ceramic membranes combining the selectivity of

polymers with the speed and additional selectivity of porous ceramics.

Hybrid organic-inorganic composites offer a unique opportunity to study transport phenomena in composite systems. In Chapter 2, it was demonstrated that sol-gel-derived glass should exhibit Knudsen diffusion based on the pore diameters typically observed. Therefore, hybrids provide a single material in which two potential separation mechanisms are possible. The word potential is used because some controversy exists surrounding the presence of open and interconnected porosity within the inorganic domains of hybrid composites. Nevertheless, this unique morphological aspect paired with the other advantages that hybridization offers is stimulating interest in the utilization of hybrid composite technology for industrial gas separation processes, dissolved oxygen sensing devices, reduced pressure oxygen sensing paint and other niche applications.[79,81,90,116-120]

Although there is seemingly little interest in rubber-porous ceramic membranes, the PTMO-polysilicate system used in this study is free of many complexities present in the study of gas transport in organic glasses such as physical aging, free volume and quasi-ordered regions within the amorphous bulk.[89] The immediate goal of this work is to measure the effect of catalyst dependent morphology upon the oxygen diffusivity of these model hybrid composites. Furthermore, it is hoped that these results will provide an assessment of the presence of multiple diffusion mechanisms indicative of open, interconnected porosity within the inorganic polysilicate phase.

Enabling Principle

The measurement technique utilized is based on the detection of oxygen by a fluorescent compound embedded within the gels. The relationship between intensity and

oxygen concentration, as indicated by these molecular probes, is described by the Stern-Volmer relationship:

$$\frac{I_o}{I_{[O2]}} = 1 + k_{QM}\tau_M[O_2]. \quad (5.1)$$

In this relation, I_o is the fluorescent intensity in the absence of oxygen, $I_{[O2]}$ is the intensity at an oxygen concentration of $[O_2]$, k_{QM} is the bimolecular quenching constant and τ_M is the lifetime of the luminescent compound in the matrix.[151,152] When the lumiphore dispersed within the sample comes into contact with molecular oxygen, the intensity at which it emits photons decreases. Therefore, this relationship predicts an increase in the intensity ratio from unity with increasing oxygen concentration. For materials such as liquids and rubbers, the concentration of a dissolved gas is directly proportional to pressure via Henry's law. The proportionality constant is the solubility, S. Therefore, the oxygen concentration, $[O_2]$, can be replaced by the quantity SP_{O2}, where P_{O2} is the partial pressure of oxygen. Since compressed air is used as the oxygen source for the experiments detailed in this chapter P_{O2}=0.21P and the solubility-pressure quantity can be substituted for $[O_2]$ in Equation. 5.1 to yield

$$\frac{I_o}{I_P} = 1 + 0.21k_{QM}\tau_M SP. \quad (5.2)$$

Therefore, the pressure-dependent phosphorescent intensity can be used to measure the concentration of molecular oxygen dissolved in the gel. Although a linear relationship is predicted, it often does not hold for polymers. The deviation from linearity is attributable to the influence of the micro-heterogeneous environment present in polymers upon the decay lifetime, τ_M, of the luminescent species.[82] For example, samples of lumiphore

coated silica particles dispersed within crosslinked polydimethylsiloxane as well as lumiphore doped polystyrene have been shown to exhibit two decay lifetimes each, albeit with different values. Although the resolved lifetime decays produce two linear Stern-Volmer responses in each of the samples over the pressure range of interest, the summation of the two linear responses leads to a nonlinear response for both samples.[82] Therefore, the presence or absence of curvature in the Stern-Volmer plots can not be rigorously used as a check for the correct assumption of Henry's law. To ensure that the pressure-concentration response is indeed linear it would be necessary to perform detailed sorption experiments employing a micro-balance or pressure-volume apparatus such as that described by Koros et al..[153] These experiments were not conducted in this study and, as stated above, Henry's law is assumed. As will be presented later, the oxygen diffusivity values obtained in this study are in good agreement with those published for other rubbers which suggests that the assumption is valid enough.

Mass Transport Equation Utilized

In the studies to be detailed shortly, lumiphore containing poly(tetramethylene oxide)-polysilicate hybrid composites were coated onto glass substrates. The rate of oxygen transport out of the exposed surface of the films is then detected by the change in oxygen concentration as assessed by the change in luminescent intensity. A special apparatus designed to do exactly this will be described in the Experimental section. The current section, however, provides the transport equations that will be applied to the data collected by this apparatus.

The solution to any time-dependent diffusion process begins by solving Fick's second law:

$$\frac{\partial C}{\partial t} = D\frac{\partial^2 C}{\partial x^2} \tag{5.3}$$

for the time, t, dependent change in concentration, C, with position x. Under the assumptions of one-dimensional flow out of a homogeneous slab of infinite length and constant average diffusivity, D, the separation of variables technique can be applied under the appropriate boundary conditions to produce the solution

$$\frac{\overline{C} - C_{Min}}{C_{Max} - C_{Min}} = 1 - \frac{8}{\pi^2}\sum_{n=0}^{\infty}\frac{1}{(2n+1)^2}\exp\left[\frac{-(2n+1)^2}{4}\cdot\frac{Dt}{L^2}\right] \tag{5.4}$$

The derivation of this expression can be found in several texts on mass transport.[104,154] In this equation, L is the sample thickness. For the time-scales examined in these studies, the first iteration of the series is sufficient and produces the expression

$$\frac{\overline{C} - C_{Min}}{C_{Max} - C_{Min}} = 1 - \frac{8}{\pi^2}\exp\left[-\frac{t}{\tau}\right] \tag{5.5}$$

where

$$\tau = \frac{4L^2}{\pi^2 D} \tag{5.6}$$

and is referred to as the time constant.[154] The best fit of Equation 5.5 to a time-dependent change in concentration allows the calculation of τ. Once τ is known, the average diffusivity can be calculated. Assuming concentration is directly proportional to pressure within the film and taking into account the partial pressure of oxygen in air, then $C_{Min} = 0.21SP_{Min}$, and $C_{max} = 0.21SP_{Max}$. This allows Equation 5.5 to be rewritten as

$$\frac{\overline{P} - P_{Min}}{P_{Max} - P_{Min}} = 1 - \frac{8}{\pi^2}\exp\left[-\frac{t}{\tau}\right] \tag{5.7}$$

which is the form most conducive to these experiments since accurate pressure values are easily obtainable.

Catalyst Effects on Polysilicate Porosity

Three different approaches have been taken to produce polysilicate phases exhibiting distinctly different continuity and levels of interaction with the surrounding polymer matrix. As the previous two chapters have elaborated upon, the choice of processing route and exposure of the gelling alkoxysilanes to different pH produces significant changes in the degree of organic/inorganic phase interaction. This chapter exploits these effects by first producing HCl catalyzed gels which dynamic mechanical spectroscopy will reveal, possess the characteristic intimate level of mixing shown to exist in Chapter 3. This level of phase interaction is decreased somewhat by prehydrolyzing equivalent amounts of tetraethoxysilane in an HCl acidified alcohol/water mixture for 2 days prior to sol addition and composite gelation. Thus allowing the polysilicate "clusters" to grow in the absence of the polymer chains and to achieve a more spatially discrete form prior to consolidation of the composite. The limit in reduced phase interaction is achieved by using a base catalyst. The catalyst employed is the same ethylamine in water solution used in Chapter 3. In this last case, prehydrolysis will not be necessary since dynamic mechanical spectroscopy results will reveal that a significant reduction in phase mixing and interaction is observed in these gels.

In addition to the phase interaction spectrum produced, it is anticipated that these processing variations will give rise to changes in the type of pore structures present. For example, Figure 5.1 schematically illustrates the type of porosity that may be formed using the acid and base catalysis route. The HCl catalyzed gels synthesized without

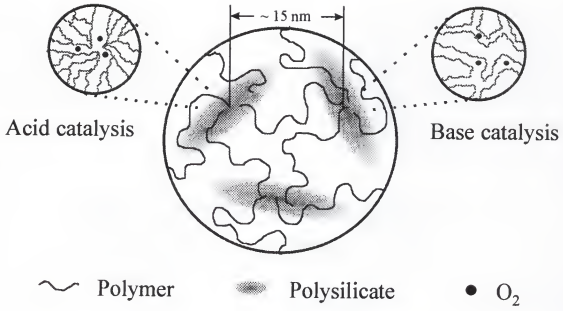

Figure 5.1 Schematic illustration of the types of porosity anticipated to be present as a result of the catalysts employed in this study.

prehydrolysis may possess polysilicate phases resembling that drawn in the upper left corner of the schematic. These pores, if present, are likely to be ill-defined, random defects within the polysilicate network resulting from incomplete hydrolysis and condensation. Consequently, they defy the traditional definition of a pore. Alternately, the ethylamine-catalyzed gels may possess inorganic phases resembling the drawing appearing in the upper right corner. The origin of the better defined pore structure would be the increased level of network development that is characteristic of base catalyzed systems and that drives enhanced phase separation. The increased level of phase separation may lead to larger agglomerates composed of smaller, more colloidal silica gel particulates. The packing defects associated with these clusters would give rise to a more traditional pore structure. By increasing the loading of polysilicate, the probability of reaching a porosity percolation limit is increased. Therefore, four polysilicate loadings have been investigated: 4.5, 11, 19 and 42% (vol/vol). Clearly stated, the objective of this study was to measure the diffusivity of the micro-phase separated composites as a function of both polysilicate loading and catalyst induced morphology.

Experimental

Triethoxysilane end functionalized PTMO of molar mass 2,495 g/mole was used for all of the compositions produced in this study. The first batching that occurred was that of the prehydrolyzed TEOS and was accomplished by adding 0.19, 0.37 and 0.64 ml of TEOS by syringe to 3ml polypropylene serum vials sealed with rubber stoppers. Each of the 3 vials contained a vigorously stirred isopropanol (IPA) solution that had been acidified with 0.87N HCl. The amount of IPA present was that necessary to produce a

volumetric ratio of 0.7:1 TEOS:IPA. Similarly, the amount of 0.87N HCl present in the IPA prior to the addition of TEOS was the stoichiometric amount required to hydrolyze every ethoxy group of every TEOS molecule added. These ratios were held constant for each of the three sols produced. Each sol was then magnetically stirred for 2 days at ambient temperature and pressure. After 2 days, each of these sols were added to vials containing stirred, pre-batched solutions of end functionalized PTMO, IPA and the amount of a toluene and platinum (II) meso-tetra(pentafluorophenyl) porphine (PtTFPP) solution required to produce a lumiphore mass loading of 0.3% in the final gel. The luminescent compound PtTFPP was obtained from Porphyrin Products and used as received. The amount of TEOS added to each vial was that necessary to produce sols of 20, 40 and 70% (mass/mass) with respect to the total mass of TEOS and PTMO. No additional catalyst was added. Each of these 3 sols were then magnetically stirred for 1 minute prior to the deposition of a sol aliquot onto 1/2" x 5/8" numbered glass substrates that had been pre-weighed 3 times each.

The processing of the remaining two sols was comparatively easy. Equivalent amounts of TEOS to those used in the prehyrolyzed sols were added via syringe directly to the PTMO, IPA, PtTFPP/toluene solutions. After 5 minutes of stirring, the appropriate amounts of 0.87N HCl or 70 wt.% ethylamine in water solution were added. The resulting mixtures were stirred for one minute then the appropriate sol aliquots were deposited onto the glass substrates. In the case of the HCl catalyzed gels, 100% of the stoichiometric water needed for complete hydrolysis was added. However, for the ethylamine catalyzed gels only 47% of the required water was added. The deficiency in water is necessary to maintain optical transparency in the resulting gels. As was the case

for the prehydrolyzed TEOS samples, the amount of PtTFPP present in each sol was that necessary to produce a final mass loading of 0.3% within the gel. Samples produced without prehydrolyzing the TEOS are henceforth referred to as in-situ precipitated. Two additional gels were produced and function as baseline samples. These two samples were HCl and ethylamine catalyzed gels that were each crosslinked by the sol-gel-processing of end functionalized PTMO without the addition of TEOS.

To produce the sample films, the appropriate amount of sol was deposited onto the glass using a volumetric pipette after 1 minute of stirring. These glass substrates were double-sided taped to the bottom of 50 mm diameter polystyrene petri dishes. After deposition, the dish was covered and tilted to spread the sol over the entire glass surface. This was done quickly so that the dish could then be set on a level plate with sufficient time remaining for the sol to redistribute evenly over the surface. Each sample was then given 4 days covered in darkness to gel, although gelation typically occurred within hours. The absence of light was necessary to prevent photodegradation of the lumiphore. After 4 days the covers were removed and residual solvent was allowed to evaporate from the gels. Next, the samples were placed into a 40°C vacuum oven and evacuated to 10 Torr under continuous pumping for 24 hours. The oven door was covered with aluminum foil to prevent the entry of ultraviolet light. Upon removal from the oven, the coated substrates were carefully detached from the petri dishes. Any adhesive remaining on the glass was removed using acetone and a tissue. All of the samples were then weighed 3 times each to determine the mass of the coating.

One final comment is due with regard to the volume of material deposited on the glass substrates. A spreadsheet has been developed which automatically performs the

calculation of the mass and volume of each component needed to produce sols with the desired catalyst equivalents, molar ratio of water-to-alkoxy and solids loading. This spreadsheet also calculates a theoretical density for gels of any composition, which is accomplished by scaling the density of the gelling species with the molar mass change of the condensing components. Agreement between predicted and measured densities is within 2% for gels containing 33% (vol/vol) polysilicate or lower. Knowing the density of the gel resulting from the sol deposited, it is possible to adjust the volume deposited on the substrate to produce a film of desired thickness once the surface area of the substrate to be coated is determined by mass, thickness and density measurements. Therefore, for this study, the volume of sol deposited has been adjusted to provide final coating thickness of 40 μm for all polysilicate loadings.

Two primary characterization techniques were employed for this investigation: dynamic mechanical spectroscopy (DMS) and a luminescence-based apparatus capable of measuring the pressure-dependent luminosity of oxygen sensitive films as a function of time. As with the DMS experiments described in Chapters 3 and 4, a heating rate of 0.75°C/min was used from -150°C to 250°C. A nitrogen atmosphere was maintained in the furnace using a flow rate of approximately 200 ml/min. The frequencies tested were 0.1, 0.5, 1, 5 and 10 Hz. All spectra displayed have been collected at 1 Hz.

The apparatus used to measure the oxygen diffusivity of the films deposited on glass was designed and built in the Department of Aerospace Engineering, Mechanics and Engineering Science at the University of Florida and is under the supervision of Dr. Bruce Carroll.[81] The apparatus, which is schematically illustrated in Figure 5.2, relies upon a photomultiplier tube to measure the pressure-dependent luminescence of polymer films

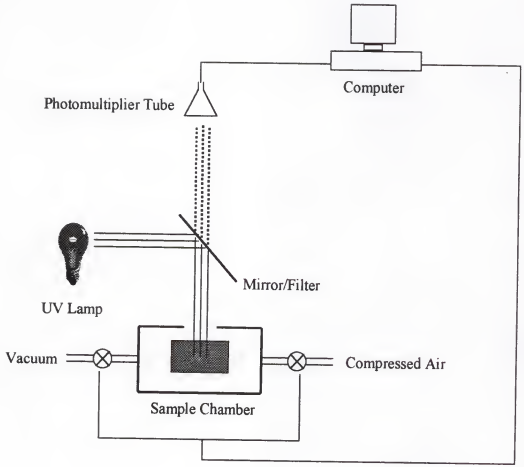

Figure 5.2 Schematic illustration of the apparatus used to measure the time dependent intensity of luminescent gel samples.

coated on impermeable substrates. The samples are contained within a small sample chamber, and a 1.26 cm^2 diameter portion of the top surface of the film is exposed to gas. The atmosphere above the sample is maintained by two computer operated valves that control the pressure of a large vacuum reservoir and a compressed air tank. The chamber possess a single window parallel to the surface of the sample through which the incident ultraviolet light can pass along with the subsequent wavelength shifted luminescent emission. Not shown are the power supplies and amplifiers necessary for the apparatus to function.

Although amplifier and power source settings have to be set manually, the software package LabView® is used to control some operations of the apparatus such as the valve positions (open or closed). The software is critical for the collection of data, which is accomplished using a three-step procedure:

1. A virtual instrument (VI) in LabView® is run, and it records the actual pressure, as measured by a transducer, and the luminescent intensity of the sample, as measured by the photomultiplier tube (PMT) voltage, at 21 different pressures between ca. 0.1 and 1.1 atms. Thirty seconds is allowed for equilibration between each data point. Upon collection of the data, a nonlinear regression through the 21 points is automatically performed thereby calibrating PMT voltage to pressure above the sample and, consequently, oxygen concentration within the sample.

2. A second VI is run that closes the "upstream" valve, thereby exposing the sample chamber to vacuum pressure of ca. 0.1 atm. A period of 60 seconds then ensues to allow equilibration. After this minute has elapsed the VI simultaneously opens the upstream valve and closes the downstream valve thereby "instantaneously" increasing or stepping the sample to a higher pressure (typically 1.1 atm). A duration of 60 seconds passes during which the VI is recording the pressure in the sample chamber via the transducer and the PMT voltage, which is calibrated to concentration of molecular oxygen within the gel sample, as a function of time. For these experiments 40 data points are collected each second for a total of 2,400 pressure/time data points.

3. The calibration VI is reopened and run again so that another calibration curve for equilibrium sample intensity (PMT voltage) as a function of pressure is obtained. The VI renames the "original" calibration data to backup files and then updates the current calibrations.

The collection of two calibration curves allows a comparison of the equilibrium pressure/intensity response of the sample both before and after the step response. This is needed to ensure that a significant amount of photodegradation has not occurred which would invalidate the step response just collected. It should be noted that no significant change occurred in the pre- and post-step calibrations for the step responses presented in this work.

The nonlinear equation regressed through the calibration data is

$$\frac{1}{V_{PMT}} = a + bP + c\left(\frac{dP_{Trans}}{1 + dP_{Trans}}\right) \tag{5.8}$$

where V_{PMT} is the PMT voltage and $P_{Trans.}$ is the transducer pressure. By allowing 30 seconds for the samples to equilibrate prior to recording the PMT voltage, it is assumed that $P_{Trans.}$ is equal to the pressure of air within the gel sample. The constants a, b, c and d are determined during the regression. The general form of the equation is that of a linear pressure-voltage response with a Langmuir term added to account for any deviation from linearity that is sometimes observable in polymeric samples, as discussed earlier in this chapter.

After the step response is collected, it is possible to curve fit a diffusion equation of the form given in Equation 5.7 using the graphical software package SigmaPlot®. This program uses a Levenberg-Marquardt least squares curve fitting routine to optimize the fit of the equation based on the parameters such as τ. Additionally, the package also produces an uncertainty in the determination of each parameter. This uncertainty is

termed the standard error and is used in the calculation for oxygen diffusivity uncertainty discussed later in this chapter.

Results and Discussion

Film Thickness Measurements

The thickness of all films used in this study is given in Table 5.1. As, the volume of sol deposited was intended to produce films 40 μm thick, in most cases, satisfactory agreement between the actual and target thickness was achieved. The error for all samples is one standard deviation of the mean arising from the three mass measurement technique. Although this standard deviation does account for the propagation of error involved, the visible rounding of the edges of the films deposited on the glass undoubtedly leads to an error exceeding that estimated from instrument uncertainty. Although more accurate techniques for film thickness measurement do exist, such as ellipsometry or spectrometric methods, the large sample surface area tested in the diffusion experiments, 1.26 cm^2, suggests that this average thickness technique may provide just as good of a value as these

Table 5.1 Estimated thickness for the samples used in oxygen diffusivity measurements.

Sample	Polysilicate Loading	Thickness (um)
HCl, 100% H_2O, in-situ TEOS	4.5	39±0.2
HCl, 100% H_2O, in-situ TEOS	11	43±0.3
HCl, 100% H_2O, in-situ TEOS	19	43±0.2
HCl, 100% H_2O, in-situ TEOS	42	50±0.2
HCl, 100% H_2O, prehy. TEOS	11	46±0.3
HCl, 100% H_2O, prehy. TEOS	19	43±0.2
HCl, 100% H_2O, prehy. TEOS	42	47±0.2
Ethyl., 47% H_2O, in-situ TEOS	4.5	44±0.2
Ethyl., 47% H_2O, in-situ TEOS	11	46±0.3
Ethyl., 47% H_2O, in-situ TEOS	19	46±0.2
Ethyl., 47% H_2O, in-situ TEOS	42	53±0.2

point source measurements. For the estimations of error used in this chapter, an uncertainty of 5% of the film thickness will be used.

Dynamic Mechanical Spectroscopy

DMS was performed on gels containing 33 vol.% polysilicate to confirm the difference in the phase interaction anticipated to be present in gels produced using the above detailed sol processing. The level of phase interaction is indicative of the spatial distribution of the polysilicate phase. Figure 5.3 displays the storage modulus, E', (top portion) and loss dispersion, tan δ, response (bottom portion) of each gel. Considering E' first, all gels exhibit nearly identical response until ca. -75°C which is the glass transition temperature of the PTMO phase. The decay in modulus occurs at approximately the same rate for all three samples until 0°C where significant changes are observable. As discussed in Chapter 3, much information can be gained regarding the level of phase interaction occurring from the rubbery regime of these hybrid composites. The fact that the HCl-100% H_2O gel possesses the highest rubbery modulus indicates that it also possesses the highest degree of phase interaction as entanglements with the polysilicate phase behave as labile crosslinks. An increase in modulus occurs beyond 175°C indicating the lack of a completely developed polysilicate network.[121] The lowest rubbery modulus is observed for the ethylamine catalyzed gel utilizing 47% water. The reduced modulus indicates a reduced level of phase interaction, and the absence of any thermally induced modulus increase indicates the development of a nearly complete polysilicate network despite the water deficient sol the gels were produced from. The prehydrolyzed, HCl catalyzed TEOS sample exhibits a rubbery response containing features of both the HCl and ethylamine catalyzed gels. At 25°C, the gel possesses a modulus nearly identical to that of

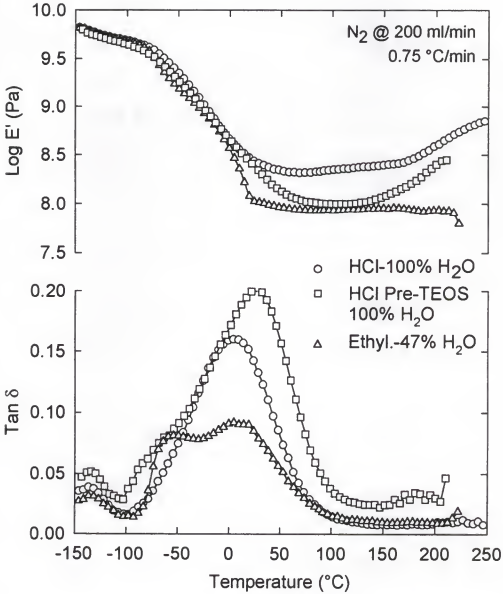

Figure 5.3 Dynamic mechanical storage modulus and tan δ response of gels containing 33 vol.% polysilicate derived from sols employing acid and base catalysts.

the HCl catalyzed, in-situ precipitated sample. As the temperature increases, the modulus continues to decay to a minimum very close to that of the ethylamine catalyzed gel. However, the syneresis typical of acid catalyzed gels is observable.

Considering the tan δ response, significant damping begins to occur at the onset of the Tg at ca. -75°C and continues until ca. 100°C for all three gels. The overall breadth of the relaxation spectra indicates that a wide variety of molecular environments exist within these gels. The most uniform or normally distributed relaxation occurs for the HCl catalyzed, in-situ precipitated polysilicate. This indicates that a high degree of phase mixing is occurring. Conversely, a bimodal distribution is observed for the ethylamine-catalyzed gel with peaks centered at ca. -50°C and 10°C. This bimodality indicates the presence of two phases with each being predominantly richer in one species than the other. The acid catalyzed, prehydrolyzed gel exhibits a fairly uniform distribution. However, a low temperature shoulder does exist at ca. -45°C indicating the presence of some phase segregation. Again, this suggests that an intermediate level of mixing is achieved. With regard to damping, i.e., the maximum value of tan δ, the prehydrolyzed gel exhibits the highest propensity to absorb energy. It is unclear at this time why the intensity does not also fall in an intermediate position. However, the above analysis of the E' response as well as the breadth and shape of the tan δ responses indicate that three varying levels of phase separation have been achieved.

Oxygen Diffusivity

The step responses of the HCl catalyzed, in-situ precipitated gels are shown in Figure 5.4, while the responses of the HCl catalyzed, prehydrolyzed TEOS and ethylamine catalyzed gels are displayed in Figures 5.5 and 5.6, respectively. Note that the ordinate of

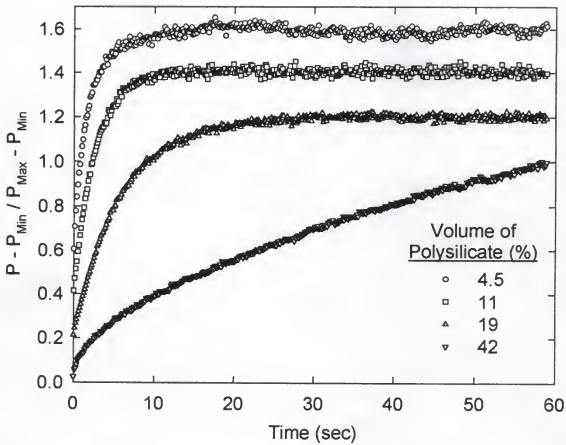

Figure 5.4 Step responses of the four HCl catalyzed gels utilizing the in-situ precipitation of polysilicate in the presence of 100% of the stoichiometric water required for hydrolysis.

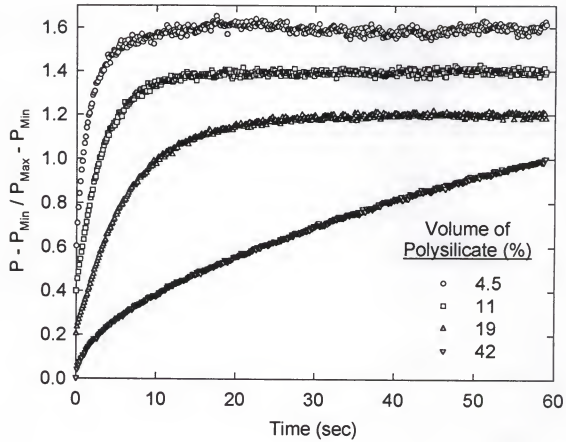

Figure 5.5 Step responses of the four HCl catalyzed gels utilizing prehydrolysis of TEOS in the presence of 100% of the stoichiometric water required for hydrolysis to produce polysilicate clusters prior to sol batching.

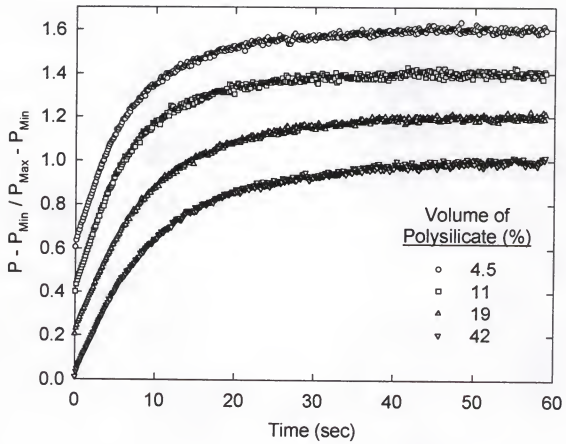

Figure 5.6 Step responses of the four ethylamine catalyzed gels utilizing in-situ precipitation of polysilicate in the presence of 47% of the stoichiometric water required for complete hydrolysis.

each of the samples is vertically shifted by 0.2 to make the response of each clearly visible. Only at the maximum loading of 42% (vol/vol) is any visually significant change in the response observed for the either class of acid catalyzed gels (Figures 5.5 and 5.6). Similarly, it can be seen that the response of the ethylamine catalyzed gels is different than that of the acid catalyzed gels. However, within this class, all four loadings of the ethylamine catalyzed gels investigated exhibit near identical responses.

As the thickness of all the samples is nearly equal, it is possible to examine the influence of processing by regrouping the step responses according to their polysilicate loadings. This has been done, and the groupings appear in Figures 5.7 through 5.10. The polysilicate loadings for each graph are given in the upper right hand corner. Also shown in these figures are the modeled responses to be discussed shortly.

Disregarding the modeled fits momentarily, a review of Figures 5.7 through 5.9 indicates that the in-situ precipitated, HCL catalyzed samples respond most quickly to the pressure change for all loading up to 19 vol.% polysilicate. Conversely, the response is slowest for the in-situ precipitated, ethylamine catalyzed samples. The prehydrolyzed gels exhibit an intermediate time response. Beyond 19% (Figure 5.10), a reversal is observed in that the ethylamine catalyzed gels now exhibit the fastest response.

The exact model fit to the step responses shown above is

$$\frac{\bar{P} - P_{Min}}{P_{Max} - P_{Min}} = B - C\exp\left[-\frac{t}{\tau}\right]. \tag{5.9}$$

The expected value of B should be unity, and the expected value of C should be $8/\pi^2$ (0.81). The parameter values, associated uncertainties and calculated oxygen diffusivity, D_{O2}, for each sample are given in Table 5.2. Visual examination of the curve fits in

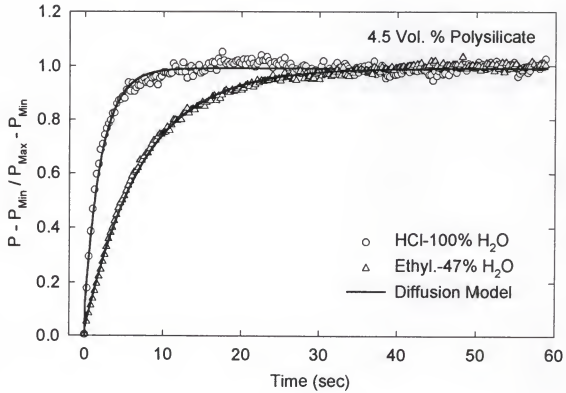

Figure 5.7 Step responses and diffusion model curve fits for HCL and ethylamine catalyzed gels containing PtTFPP and an estimated 4.5 vol.% polysilicate.

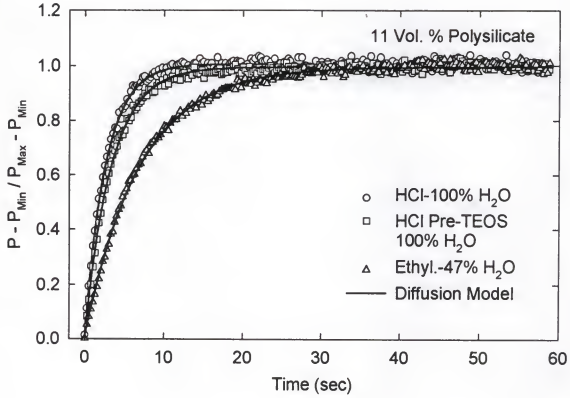

Figure 5.8 Step responses and diffusion model curve fits for the in-situ precipitated and prehydrolyzed HCL catalyzed gels, as well as the ethylamine catalyzed gels. All samples contain PtTFPP and an estimated 11 vol.% polysilicate.

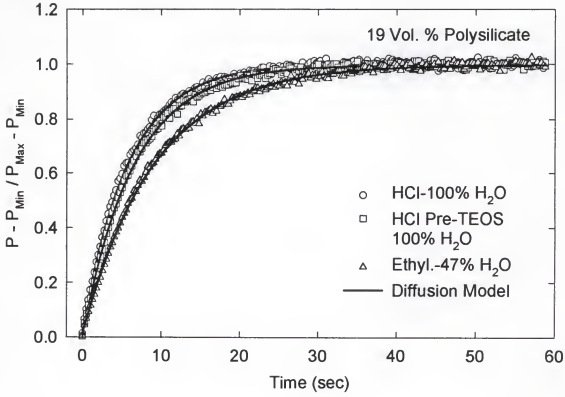

Figure 5.9 Step responses and diffusion model curve fits for the in-situ precipitated and prehydrolyzed HCL catalyzed gels, as well as the ethylamine catalyzed gels. All samples contain PtTFPP and an estimated 19 vol.% polysilicate.

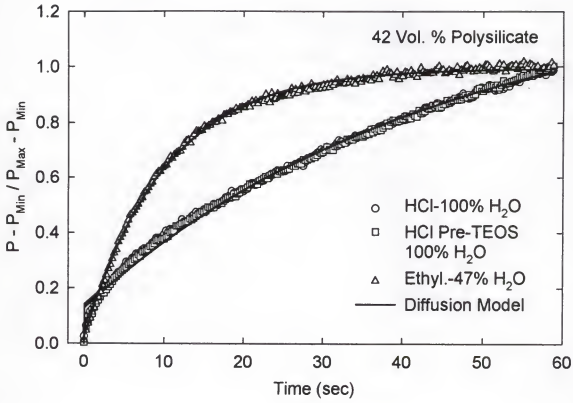

Figure 5.10 Step responses and diffusion model curve fits for the in-situ precipitated and prehydrolyzed HCL catalyzed gels, as well as the ethylamine catalyzed gels. All samples contain PtTFPP and an estimated 42 vol.% polysilicate.

Figures 5.7 through 5.10 indicates good agreement with the exception of the 42% HCl catalyzed gels. These two samples exhibit step responses during the first 3 seconds that can not be described by this model. The most likely explanation is that insufficient time has been allowed for the samples to reach equilibrium luminescence. This is supported by the estimated B values of 1.27 and 1.28.

Although the parameter uncertainties are automatically estimated by the curve fitting routine, the uncertainty associated with the diffusivity measurements in Table 5.2 must be estimated using an uncertainty analysis of the relevant parameters. Equation 5.6 can be written in terms of the diffusivity to yield:

$$D = \frac{4L^2}{\pi^2 \tau}. \tag{5.10}$$

The uncertainty in this measurement can be estimated from the summation of the partial derivatives with respect to thickness and τ

$$dD_{O2} = \left[\left(\frac{8L}{\pi^2 \tau} \cdot w_L \right)^2 + \left(\frac{4L^2}{\pi \tau^2} \cdot w_\tau \right)^2 \right]^{\frac{1}{2}}, \tag{5.11}$$

Table 5.2 Diffusion model parameters and resulting oxygen diffusivity.

Sample	B	C	τ (sec)	D_{O2} (10^6 cm2/sec)
4.5%, HCl, in-situ	0.991	0.874±4.18E-3	2.13±0.015	2.9±0.30
11%, HCl, in-situ	1.01	0.982±2.64E-3	2.63±0.011	2.8±0.28
19%, HCl, in-situ	1.00	0.972±1.32E-3	5.81±0.013	1.3±0.13
42%, HCl, in-situ	1.27	1.13±3.84E-3	43.4±0.31	0.24±0.024
11%, HCl, prehy.	0.995	0.979±2.01E-3	3.32±0.010	2.6±0.26
19%, HCl, prehy.	0.996	0.986±1.20E-3	6.50±0.013	1.1±0.11
42%, HCl, prehy.	1.28	1.15±3.91E-3	43.6±0.31	0.20±0.021
4.5%, Ethyl., in-situ	0.993	0.961±1.47E-3	7.33±0.019	1.1±0.11
11%, Ethyl., in-situ	0.996	0.982±1.37E-3	6.94±0.017	1.3±0.13
19%, Ethyl., in-situ	0.997	0.980±1.03E-3	9.09±0.018	0.92±0.093
42%, Ethyl., in-situ	0.994	0.967±1.12E-3	10.1±0.023	1.1±0.11

where L is the sample thickness, and w_L and w_τ are the uncertainties in the values of the thickness and τ, respectively.[155,156] Although a measure of error does exist for the thickness of each gel and is given in Table 5.1, a ballpark uncertainty of 5% is assumed to allow for the assumptions made in the film thickness calculation. Since the uncertainty of τ for each gel has been given in Table 5.2, it is possible to calculate the oxygen diffusivity uncertainty for each sample. An assessment of the resulting uncertainty for these D_{O2} values indicates that ca. 10% error exists in the measurements.

The graphical display of the oxygen diffusivity as a function of polysilicate loading is given in Figure 5.11. These results reveal that the oxygen diffusivity of the acid catalyzed, unfilled gel, i.e., crosslinked in the absence of additional TEOS, is ca. $3x10^{-6}$ cm^2/sec while that of the base catalyzed, unfilled gel is three times lower. The first check that must be made is the validity of these values. Since no published values of the oxygen diffusivity of PTMO can be found, comparisons must be made to other rubbers. Poly(dimethyl siloxane) (PDMS), which is the most permeable rubber known, possesses an oxygen diffusivity estimated by a similar technique at $3.55x10^{-5}$ cm^2/sec at 25°C.[152] Additionally, values of $1.75x10^{-6}$ and $1.5x10^{-6}$ cm^2/sec at 25°C for natural rubber and polybutadiene, respectively, have been published.[157] That good agreement is found between the oxygen diffusivity of these unfilled composites (both acid and base catalyzed) and these published values of natural rubber and polybutadiene is encouraging. This validity is enhanced by the fact that all of these published values are less than that of PDMS measured using a similar fluorescence technique.[152] Having established that the values measured are reasonable, it becomes necessary to explain why the acid catalyzed

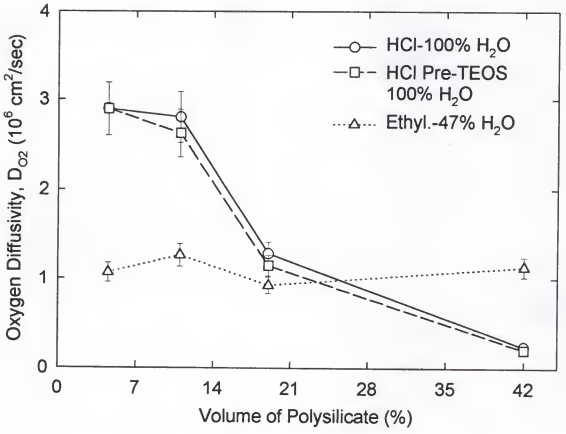

Figure 5.11 Oxygen diffusivity as a function of polysilicate loading for all three classes of gels produced.

unfilled gels, i.e., 4.5 vol.% polysilicate, has a diffusivity that is different from the base catalyzed gel. No complimentary data exists for these 4.5 vol.% polysilicate gels. However, insights can be gained from examination of more highly loaded gels, e.g. 33 vol.%. A review of Figure 5.3 reveals that the storage modulus at 25°C for the ethylamine catalyzed gel is lower than that of the HCl catalyzed gel. This reduced value is attributed to the diminished reinforcing effect induced by the more phase separated, base catalyzed polysilicate phase. This conclusion is reinforced by the fact that swelling of both the HCl and ethylamine catalyzed, in-situ precipitated gels in tetrahydrofuran for 24 hr results in mass uptakes of 19.8±1.22% and 31.1±2.60%, respectively. Therefore, the ethylamine catalyzed gel likely possesses a lower crosslink density which should lead to increased diffusivity. Figure 5.11 indicates that this is indeed observed. It is reasonable to assume that this trend of decreased phase interaction leading to increased diffusivity would hold for all polysilicate loadings generated using base catalysis. Consequently, the 4.5 vol.% ethylamine catalyzed gel should still possess a greater diffusivity than the HCl catalyzed gel. However, the opposite is observed. This indicates that the slight variation in measured diffusivity may be due to the environment the lumiphore resides. Published results indicate that this is quite possible.[82,158,159] The result of a slight change in the pressure-luminescence response would be slightly different step responses. The values of τ calculated would then be different, as would the calculated diffusivity. Recall that exposure of HCl catalyzed gels to ethylamine in Chapter 2 resulted in a significant reduction in the silanol concentration within the gels. It is quite possible that the in-situ precipitation of the polysilicate phase in the presence of ethylamine would result in a similar reduction in the number of silanol species present in the inorganic phase.

Therefore, the difference in measured diffusivities may reflect this change in chemical environment within the two gel classes. However, within each class the influence of polysilicate environment remains constant and the luminescent characteristics of the probe should remain the same.

Considering next the influence of processing, a significant difference is observable between the acid and base catalyzed gel classes as the polysilicate loading increases. The diffusivity of both classes of the HCl catalyzed gels decreases with increased polysilicate loading while the ethylamine catalyzed gels exhibit virtually no change. Few studies have been published detailing transport phenomena in hybrids because the emphasis has been on device production and performance. Insights can be gained, however, by adapting the analysis used to explain both the influence of crystallinity, phase separation and impermeable particles, such as zeolites, upon diffusion characteristics.[106,108,109,160] Although different symbols and accompanying terminology are used to express the effect, the overall result is that the diffusivity of crystalline polyethylene, SBS block copolymers, filled rubbers and zeolite embedded polydimethylsiloxane decreases by a factor of κ according to the relation

$$D = \frac{D_{amorphous}}{\kappa} \tag{5.12}$$

where $D_{amorphous}$ is the diffusivity of the amorphous or "high diffusivity" region. The term κ is essentially interpreted as the geometric impedance factor intended to account for the tortuosity of the diffusion pathways resulting from the presence of the less permeable or absorptive domains. In the polyethylene studies, it was demonstrated that at 22 vol.% crystallinity, the oxygen diffusivity is 1/10 of that estimated for amorphous

polyethylene.[160] In the case of polydimethylsiloxane containing dispersed zeolites, it was demonstrated that the presence of these gas immobilizing fillers delays the time necessary to reach the steady-state permeation required by the time-lag technique. However, only a 1/4 reduction in the oxygen diffusivity of the composite system occurred at a 21 vol.% loading.[106] This is a significant difference in the tortuosity, or κ-value, for these two types of fillers and indicates that as the oxygen absorptive ability of the second phase increases the impact it has upon reduced diffusivity is diminished. The minimum pore diameter present in the embedded zeolites was 0.45 nm. It is anticipated that the pores present within the polysilicate domains of these hybrids could be as much as an order of magnitude larger. Therefore, it is not unreasonable to conclude that the effect of such an absorptive second phase may be insignificant. As Figure 5.13 reveals, the ethylamine catalyzed gels do not exhibit any change in oxygen diffusivity with increased loading suggesting that the polysilicate domains present do contain significant porosity. It is possible that the diffusivity of these pores is on the order of the polymer matrix they reside in. For example, the published value of the diffusivity of methane at ambient temperature in a single zeolite possessing 0.56 nm minimum pore diameter is 8×10^{-6} cm^2/sec.[100] This value is quite close to the measured 1×10^{-6} cm^2/sec for the hybrids. Therefore, if the pores present in the base catalyzed polysilicate phases are of comparable size then increased polysilicate loading would have no effect. In relation to Equation 5.12, this would constitute κ equal to unity.

The HCl catalyzed gels exhibit a much different response and undergo significant reductions in the composite diffusivity with increasing polysilicate loadings. This suggests

that these domains contain less absorptive ability, such as smaller pores, and are much more impenetrable to the diffusing oxygen. The κ values for increasing polysilicate loadings are given in Table 5.3 and reflect the increasing tortuosity of the diffusion pathways induced by the comparatively impenetrable polysilicate phase. Interestingly, there is very little difference in diffusivity induced by prehydrolyzing the TEOS compared to in-situ precipitation. This is most likely due to the similar "effective crosslink density" indicated by the near equivalent DMS storage modulus values at 25°C in Figure 5.3.

One method of assessing the porosity present in the polysilicate domains of the gels is to force-fit a double-exponential diffusion equation of the form

$$\frac{\overline{P} - P_{Min}}{P_{Max} - P_{Min}} = B - \left[C_1 \exp\left(-\frac{t}{\tau_1}\right) + C_2 \exp\left(-\frac{t}{\tau_2}\right) \right] \tag{5.13}$$

to determine the diffusivity of both the PTMO and polysilicate phase. Despite the fact that very good agreement already exists for the single-exponential model, this was done for the 19 vol.% ethylamine catalyzed gel. Only one gel was needed as the diffusivity is independent of the loading. The resulting fit is not shown as no discernible difference in the quality of the single-exponential and double-exponential fits is observable. The resulting D_{O2} values are $1.2\pm0.24\times10^{-6}$ cm^2/sec and $0.63\pm0.18\times10^{-6}$ cm^2/sec for the PTMO and polysilicate phases, respectively. The diffusivity of oxygen undergoing transport in

Table 5.3 Tortuosity factors as a function of increasing polysilicate loading for the HCl catalyzed gels.

Acid Catalyzed Polysilicate Volume (%)	κ
11	1.0
19	2.2
42	12

the Knudsen regime is given as

$$D_K = \frac{4r}{3}\left(\frac{2RT}{\pi M}\right)^{\frac{1}{2}} \quad (5.14)$$

For an assumed D_K of 1.2×10^{-6} cm^2/sec the calculated pore diameter is ca. 4×10^{-4} nm. This value is nonsensical, and suggests that although diffusion is occurring within the polysilicate phase it is most likely occurring in transport pathways that are considerably smaller than those necessary for Knudsen diffusion. Since the size of the pores strongly influences diffusion, these hybrids must possess pore diameters that are very near the collision diameter of the gas, i.e., 0.2 nm to 1 nm. Furthermore, the acid catalyzed domains are smaller and less well defined. The review of the literature concerning hybrid membranes given in Chapter 2 strongly supports these observations in that near universal absence of Knudsen diffusion was observed.[116-119]

Conclusions

A luminescence-based technique for measuring the oxygen diffusivity of homogeneous materials has been applied to hybrid organic-inorganic composites. The near molecular level of mixing present in these sol-gel-derived composites has been tuned to produce three differing levels of polysilicate structure through the use of both acidic and basic catalysts as well as the prehydrolysis of the silicon alkoxide during sol processing. The results of this testing indicate that the technique is valid since the oxygen diffusivity values calculated from the application of a single-exponential diffusion model appear to be in agreement with the published results on other types of rubbers. Some

indication is present, however, that the molecular environment that the lumiphore probes reside within influences the measured oxygen diffusivity.

One of the goals of this work was to assess the potential for well-defined, open porosity within these hybrid gels. It was anticipated that if porosity was indeed present the diffusion would likely be occurring in the Knudsen regime. The results collected in this study indicate that this is not the case. Although the polysilicate phases do possess some absorptive nature, with the ethylamine catalyzed gels exhibiting the highest propensity to absorb and/or immobilize oxygen, theoretical Knudsen diffusion models are unable to accurately predict realistic pore diameters. Therefore, the pore structures present in these hybrid composites most likely exhibit a configurational influence upon the diffusing oxygen, i.e., the types of pores present have dimensions approaching the collision diameter of the diffusing oxygen.

CHAPTER 6
CLOSING REMARKS

Rubber Elasticity and Nonideal Networks

In Chapter 3, the average molar mass between crosslinks was estimated using elementary rubber elasticity theory in conjunction with DMS. The resulting values were shown to be in excellent agreement with those obtained using traditional swelling studies. These results reveal that under the conditions of low strain amplitude and in the absence of thermally induced chemistry/curing, the combination of dynamic mechanical data and rubber elasticity theory are complimentary and do provide seemingly accurate values of network parameters. Perhaps, the most important word is complimentary. DMS is a widely used tool for evaluating the modulus, Tg, damping characteristics and phase homogeneity of polymers. Frequently, thermo-mechanical scans are performed on thermosets, and these parameters are tabulated. Less frequently, however, is additional information extracted from these spectra. The investigation detailed in Chapter 3 reveals that application of an idealized theory to a nonideal system can provide much additional information concerning phase mixing. Although the results of the analysis appear to be valid for this system, some would surely question the credibility of the approach. However, other evidence attesting to the success of rubber elasticity theory in evaluating nonideal networks exists.

Although the elasticity of bimodal networks has been analyzed extensively over the past decade, these investigations have exclusively utilized the Mooney-Rivlin equation.[161] Only recently have preliminary findings of swelling-based elasticity studies been reported. However, like elastomeric hybrid composites, the results suggest that these nonideal networks behave in a much more ideal way than expected. In many respects, the two systems are similar. For example, bimodal networks are comprised of exceptionally short oligomers and higher molar mass chains, e.g., 500 and 10,000 g/mole, respectively. Current thinking on these networks is that the short chains coalesce and form macro-sized crosslink junctions spanned by the longer chains. By analogy, the hybrids discussesd in this work possess macro-sized domains rich in polysilicate, a highly crosslinked network. These domains are the crosslink junctions spanned by the PTMO. When these results are taken as a whole, they suggest that rubber elasticity theory is quite capable of evaluating these heterogeneous networks, and it provides a very useful tool for examining phase mixing.

However, several important issues remain to be answered. One of the underlying assumptions in the analysis used in Chapter 3 concerns the use of dynamic moduli data in place of equilibrium modulus values. The assumption made in applying the dynamic data is that if the characteristic relaxation time of the material is less than the time-scale of the DMS measurement then essentially the material is at equilibrium. The time required to obtain the dynamic modulus is approximated by the frequency of the applied strain. At 0.1 Hz, the time required for testing is 10 seconds. Several attempts have been made to determine the characteristic relaxation times for these gels. Although not reported on in Chapter 3, the results are interesting in that virtually no relaxation is observable at room

temperature. However, upon heating to 70°C, significant stress relaxation/retardation occurs. Attempts at using these equilibrium modulus/temperature data points to calculate the average number of covalently bonded, elastically active chains proved unsuccessful owing to the low number of data points and large scatter in the values. A better designed and more rigorous analysis of the stress relaxation and temperature response of these gels as a function of both polysilicate loading and spatial distribution would provide valuable insight into the extent of phase mixing occurring. This analysis could then be compared to the network parameters measured using the DMS-based technique and swelling-based assessment of the same parameters. Taken as a whole, this would constitute an excellent study of the network homogeneity and ideallity present in hybrid composites. No such studies have been published in the hybrid community.

High Performance SIPNs

The origin of the investigation detailed in Chapter 4 was the high strength, high elongation and yielding previously observed for SIPNs containing poly(methacrylic acid) (PMAA) as the "thermoplastic" interpenetrating phase.[123] The classification of these materials as semi-interpenetrating polymer networks is based on the fact that the PTMO and polysilicate hybrids from which the "SIPNs" are produced are pre-established thermoset networks. Swelling this network with an acrylic monomer and then polymerizing it in-situ produces the thermoplastic interpenetrating chains. Realistically, the high energy of γ radiation induces chain scission and leads to increased modulus and strength and decreased elongation at break in the elastomeric hybrid gels. Therefore, when the monomer swollen gels are exposed to the radiation, it is quite probable that

some methacrylic acid segments or PMAA oligomers are incorporated into the PTMO chains. Furthermore, some crosslinking may be induced in the PMAA. These possibilities were part of the reason for addressing the issue of polysilicate loading and spatial distribution in the SIPNs. By varying the amount and distribution of this reinforcing phase, insights into the factors contributing to the high strength and elongation were identified.

The results of Chapter 4 revealed that as the loading of polysilicate increased the elongation at failure decreased without a significant gain in strength. Similarly, when the degree of hydrogen bonding likely occurring was reduced by replacing THF with DMF in the sol, the elongation at failure decreased without a significant gain in strength. Accompanying the decreased elongation values were decreased post-yield elongation prior to strain hardening. These trends indicate that as the polysilicate loading and connectivity increases the glassy network is capable of less deformation under the load. Therefore, since the use of an acid catalyzed or THF-based sol promotes the development of a less connected polysilicate phase, it is the ability of this network to deform that allows the high elongation. Inherent in this finding is that the unhindered PTMO-PMAA phases are capable of significant deformation.

Several additional studies would compliment these findings well. For example, obtaining the mechanical tensile response of PMAA would provide a baseline against which the response of the hybrid SIPNs could be compared. However, efforts to compression mold PMAA of ca. 100,000 g/mole polymer have produced brittle glasses from which tensile samples could not be obtained. It is arguable that this relatively low molar mass is below the critical molar mass for entanglement and that this explains the

brittle nature. This is quite possible. Until higher molar mass polymer can be produced or synthesized, this baseline response can not be obtained. One advantage that this lower molar mass material may provide is enhanced diffusion rates. An interesting study would be to dissolve the 100 kg/mole PMAA in an alcohol and then swell pieces of the hybrid in this solution. If a significant amount of PMAA can be absorbed, it would result in a more ideal SIPN. Therefore, it would be possible to investigate the influence of the organic phase connectivity, or lack of, upon the mechanical response of the hybrids. Such a study would compliment the investigation of inorganic phase connectivity upon mechanical response.

Gas Transport in Hybrid Composites

The origin of this study was the distinct lack of information addressing gaseous diffusion in hybrid composites composed of a significant amount of the organic phase. This is in contrast to the organically modified glasses described in Chapter 2. The central theme of the study was to measure the diffusivity of a common, inert gas as a function of the polysilicate loading and structure. Again, it is the wide-variety of morphologies that can be produced in hybrid composites that make them such ideal models for many studies of mixed phase systems. In this study, it was hoped that the diffusivity values measured and trends observed would provide an assessment of the types of pore structures present in the polysilicate phase. The ability to detect significant porosity would substantiate the notion that pores do exist in these composites.

The results were highly informative. Initially, it was thought that if pores do exist in the polysilicate phase, then Knudsen diffusion would predominate, as is the case in sol-

gel-derived membranes. Therefore, hybrid composites may possess two gas separation mechanisms. Evidence of this mixed-mode diffusion would have been step responses that could only be fit by a dual-exponential diffusion model. However, in agreement with the majority of literature published on organically doped sol-gel membranes, Knudsen diffusion was not observed. Rather, the materials exhibited diffusion responses indicative of configurational transport at best. Valuable insights were gained, however, from the trends in diffusivity with increased polysilicate loading. Perhaps most enlightening was the evidence that base catalysis produces polysilicate phases that are much more absorptive in nature than acid catalysis. Taken as a whole, the results point to sub-nanometer porosity within the base catalyzed inorganic domains and even smaller pores, essentially bonding defects, within the acid catalyzed polysilicate domains.

An additional level of complexity was present in this study in that a luminescence-based technique was used to measure the diffusivity. While this technique is certainly not difficult, the influence of molecular environment upon the luminescence characteristics of the compound becomes important. This technique also limits the results somewhat in that no measure of permeability exists, and consequently, no method of calculating an average solubility exists. This is important because there is no way of checking the validity of the Henry's law assumption this luminescent technique relies upon. Traditional concentration-pressure studies utilizing a micro-balance or other technique need to be performed. The insights gained from such sorption studies would undoubtedly provide a valuable second opinion of the absorptive capabilities of the inorganic phases in these gels.

Another approach that warrants utilization is that of preferentially localizing the lumiphores within each phase. For example, many different types of luminescent

compounds exist. If a salt-based lumiphore were to be present during the prehydrolysis of TEOS, then it is likely that polar interactions between the silanol groups of the gelling polysilicate and lumiphore would result in incorporation of the probe into the glassy network. These doped polysilicate structures could then be processed with the end functionalized PTMO and gels cast. For the sake of comparison, the same probe could be dispersed into the PTMO sol and the prehyrolyzed TEOS added immediately prior to casting. This would force the lumiphore into the PTMO rich phase. By measuring the diffusivity of both types of gels as a function of polysilicate loading, the effects of environment upon diffusivity could be discerned and a check made of the premise that the lumiphore must be present in every phase for which it is assessing the diffusivity.

LIST OF REFERENCES

1. Sur, G.S. and Mark, J.E., *Eur. Poly. J.*, **21**, 1051 (1985).

2. Mark, J.E., Jiang, C-Y. and Tang, M-Y., *Macromolecules*, **17**, 2613 (1984).

3. Ning, Y-P., Tang, M-Y., Jiang, C-Y., Roth, W.C. and Mark, J.E., *J. Appl. Poly. Sci.*, **29**, 3209 (1984).

4. Mark, J.E., Ning, Y-P., Jiang, C-Y. and Tang, M-Y., *Polymer*, **26**, 2069 (1985).

5. Schaefer, D.W., Jian, L., Sun, C-C., McCarthy, D., Jiang, C-Y., Ning, Y-P. and Mark, J.E., *Poly. Prep.*, **30**, 102 (1989).

6. Sun, C-C. and Mark, J.E., *Polymer*, **30**, 104 (1989).

7. Wang, S.B. and Mark, J.E., *Poly. Prep.*, **32**, 523 (1991).

8. Sohoni, G.B. and Mark, J.E., *J. Appl. Poly. Sci.*, **45**, 1763 (1992).

9. Wilkes, G.L., Orler, B. and Huang, H-H., *Poly. Prep.*, **26**, 300 (1985).

10. Huang, H-H., Orler, B. and Wilkes, G.L. *Poly. Bull.*, **14**, 557 (1985).

11. Huang, H.-H., Orler, B. and Wilkes, G.L., *Macromolecules*, **20**, 1322 (1987).

12. Wen, J. and Wilkes, G.L., *Chem. Mater.*, **8**, 1667 (1996).

13. Chung, Y.J., Ting, S-J. and Mackenzie, J.D., *Better Ceramics Through Chemistry IV*, Zelinski, B.J.J., Brinker, C.J., Clark, D.E. and Ulrich, D.R., Eds., Mat. Res. Soc. Symp. Proc., **180**, 981 (1990).

14. Hu, Y. and Mackenzie, J.D., *J. Mater. Sci.*, **27**, 4415 (1992).

15. Schmidt, H., *Better Ceramics Through Chemistry*, Brinker, C.J., Clark, D.E. and Ulrich, D.R., Eds., Mat. Res. Soc. Symp. Proc., **32**, 327 (1984).

16. Kohjiya, S., Kenichiro, O. and Yamashita, S., *J. Non-Cryst. Solids*, **119**, 132 (1990).

17. Surivet, F., Lam, T.M., Pascault, J-P. and Mai, C., *Macromolecules*, **25**, 5742 (1992).

18. Huang, H-H. and Wilkes, G.L., *Poly. Prep.*, **28**, 244 (1987).

19. Huang, H-H., Glaser, R.H. and Wilkes, G.L., *Inorganic and Organometallic Polymers*, Zeldin, M., Wynne, K.J. and Allcock, H.R., Eds., ACS Symp. Series, **360**, 355 (1987).

20. Brennan, A.B., Huang, H.-H and Wilkes, G.L. *Poly. Prep.*, **30**, 105 (1989).

21. Wang, B., Huang, H-H., Brennan, A.B. and Wilkes, G.L., *Poly. Prep.*, **30**, 146 (1989).

22. Rodrigues, D.E. and Wilkes, G.L., *Poly. Prep.*, **30**, 227 (1989).

23. Huang, H-H., Wilkes, G.L. and Carlson, J.G., *Polymer*, **30**, 2001 (1989).

24. Wilkes, G.L., Brennan, A.B., Huang, H.-H., Rodrigues, D. and Wang, B. *Polymer Based Molecular Composites*, Schaefer, D.W. and Mark, J.E., Eds., Mat. Res. Soc. Symp. Proc., **171**, 15 (1990).

25. Wang, B., Brennan, A.B., Huang, H.-H. and Wilkes, G.L., *J. Macromol. Sci., Chem.*, **A27**, 1447 (1990).

26. Brennan, A.B., Wang, B., Rodrigues, D.E. and Wilkes, G.L. *J. Inorgan. Organomet. Poly.*, **1**, 167 (1991).

27. Wang, B. and Wilkes, G.L., *J. Poly. Sci., Poly. Chem.*, **29**, 905 (1991).

28. Brennan, A.B. and Wilkes, G.L., *Polymer*, **32**, 733 (1991).

29. Rodrigues, D.E., Brennan, A.B., Betrabet, C., Wang, B. and Wilkes, G.L., *Poly. Prep.*, **32**, 525 (1991).

30. Rodrigues, D.E., Brennan, A.B., Betrabet, C., Wang, B. and Wilkes, G.L., *Chem. Mater.*, **4**, 1437 (1992).

31. Brennan, A.B. and Rabbani, F., *Poly. Prep*, **32**, 496 (1991).

32. Mauritz, K.A. and Jones, C.K., *J. Appl. Poly. Sci.*, **40**, 1401 (1990).

33. Surivet, F., Lam, T.M., Pascault, J.-P. and Pham, Q.T., *Macromolecules*, **25**, 4309 (1992).

34. David, I.A. and Scherer, G.W., *Poly. Prep.*, **32**, 530 (1991).

35. Saegusa, T., *J. Macromol. Sci., Chem.*, **A28**, 817 (1991).

36. Fitzgerald, J.J., Landry, C.J.T., Schillace, R.V. and Pochan, J.M., *Poly. Prep.*, **32**, 532 (1991).

37. Landry, C.J.T., Coltrain, B.K., Wesson, J.A., Zumbulyadis, N. and Lippert, J.L., *Polymer*, **33**, 1496 (1992).

38. Toki, M., Chow, T.Y., Ohnaka, T., Samura, H. and Saegusa, T., *Poly. Bull.*, **29**, 653 (1992).

39. Novak, B.M. and Ellsworth, M.W., *Mater. Sci. and Engr.*, **A162**, 257 (1993).

40. Landry, C.J.T. and Coltrain, B.K., *Poly. Prep.*, **32**, 514 (1991).

41. Landry, C.J.T., Coltrain, B.K. and Brady, B.K., *Polymer*, **33**, 1486 (1992).

42. Pope, E.J.A., Asami, M. and Mackenzie, J.D., *J. Mater. Res.*, **4**, 1018 (1989).

43. Klein, L.C. and Abramoff, B., *Poly. Prep.*, **32**, 519 (1991).

44. Wei, Y., Bakthavatchalam, R., Yang, D. and Whitecar, C.K., *Poly. Prep.*, **32**, 503 (1991).

45. Noell, J.L.W., Wilkes, G.L., Mohanty, D.K. and McGrath, J.E., *J. Appl. Poly. Sci.*, **40**, 1177 (1990).

46. Gillham, J.K., *Poly. Eng. Sci.*, **16**, 353 (1976).

47. Brennan, A.B., Ph.D. Dissertation, Virginia Polytechnic Institute and State University, Blacksburg, VA, 1990.

48. Morikawa, A., Iyoku, Y., Kakimoto, M. and Imai, Y., *Poly. J.*, **24**, 107 (1992).

49. Deng, Q., Hu, Y., Moore, R.B., McCormick, C.L. and Mauritz, K.A., *Chem. Mater.*, **9**, 36 (1997).

50. Mauritz, K.A., Storey, R.F. and Jones, C.K., *Multiphase Polymer Materials: Blends, Ionomers and Interpenetrating Networks*, Ultracki, L.A. and Weiss, R.A., Eds., ACS Symp. Series., **395**, 401 (1989).

51. Mauritz, K.A. and Warren, R.M., *Macromolecules*, **22**, 1730 (1989).

52. Stefanithis, I.D., Mauritz, K.A., Wilkes, G.L. and Huang, H.-H., *Poly. Prep.*, **32**, 236 (1991).

53. Mauritz, K.A., Stefanithis, J.D., Davis, S.V., Scheetz, R.W., Pope, R.K., Wilkes, G.L., Huang, H-H., *J. Appl. Poly. Sci.*, **55**, 181 (1995).

54. Gummaraju, R.V., Moore, R.B. and Mauritz, K.A., *J. Poly. Sci., Poly. Phys.*, **34**, 2383 (1996).

55. Apichatachutapan, W., Moore, R.B. and Mauritz, K.A., *J. Appl. Poly. Sci.*, **62**, 417 (1996).

56. Giannelis, E.P., *Adv. Mater.*, **8**, 29 (1996).

57. Kojima, Y., Usuki, A., Kawasumi, M., Okada, A., Fukushima, Y., Kurauchi, T., Kamigaito, O., *J. Mater. Res.*, **8**, 1185 (1993).

58. Yano, K., Usuki, A., Okada, A., Kurauchi, T. & Kamigaito, O., *Poly. Prep.*, **32**, 65 (1991).

59. Okada, A., Kawasumi, M., Kurauchi, T. & Kamigaito, O., *Poly. Prep.*, **28**, 447 (1987).

60. Okada, A., Kawasumi, M., Usuki, A., Kojima, Y., Kurauchi, T., Kamigaito, O., *Polymer Based Molecular Composites*, Schaefer, D.W. and Mark, J.E., Eds., Mat. Res. Soc. Symp. Proc., **171**, 45 (1990).

61. Okada, A., K. Fukumori, A. Usuki, Y. Kojima, N. Sato, Kurauchi, T., Kamigaito, O., *Poly. Prep.*, **32**, 540 (1991).

62. Avnir, D., Braun, S., Lev, O., Levy, D. and Ottolenghi, M., *Sol-Gel Optics: Processing and Applications*, Klein, L.C., Ed., Kluwer Academic Press, Boston, 539 (1994).

63. Schmidt, H. and Wolter, H., *J. Non. Cryst. Solids*, **121**, 428 (1990).

64. Popall, M., Meyer, H., Schmidt, H. and Schulz, J., *Better Ceramics Through Chemistry IV*, Zelinski, B.J.J., Brinker, C.J., Clark, D.E. and Ulrich, D.R., Eds., Mat. Res. Soc. Symp. Proc., **180**, 995 (1990).

65. Wang, B., Gungor, A., Brennan, A.B., Rodrigues, D.E., McGrath, J.E., Wilkes, G.L., *Poly. Prep.*, **32**, 521 (1991).

66. Betrabet, C. and Wilkes, G.L., *Poly. Prep.* **32**, 286 (1992).

67. Tamami, B., Betrabet, C. and Wilkes, G.L., *Poly. Bull.*, **30**, 39 (1993).

68. Fujita, M. and Honda, K., *Poly. Comm.*, **30**, 200 (1989).

69. Munteanu, D., *Metal Containing Polymeric Systems*, Sheats, J.E., Camahar, C.E. and Pittman, C.U., Eds., Plenum Press, New York, 479 (1985).

70. Prasad, P. and Williams, D.J., *Introduction to Nonlinear Optical Effects in Molecules and Polymers*, John Wiley & Sons, Inc., New York (1991).

71. Puccetti, G., Toussaere, E., Ledoux, I. and Zyss, J., *Poly. Prep.*, **32**, 61 (1991).

72. Hsiue, G-H., Lee, R-H. and Jeng, R-J., *Chem. Mater.*, **9**, 883 (1997).

73. Lebeau, B., Brasselet, S., Zyss, J. and Sanchez, C., *Chem. Mater.*, **9**, 1012 (1997).

74. Miller, R.D. and Michl, J., *Chem. Rev.*, **89**, 1405 (1989).

75. Wung, C.J., Pang, Y., Prasad, P.N. and Karasz, F.E., *Polymer*, **32**, 605 (1991).

76. Ellerby, L.M., Nishida, C.R. and Nishida, F., *Science*, **225**, 1113 (1992).

77. McEvoy, A.K., McDonagh, C.M. and MacCraith, B.D., *Chemical, Biochemical and Environmental Fiber Sensors VII*, SPIE Symp. Series, **2508**, 190 (1995).

78. McEvoy, A.K., McDonagh, C.M. and MacCraith, B.D., *Analyst*, **121**, 785 (1996).

79. Krihak, M., Murtagh, M. and Shahriari, M.R., *Chemical, Biochemical, and Environmental Fiber Sensors VIII,* SPIE Symp. Series, **2836**, 105 (1996).

80. Baron, A.E., Danielson, J.D.S, Gouterman, M., Wan, J.R., Callis, J.B., McLachlan, B., *Rev. Sci. Inst.*, **64**, 3394 (1993).

81. Carroll, B.F., Abbitt, J.D., Lukas, E.W. and Morris, M.J., *AIAA J.*, **34**, 521 (1996).

82. Hartmann, P., Leiner, M.J.P. and Lippitsch, M.E., *Sensors and Actuators*, **B29**, 251 (1995).

83. Badini, G.E., Grattan, K.T.V. & Tseung, A.C.C., *Rev. Sci. Inst.*, **66**, 4034 (1995).

84. Badini, G.E., Grattan, K.T.V., Tseung, A.C. and Palmer, A.W., *J. Sol-Gel Sci. Tech.*, **6**, 269 (1996).

85. Jin, T., Tsutsumi, S., Deguchi, Y., Machida, K. and Adachi, G., *J. Electrochem. Soc.*, **143**, 3333 (1996).

86. Chang, W.-P. and Whang, W-T., *Polymer*, **37**, 4229 (1996).

87. Corriu, R.J.P., Hesemann, P. and Lanneau, G.F., *Chem. Comm.*, **15**, 1845 (1996).

88. Schutte, C.L., Williams, K.W. and Whitesides, G.M., *Polymer*, **34**, 2609 (1993).

89. Kesting, R.E. and Fritzsche, A.K., *Polymeric Gas Separation Membranes*, John Wiley & Sons, Inc., New York (1993).

90. Chung, T-S., *Poly. and Poly. Comp.*, **4**, 269 (1996).

91. Freeman, B. and Pinnau, I., *TRIP*, **5**, 167 (1997).

92. Cunningham, R.E. and Williams, R.J.J., *Diffusion in Gases and Porous Media*, Plenum Press, New York, 1980.

93. McLachlan, B.G. and Bell, J.H., *Exp. Therm. and Fluid Sci.*, **10**, 470 (1995).

94. Koros, W.J., Chan, A.H. and Paul, D.R., *J. Membr. Sci.*, **2**, 165 (1977).

95. McHattie, J.S., Koros, W.J. and Paul, D.R., *J. Poly. Sci., Poly. Phys.*, **29**, 731 (1991).

96. Rautenbach, R. and Albrecht, R., *Membrane Processes*, John Wiley and Sons, Inc., New York (1989).

97. La Torre, G.P. and West, J.K., *Chemical Processing of Advanced Materials*, Hench, L.L. and West, J.K., Eds., John Wiley and Sons, Inc., New York, 891 (1992).

98. Fosmoe, A. and Hench, L.L., *Chemical Processing of Advanced Materials*, Hench, L.L. and West, J.K., Eds., John Wiley and Sons, Inc., New York, 897 (1992).

99. Klein, L.C. and Giszpenc, N.G., *Amer. Cer. Soc. Bull.*, **69**, 1821 (1990).

100. Sun, M.S., Talu, O. and Shah, D.B., *AIChE J.*, **42**, 3001 (1996).

101. Stannett, V., *J. Membrane Sci.*, **3**, 97 (1978).

102. Graham, T., *Roy. Inst. J.*, (1829).

103. Vieth, W.R., *Diffusion in and Through Polymers*, Hanser Publishers, New York (1991).

104. Crank, J., *The Mathematics of Diffusion*, 2nd Ed., Oxford University Press, London (1975).

105. Paul, D.R., *J. Poly. Sci., A-2*, **7**, 1811 (1969).

106. Paul, D.R. and Kemp, D.R., *J. Poly. Sci., Symp.*, **41**, 79 (1973).

107. Paul, D.R. and Koros, D.R., *J. Poly. Sci., Poly. Phys.*, **14**, 675 (1976).

108. van Amerongen, G.J., *Rubber Chem. and Tech.*, **37**, 1065 (1964).

109. Kinning, D.J., Thomas, E.L. and Ottino, J.M., *Macromolecules*, **20**, 1129 (1987).

110. Paul, D.R., *J. Polym. Sci., A-2*, **7**, 1811 (1969).

111. Muruganandam, N., Koros, W.J. and Paul, D.R., *J. Poly. Sci., Poly. Phys.*, **25**, 1999 (1987).

112. McHattie, J.S., Koros, W.J. and Paul, D.R., *Polymer*, **32**, 840 (1991).

113. McHattie, J.S., Koros, W.J. and Paul, D.R., *Polymer*, **32**, 2618 (1991).

114. Aitken, C.L., Koros, W.J. and Paul, D.R., *Macromolecules*, **25**, 3651 (1992).

115. Hellums, M.W., Koros, W.J., Husk, G.R. and Paul, D.R., *J. Appl. Poly. Sci.*, **43**, 1977 (1991).

116. Shelekhin, A.B., Grosgogeat, E.J. and Hwang, S-T., *J. Membrane Sci.*, **66**, 129 (1991).

117. Cao, G., Lu, Y., Laurent, D., Brinker, C.J. and Lopez, G.P., *Adv. Mater.*, **8**, 588 (1996).

118. Okui, T., Yuriko, S., Okubo, T. and Sadakata, M., *J. Sol-Gel Sci. and Tech.*, **5**, 127 (1995).

119. Smaihi, M., Jermoumi, T., Marignan, J. and Noble, R.D., *J. Membrane Sci.*, **116**, 211 (1996).

120. Guizard, C. and Lacan, P., *New J. Chem.*, **18**, 1097 (1994).

121. Brennan, A.B. and Miller, T.M., *Chem. Mater.*, **6**, 262 (1994).

122. Brennan, A.B., Miller, T.M. and Vinocur, R.B., *Hybrid Organic-Inorganic Composites*, Mark, J.E., Lee, C.Y-C. and Bianconi, P.A., Eds., ACS Symp. Series, **585**, 144 (1995).

123. Miller, T.M., M.S. Thesis, University of Florida, Gainesville, FL 1993.

124. Iler, R.K., *The Chemistry of Silica*, John Wiley and Sons, Inc., New York (1979).

125. Wilkes, G.L., *Polymer Science and Technology: An Interdisciplinary Approach*, American Chemical Society, Washington DC (1978).

126. Flory, P.J., *J. Chem. Phys.*, **18**, 108 (1950).

127. Flory, P.J., *Principles of Polymer Chemistry*, Cornell University Press, Ithaca, New York (1953).

128. Bristow, G.M. and Watson, W.F., *Trans. Faraday Soc.*, **54**, 1731 (1958).

129. Glaser, R.H., Wilkes, G.L. & Bronnimann, C.E., *J. Non-Cryst. Solids*, **113**, 73 (1989).

130. Almeida, R.M. and Pantano, C.G., *J. Appl. Phys.*, **68**, 4225 (1990).

131. Wood, D.L. and Rabinovich, E.M., *Appl. Spec.*, **43**, 263 (1989).

132. Bertoluzza, A., Fagnano, C., Morelli, M.A., Gottardi, V. and Guglielmi, M., *J. Non-Cryst. Solids.*, **48**, 117 (1982).

133. Yoshino, H., Kamiya, K. and Hiroyuki, N., *J. Non-Cryst. Solids*, **126**, 68 (1990).

134. Harrick, N.J., *Internal Reflection Spectroscopy*, John Wiley and Sons, Inc., New York (1967).

135. Orcel, G., Ph.D. Dissertation, University of Florida, Gainvesville, FL 1987.

136. Orcel, G., Hench, L.L., Artaki, I., Jonas, J. and Zerda, T.W., *J. Non-Cryst. Solids*, **105**, 223 (1988).

137. Artaki, I., Zerda, T.W. and Jonas, J., *J. Non. Cryst. Solids*, **81**, 381 (1986).

138. Yasumori, A., Anma, M. and Yamane, M., *Phys. Chem. of Glasses*, **30**, 193 (1989).

139. Porod, G., *Kolloid Z.*, **124**, 83 (1951).

140. Silverstein, R.M., Bassler, G.C. and Morrill, T.C., *Spectrometric Identification of Organic Compounds,* 5th Ed., John Wiley and Sons, Inc., New York (1991).

141. Matos, M.C., Ilharco, L.M. and Almeida, R.M., *J. Non. Cryst. Solids*, **147&148**, 232 (1992).

142. Lippincott, E.R., Van Valkenburg, A., Weir, C.E. and Bunting, E.N., *J. Res. Nat. Bur. of Stds.*, **61**, 61 (1958).

143. Niznansky, D. and Rehspringer, J.L., *J. Non. Cryst. Solids*, **180**, 191 (1995).

144. Ying, J.Y. and Benziger, J.B., *J. Non. Cryst. Solids*, **147&148**, 222 (1992).

145. Little, L.H., *Infrared Spectra of Absorbed Species*, Academic Press, New York (1966).

146. Smith, B.C., *Fundamentals of Fourier Transform Infrared Spectroscopy*, CRC Press, Boca Raton, FL (1996).

147. Scherer, G.W., *J. Non-Cryst. Solids*, **109**, 183 (1989).

148. Nielsen, L.E. & Landel, R.R., *Mechanical Properties of Polymers and Composites* Marcel Dekker, Inc., New York (1994).

149. Peyser, P., *Polymer Handbook*, Brandrup, J. and Emmergut, E.H., Eds., John Wiley and Sons, Inc., New York, VI-209 (1989).

150. Kim, T.-H., Koros, W.J., Husk, G.R. and O'Brien, K.C., *J. Membr. Sci.*, **37**, 45 (1988).

151. Stern, O. and Volmer, M., *Phys. Z.*, **20**, 183 (1919).

152. Cox, M.E., *J. Poly. Sci., Poly. Chem.*, **24**, 621 (1986).

153. Koros, W.J., Paul, D.R. and Rocha, A.A., *J. Poly. Sci., Poly. Phys.*, **14**, 687 (1976).

154. Poirier, D.R. and Geiger, G.H., *Transport Phenomena in Materials Processing*, The Minerals, Metals & Materials Society, Warrendale, Pennsylvania (1994).

155. Holman, J.P. and Gajda, W.J., *Experimental Methods for Engineers*, 5th Ed, McGraw-Hill, Inc., New York (1989).

156. Kline, S.J. and McClintock, F.A., *Mech. Eng.*, **75**, 3 (1953).

157. van Amerongen, G.J., *J. Appl. Phys.*, **17**, 972 (1946).

158. Smirnova, N.P., Kikteva, T.A., Kondilenko, V.P., Chorny, V.J., Eremenko, A.M., Ogenko, V.M., *Coll. Surf.*, **101**, 207 (1995).

159. Cox, M.E. and Dunn, B., *Appl. Optics*, **24**, 2114 (1985).

160. Michaels, A.S. and Parker, R.B., *J. of Poly. Sci*, **41**, 53 (1959).

161. Mark, J.E. and Erman, B. *Rubberlike Elasticity: A Molecular Primer*, John Wiley & Sons, Inc., New York (1988).

BIOGRAPHICAL SKETCH

The author was born in St. Louis, Missouri, in 1969. His father, Wayne Miller, was a pilot in the United States Army. His father's occupation resulted in twenty-one changes of address throughout the eastern U.S. before the author was 10 years old. The families twenty-second move was to Paducah, Kentucky, where the author and parents began life as civilians. While growing up in Kentucky, the author enjoyed hobbies of fishing, target shooting and especially windsurfing on nearby Kentucky Lake. In 1987 he began his studies in ceramic engineering at the University of Missouri at Rolla. He graduated with a Bachelor of Science degree and became engaged to Yvonne Gander in the fall of 1991. He immediately began pursuing a master's degree in materials science at the University of Florida. In May of 1992 he married. His studies and research focused on the sol-gel synthesis and characterization of organic-inorganic hybrid composites. He earned the master's degree in December of 1993. With the exception of a two year long quest in search of the ultimate slow-to-gel, thermal shock resistant epoxy, his efforts continued in the field of hybrid technology. Upon receiving his doctorate, he will immediately begin working in industry, which he considers the reward for the many years invested in formal education.

I certify that I have read this study and that in my opinion it conforms to acceptable standards of scholarly presentation and is fully adequate, in scope and quality, as a dissertation for the degree of Doctor of Philosophy.

Anthony B. Brennan, Chairman
Associate Professor of Materials Science and Engineering

I certify that I have read this study and that in my opinion it conforms to acceptable standards of scholarly presentation and is fully adequate, in scope and quality, as a dissertation for the degree of Doctor of Philosophy.

Christopher D. Batich
Professor of Materials Science and Engineering

I certify that I have read this study and that in my opinion it conforms to acceptable standards of scholarly presentation and is fully adequate, in scope and quality, as a dissertation for the degree of Doctor of Philosophy.

Elliot P. Douglas
Assistant Professor of Materials Science and Engineering

I certify that I have read this study and that in my opinion it conforms to acceptable standards of scholarly presentation and is fully adequate, in scope and quality, as a dissertation for the degree of Doctor of Philosophy.

Eugene P. Goldberg
Professor of Materials Science and Engineering

I certify that I have read this study and that in my opinion it conforms to acceptable standards of scholarly presentation and is fully adequate, in scope and quality, as a dissertation for the degree of Doctor of Philosophy.

Kenneth B. Wagener
Professor of Chemistry

This dissertation was submitted to the Graduate Faculty of the College of Engineering and to the Graduate School and was accepted as partial fulfillment of the requirements for the degree of Doctor of Philosophy.

December, 1997

Winfred M. Phillips
Dean, College of Engineering

Karen A. Holbrook
Dean, Graduate School